CRANFIELD UNIVERSITY

Yu Jie

Novel Swing Arm Mechanism Design for Trailing Edge Flaps on Commercial Airliner

SCHOOL OF ENGINEERING

MSc by research thesis

Jan. 2009

Cranfield University

School of Engineering

MSc by research thesis

Academic Year 2008-2009

Yu Jie

Novel Swing Arm Mechanism Design
for Trailing Edge Flaps on Commercial Airliner

Supervisor: **Mr. Phillip Stocking**
Dr. Craig Lawson

January 2009

ABSTRACT

This thesis will describe the works had been done by the author in the Flying Crane aircraft group design project and the new design of a novel swing arm mechanism which can be applied in the trailing edge high lift devices for this aircraft concept.

Flying Crane aircraft is a new generation commercial airliner concept as the result of group design project conducted by China Aviation Industry Corporation I (AVIC I) and Cranfield University. At the end of the group design project, parameters such as take-off and landing distance, trailing edge flap type and deflection in take-off and landing configuration of the Flying Crane concept have been determined. These parameters are design input of the novel trailing edge high lift device mechanism for this aircraft concept.

The idea of this innovative mechanism comes from the research achievement of a previous MSc student, Thomas Baxter, which applied swing arm mechanism into a passenger aircraft's leading edge slat. This thesis applied this idea to trailing edge flap and modeled the mechanism on CATIA software to yield a kinematic simulation for the purpose of check motion trail and force transfer in this mechanism. Relevant works such as actuation, mass and stress analysis are also involved.

As the result of this research project, it was found that swing arm mechanism trends to require relatively small fairings for supports and attachments due to its high stowed space utilizing efficiency. Initial mass estimation carried out in this thesis also indicates that the new design takes advantage in terms of weight comparing with traditional trailing edge flap mechanisms. Thus, swing arm mechanism is supposed to show great competitive potential for commercial airliner's trailing edge flaps after further analysis has been done in the detail design phase.

Keywords:

high lift devices, trailing edge flap, swing arm mechanism, kinematic simulation

ACKNOWLEDGEMENTS

I want to thank Mr. Phillip Stocking, Dr Craig Lawson, Dr Shijun Guo and other staff of School of Engineering who help me lot in my research project.

Moreover, I would like to show my great appreciation to our mentors and colleagues who worked hard and cooperated closely and helped me so much in both group design project and my individual research.

I also appreciate my family in China, my dear wife, my lovely little boy and my parents who supported me unselfishly during this year.

CONTENTS

TABLE OF FIGURES

TABLE OF TABLES

1 Introduction

1.1 General

High lift devices are introduced into modern transport aircraft to cope with the conflict between economical considerations and lift requirements at low flight speed. When a procedure of aircraft design starts, there are many aspects which should be considered carefully. A very important one is the aerodynamic performance of the wing. Most of modern wing profiles are optimized for cruise flight efficiency due to cruise flight phase occupies most proportion of the whole mission profile, and this optimization can reduce direct operating cost (DOC) of the aircraft for reduction of fuel consumption. However, this kind of airfoil is rather inefficient at low speeds and can not provide sufficient lift. Hence, high lift devices are adopted for the purpose of yielding more lift of the wing at low speeds, i.e. in take-off and landing stage.

A well-known lift coefficient to angle of attack (AoA) diagram is shown in Figure1.1 [1]. The curve at the bottom which is pointed by 'FLAPS UP' represents the lift coefficient of the basic airfoil. And the other above curve represents the lift coefficient of the wing when trailing edge flaps are deployed. The whole curve moves upward which means C_L has been increased with the same fuselage AoA because the trailing edge flaps increase the wing camber and improve the flow at trailing edge. But it may also cause a reduction in the stalling AoA due to it promotes leading edge stall on thin sections. Leading edge high lift devices can delay or eliminate leading edge stall so that to enlarge stall angle. The impact to C_L of leading edge devices is represented by dashed in the diagram.

The design process of high lift devices is more an empirical job than an analytic one. First of all, basic airfoil of the wing should be determined, and then the maximum lift coefficient ($C_{Lmax)}$ of this basic airfoil can be attained from either approximate calculation by empirical and statistic formulas or existing experimental data. Initial field performance parameters of the aircraft such as take-off and landing distance are relevant to the vehicle's mission type and can be set through consideration about the airport

condition. Then the increments of C_{Lmax} due to high lift devices during take-off and landing phases can be calculated from those parameters. So a certain suitable high lift devices type could be picked up via consideration about its high-lift capability, weight, complexity, cost, reliability and maintainability. The Fowler motion and deflection of the high-lift surfaces (flaps or slats) in take-off and landing stage can also be determined respectively. Once the motive track of high-lift surfaces is defined, the next job is preliminary design of the device's actuating mechanism. CAD software like CATIA would be used to help modeling and analysis. After an estimated aerodynamic loading is performed on the high-lift surfaces, we can calculate stress in the mechanism and analyze its strength to check whether the structure size is practical and feasible.

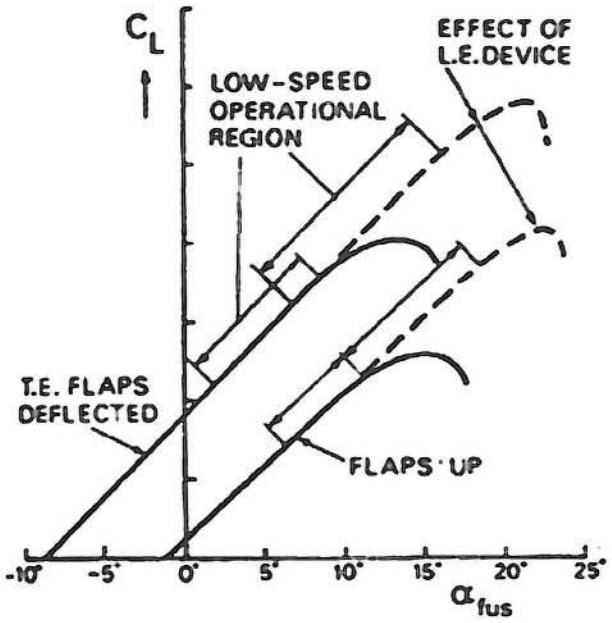

Figure 1.1 Lift curve with and without high lift devices [1]

1.2 Research background

1.2.1 Aircraft to be modeled

Flying Crane aircraft concept was developed by AVIC 1 aerospace vehicle design group under supervision of staff from Aerospace Science Department, School of Engineering, Cranfield University in 2008. This concept is a new generation airliner and mainly aims to domestic aviation market of China and may be rolled out in 10 to 15 years. The

whole project was built on a totally blank base, and the group experienced a complete series of processes including market survey, data collection, requirements analysis, initial parameters configuration, iterative procedures, comparison and filtration, and so on. As a member of the group, the author went through the whole flow and accomplished different tasks during each phase. The Group Design Project report is attached in appendix A of this thesis, which can provide more detailed introduction about works had been done in the group design project.

After comprehensive investigation about market prediction, its design point was defined to have 128-passenger capacity with 2,000nm range, which makes the airliner more efficient in operation, particularly in Chinese domestic market. Due to runway condition of existing airports and requirement of operating this aircraft in some high altitude airports, efficient high lift devices need to be designed for this concept to improve its field performance. Following parameters of Flying Crane which are close relevant to high lift devices design all come from reference [2].

Maximum Lift Coefficient (Flap and slats at take-off setting): 2.5

Maximum Lift Coefficient (Flap and slats at landing setting): 3.0

Aerofoil section: NASA SC(2)-0612

Trailing edge flap type: single slotted flap

Flap chord / local wing chord: 30%

Take-off flap angle: 25°

Landing flap angle: 45°

Outboard flap:

Inboard end from aircraft centreline: 6.868 m

Outboard end from aircraft centreline: 12.221 m

Inboard flap:

Inboard end from aircraft centreline: 2.3 m

Outboard end from aircraft centreline: 6.5 m

Figure1.2 [2] shows a 3-view drawing of the Flying Crane concept.

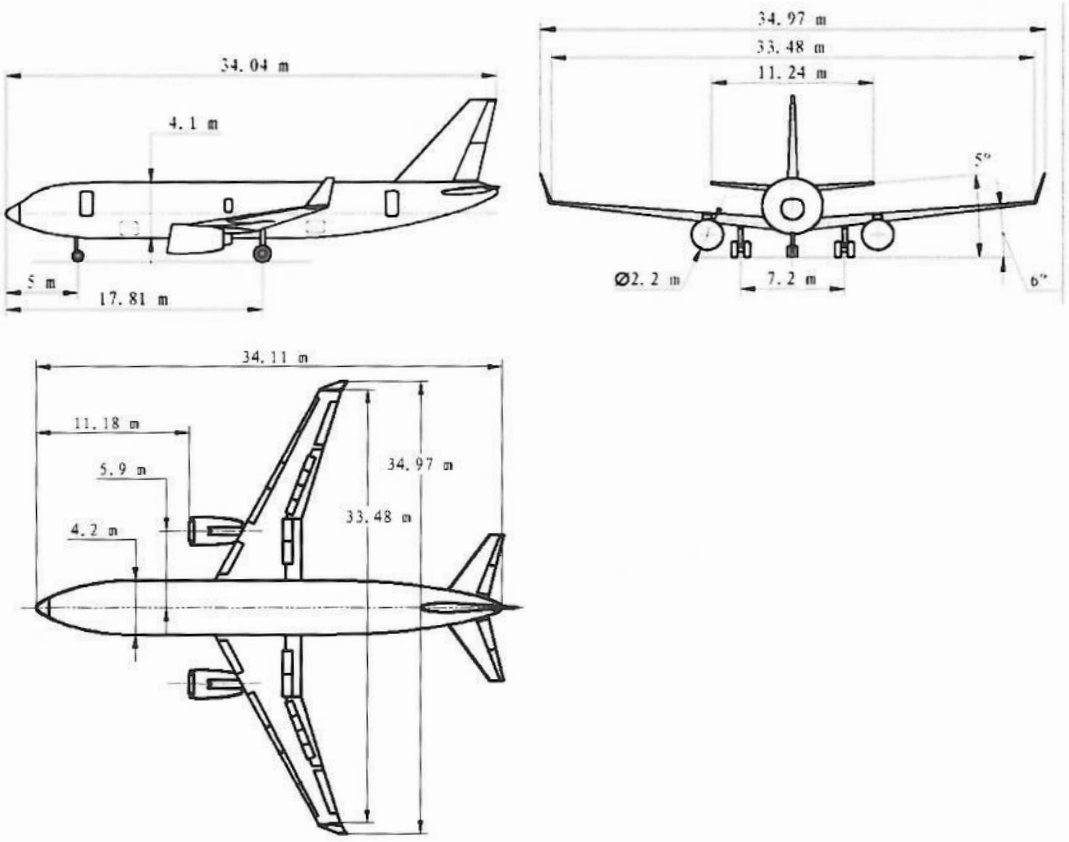

Figure 1.2 3-view drawing of the Flying Crane concept [2]

1.2.2 Swing arm mechanism specification

Mr. Craig Broadbent brought out the design of a swing arm mechanism which can deploy a moveable wing surface from a main wing section [3]. This mechanism consists of at least one first swing arm and another swing arm which connect the slat to the main wing section. This idea explored a new novel driven mechanism for high lift devices besides the bar-linkage mechanism and paired track mechanism which are adopted on most modern passenger aircrafts. Swing arm mechanism has advantages of lighter weight and more effective flat packed characteristic at stowed position which means less storage volume. Figure1.3 demonstrates sketches of the mechanism in detracted position, take-off position and full deployed position (landing configuration) respectively. [3]

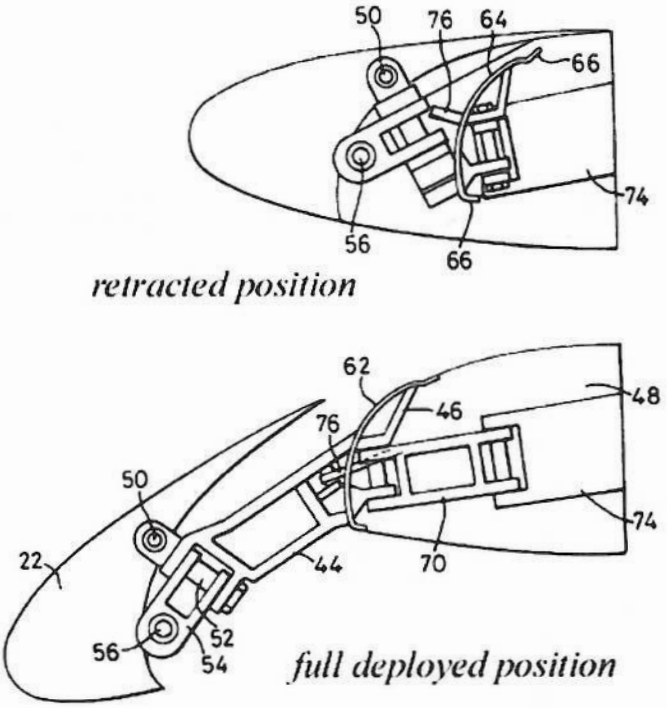

Figure 1.3 Broadbent's swing arm mechanism for slat system [3]

A previous MSc student, Mr. Thomas Baxter, looked at the feasibility of Craig Broadbent's design by modeling the mechanism and establishment its kinematic simulation using CAD software. He also finished the work of application this mechanism on the leading edge slats of A82, a short/medium range airliner, to value it against traditional rack and pinion slat system in terms of weight, volume, strength and fatigue trade-offs. The research conclusion is that the swing arm mechanism does work for thicker wing sections and has a good possibility of demonstrating competition against existing track mechanisms. [4]

1.3 Research objective

The objective of this thesis is to apply swing arm concept on trailing edge flap mechanisms of Flying Crane aircraft. The work consists of preliminary mechanical and actuating method design, actuator choice and strength analysis of the mechanism. After the mechanism is designed, it is also necessary to compare this new design with conventional trailing edge flap mechanisms in terms of weight and volume.

Baxter's thesis pointed out that the main problem attributed to the swing arm

mechanism is the sideways translation [4]. The loss in spanwise slat length may cause aerodynamic performance reduction and impact its competition consequently. Hence, it is an objective of the new mechanism to provide deployment that mitigates or eliminates the spanwise translation of the surface.

1.4 Research method

The author used method presented below in this research study.

Review about existing trailing edge high lift devices and their mechanisms

This research project began with a comprehensive investigation of existing trailing edge high lift devices. Review of their aerodynamic performance and structural and mechanical characteristics may help the author to understand advantages and disadvantages of each type and figure out which one is suitable for Flying Crane concept.

Modeling and simulation with CAD software

The whole process of the mechanism design from principle definition to components design was completed by CATIA V5. This software has excellent 3D modeling capability which could shorten design term and present the design results directly. With this characteristic, motion track of the mechanism and flaps from stowed position to full deployed position could be checked as soon as modeling and simulation work has been done.

Load calculation and strength analysis

Calculation of load on flaps bases on chordwise and spanwise pressure distribution curves coming from a previous PhD thesis written by Mr. Ammoo [5]. And strength analysis method comes from lecture notes of the college courses [6].

Discussion and comparison

The results of design and calculation were discussed around benefits and limitations of the new-designed novel swing arm mechanism.

Conclusions and recommendations

Conclusions coming from the whole research project were drawn. Some recommendations about future work were also given.

Figure1.4 demonstrates the flow chart of the design procedure.

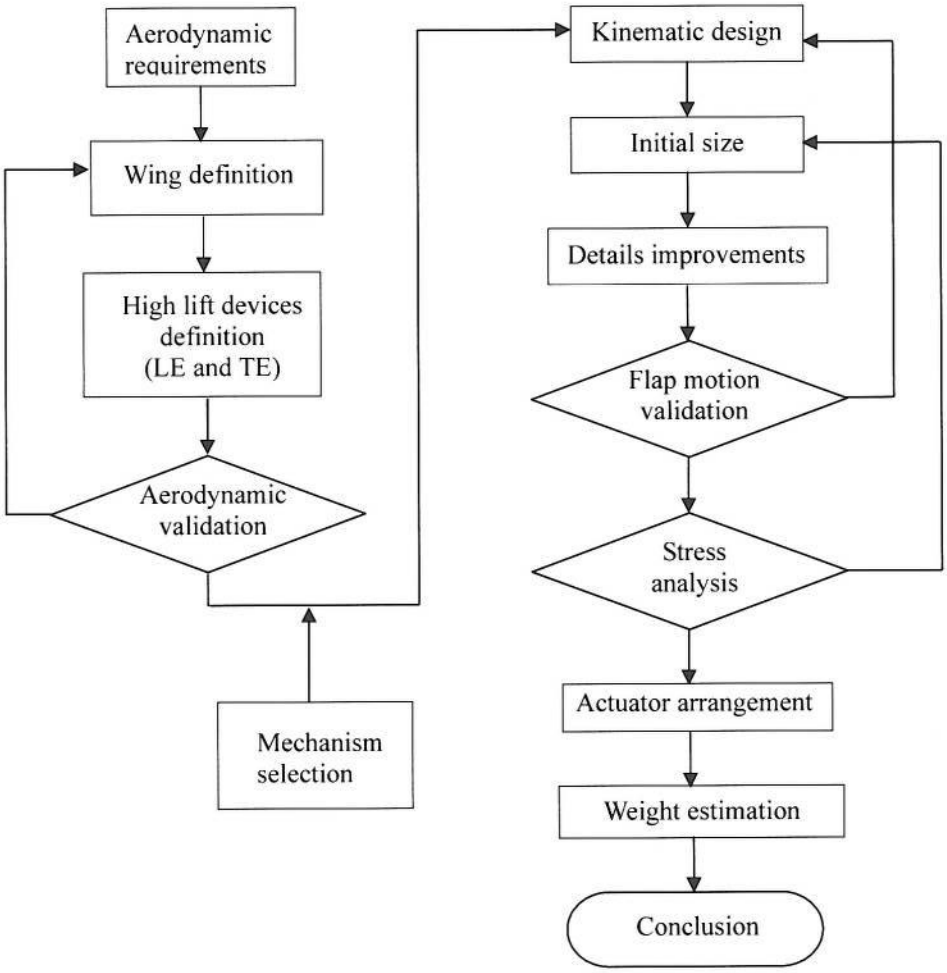

Figure 1.4 Flow chart of design procedure

1.5 Thesis structure

The first paragraph of this thesis presented general knowledge about trailing edge high lift devices and research background of swing arm mechanism for trailing edge flaps. The objective and method of this research which was aimed and chosen by the author is also introduced briefly in this paragraph. The second paragraph reviewed existing trailing edge flap devices in terms of structure and mechanism characteristics. Then the author described design procedure of the new mechanism in details in the third paragraph. The fourth paragraph compared mass characteristics between the new design and conventional mechanisms. And the last paragraph drew a conclusion about potential of the new mechanism.

The four appendices from A to D are group design project report, lift coefficient calculation, flap motion validation and mechanical stress analysis respectively.

2 Literature Review

2.1 Basics of high lift devices

For the design of high lift devices, the main objectives and constraints are shown below:

- High lift requirements
- Trim considerations
- Drag considerations
- Mass
- Cost, complexity and maintenance

The main aim of using high lift devices is to provide aircraft with adequate field performance during take-off and landing phases. The most important factor in take-off phase is climb rate, and in landing phase it is landing speed. And this speed is dominated by wing load (W/S) and maximum lift coefficient (C_{LMAX}).

2.1.1 Take-off requirements

For civil aircraft, take-off field length is defined as the total rolling distance on ground to lift off plus the airborne distance to over fly a 35-foot obstacle.

In second segment climb, which means one engine failed:

$\tan \gamma \geqslant 0.03$ (4 engines)

$\tan \gamma \geqslant 0.023$ (2 engines) where γ is climb gradient

The climb rate (R/C) can be gotten basing on the thrust-to-weight ratio (T/W) and lift-drag ratio (L/D) given through following equation:

$R/C=[T/W-(L/D)^{-1}]\times V$ where V is the aircraft speed

2.1.2 Landing requirements

Stalling speed can be reduced by increasing C_{LMAX} through the method of high lift devices. Stalling speed is given by the following equation:

$$Vs = \sqrt{\frac{2W}{S \times \rho \times C_{LMAX}}}$$

Where W is weight of aircraft

S is wing area

ρ is air density

C_{LMAX} is maximum lift coefficient of aerofoil

There are 3 basic means to increase lift via the use of high lift devices:

- To vary wing camber
- To increase effective wing area
- Boundary layer control

Trailing edge flaps can not only increase wing camber but also increase wing effective area. In terms of the change of wing's lift curve due to high lift devices, trailing edge flaps make the curve move to up-left direction without change on slope of the curve. It means that the maximum lift is increased, but the stalling angle is reduced. This problem is resolved with the adoption of leading edge devices, which increase both stall angle and maximum lift. The flaps increasing wing area can produce more lift and less drag than that only change the camber.

As improvement of trailing edge flaps' aerodynamic effectiveness, its mechanical complexity also rises. And this rise may induce worse reliability and rising manufacture and maintenance cost. Figure2.1 presents comparison between different trailing edge flaps. The high-lift capability is not the only constraint of high lift device design, whilst its mass and mechanical complexity is also important aspects which should be considered carefully. And the final design is compromise of all these constraints.

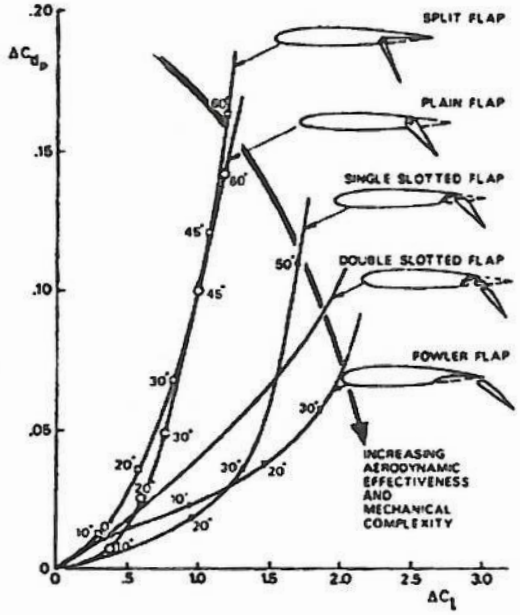

Figure 2.1 Trends in performance of trailing edge flaps [1]

2.2 Conventional trailing edge high lift devices

2.2.1 Plain flap

Plain flap (Figure2.2) is a simple hinged part of the wing trailing edge which is pivoted in a chord line. This allows the trailing edge to be deployed by downward rotation inducing an increment of the local wing camber and lift. The flap deployment is limited to an angle around 20° because of the fact that the flow separates on the upper surface at higher angle. Hence, this kind of flap can only provide limited lift increment. Plain flap is also a mechanically simple device. But it's not used on any modern airliner because of the deployment angle limitation.

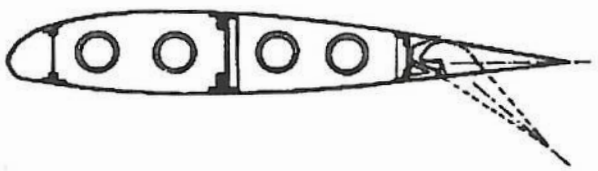

Figure 2.2 Plain flap [1]

2.2.2 Split flap

Split flap (Figure2.3) consists of a simple stiffened plate which is hinged in the wing lower surface. It deflects downwards and effectively varies the local camber of the wing section. The flow always separates when this device is deployed. This device is structurally and mechanically simple and with low weight. This type of flap produces a slightly greater increase in lift than plain flap but generates more drag. Thus it is not applied on any modern commercial aircraft.

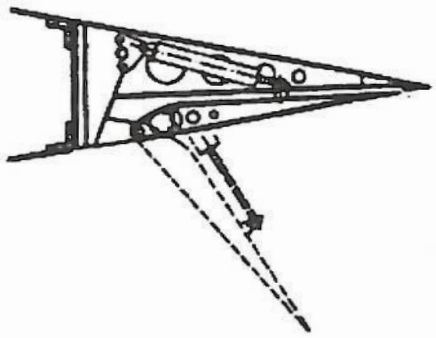

Figure 2.3 Split flap [1]

2.2.3 Simple slotted flap

Simple slotted flap (Figure2.4) is similar to plain flap and the major difference is that it introduces a gap between the main wing section and the flap's leading edge when the device is in deployed position. This gap allows high-pressure air to flow in the upper surface from the lower surface, re-energizing and stabilizing the boundary layer. It delays the flow separation problem and causes much greater increase in lift than previous devices. The performance of this device is sensitive to the shape of slot and requires a very careful aerodynamic design for the leading edge of flap. The introduction of the gap also increases the mechanical complexity.

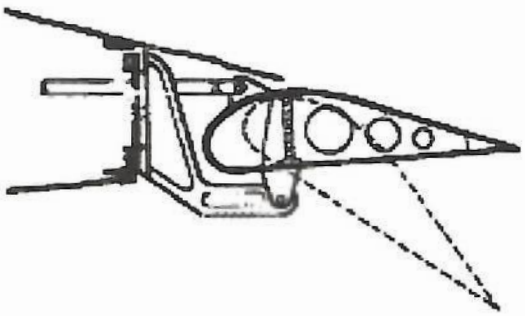

Figure 2.4 Simple Slotted Flap [1]

2.2.4 Single slotted Fowler flap

Fowler flap (Figure2.5) is similar to simple slotted flap. The slot between flap and main wing section improves the flap's efficiency. The difference comes from that this device travels rearward at the same time when it is rotated downwards. This displacement generates an increase in wing camber as well as a significant increase in effective wing area. It has a very good efficiency because it yields a large increase in lift for very little changes in drag. That is why it is so popular in transport aircraft and it is used in many airliners on the wing trailing edge or only on the outboard wing. Fowler flap can be attached by a track carriage assembly, or by means of simple hinges below the wing. Meanwhile, these attachments also lead to penalty of weight and mechanical complexity increase.

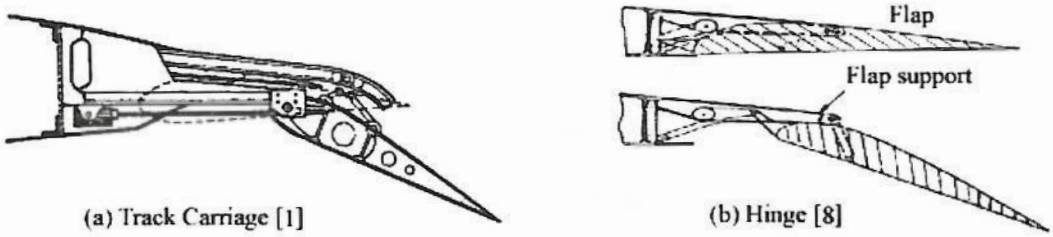

(a) Track Carriage [1]

(b) Hinge [8]

Figure 2.5 Single Slotted Fowler Flap [1][8]

2.2.5 Double slotted flap

To take more advantages of the Fowler flap good qualities, double-slotted and even triple-slotted flaps are applied in some airliners. The utilization of more than one slot makes the re-energizing of the airflow over the wing upper surface much more effective and allows even larger flap deflection angles. However, the introduction of one or more slots means that devices will be more complex and heavier. And in some cases this penalty is too fatal to ignore and leads to results that more slotted flaps are not adopted finally. Moreover, big size of fairing is also problem of more slotted flaps.

Three ways of using double slotted flap are listed below:

- Fixed vane/main double-slotted flap (Figure2.6)
- Articulating vane/main double-slotted flap (Figure2.7)
- Main/aft double-slotted flap (Figure2.8)

The first way faces a problem that it may cause high profile drag during take-off phase

because of its fixed slot. The second and third lighten the drag issue with expense of mass and complexity rise.

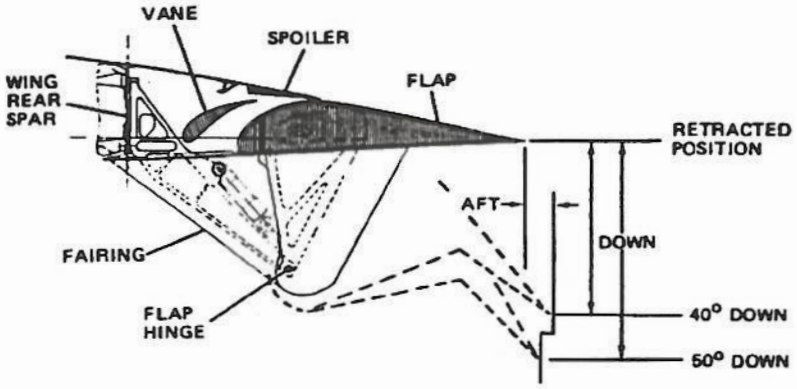

Figure 2.6 **Fixed Vane/Main Double-Slotted Flap [8]**

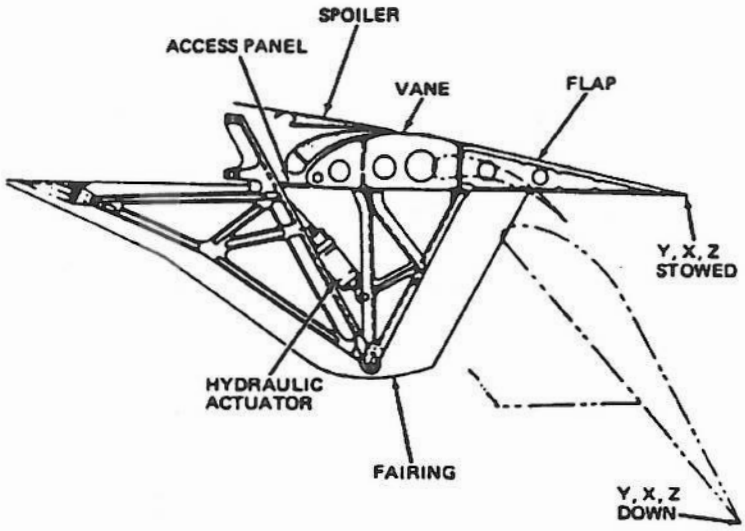

Figure 2.7 **Articulating Vane/Main Double-Slotted Flap [8]**

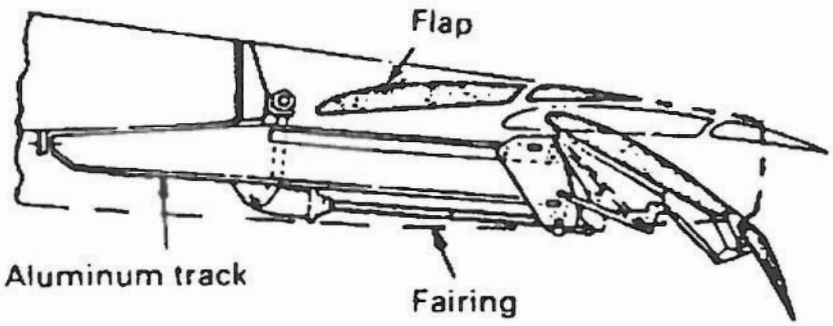

Figure 2.8 **Main/Aft Double-Slotted Flap [8]**

2.2.6 *Triple slotted flap*

Triple slotted flap (Figure2.9) is a combination of articulating vane/main and main/aft double-slotted flaps. Aircraft which have high wing loads usually uses this kind of flaps. It provides the highest sectional lift compared with other types of flaps. However, the high edge losses due to tip vortex at each flap panel edge and the higher nose-down pitching moment associated reduce its benefits of high lift capability. With another moving part being introduced, the mechanical complexity is increased even more. And in some cases the penalties associated with the complexity have outweighed the aerodynamic gains. It also requires complicated flap supports and controls which make it a heavy mechanism.

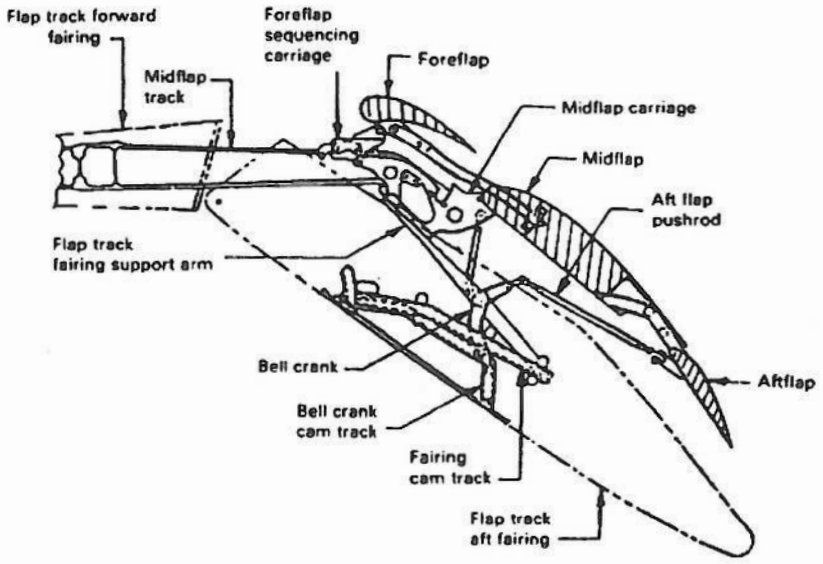

Figure 2.9 Triple-Slotted Flap [8]

Table2.1 demonstrates comparison between different trailing edge flaps described above. This comparison is not quantitative but qualitative and just tries to give a general idea about how the penalties such as drag, mass and complexity increase as the advance of high lift capability. From this table it could be seen that single slotted flap could achieve a significant lift increment without too much drag and mass drawback. That is the reason that single slotted flap is adopted as trailing edge high lift device by many commercial airliners, i.e. A320, A330/340, and Boeing 767/777's outboard flaps.

		lift	Fowler motion	drag	fairing size	mass	complexity
plain flap		low	none	low	none	light	low
split flap		low	none	medium	none	light	low
simple slotted flap		medium	little	medium	small	light	medium
single slotted flap		medium	medium	medium	small	medium	medium
double slotted flap	Fixed vane/main	medium	medium	high	large	medium	medium
	Articulating vane/main	medium	medium	medium	large	medium	high
	Main/aft	high	much	medium	medium	heavy	high
triple slotted flap		high	much	high	large	heavy	high

Table 2.1 Qualitative comparison of different trailing edge flaps

Table2.2 presents the approximate lift contributions for different types of high lift devices.

devices	Max. increment in lift coefficient	
	2D potential	Typical 3D dimension value
Basic aerofoil –subsonic	1.6	1.5
Basic aerofoil –sharp nose	1.0	0.95
Plain trailing edge flap: 20% chord	0.8	0.55
40% chord	1.1	0.75
Split flap (no gap) t/c=0.15, 20% chord	0.9	0.6
40% chord	1.4	0.95
Single-slotted flap: 20% chord	1.2	0.8
40% chord	1.8	1.2
Double-slotted flap: 40%(+26%) chord	2.5	1.65
Triple-slotted flap: 40% chord overall	2.9	1.9
Fowler flaps: 20% chord	1.2	0.8
40% chord	1.8	1.2
Fowler plus split flap: 40% chord	2.2	1.45
Plain leading edge flap: 15% chord	0.5	0.4
Vented slat: 18% chord	1.0	0.85
Kruger flap: 20% chord	0.8	0.65
Vented Kruger flap: 20% chord	1.0	0.85

Table 2.2 Lift contributions for different types of HLD [7]

2.3 Mechanism types of trailing edge high lift devices

Selection of mechanism is a trade-off between flap performance, cruise drag, weight and complexity. Table2.3 presents a list of mechanical applications in current dominant civil transport aircraft.

manufacture	prototype	mechanism
Boeing	707	internal track
	727	external hooked track
	737	external hooked track
	747	external hooked track
	747SP	four-bar linkage
	757	external hooked track
	767	complex four-bar linkage
	777	simple four-bar linkage
McDonnell Douglas	DC-8	internal four-bar linkage
	DC-9	external hinge
	DC-10	external hinge
	MD-80	external hinge
	MD-81	external hinge
	MD-11	external hinge
Airbus	A300	external straight track
	A310	external hooked track
	A320	link/track mechanism 1
	A321	link/track mechanism 1
	A330	link/track mechanism 2
	A340	link/track mechanism 2

Table 2.1 Applications of trailing edge flap mechanisms [8]

2.3.1 Simple hinge

Simple hinge mechanisms (Figure2.10) have superiority on terms of simplicity and light weight. Fairing for these mechanisms is prone to get fairly deep. Sometimes they yield additional frontal areas because of motion not aligned with flight and this will increase drag. [8]

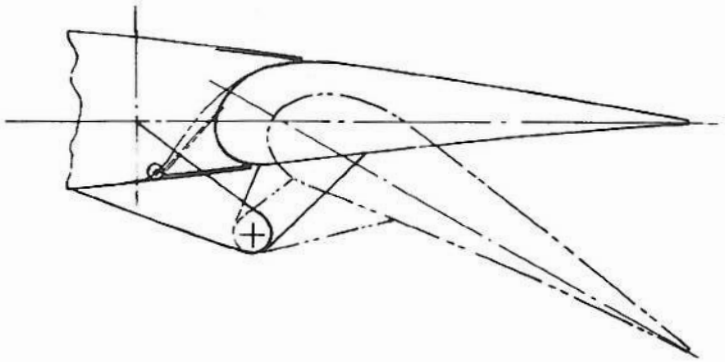

Figure 2.10 Simple Hinge Application [8]

2.3.2 Linkage systems

Four-bar linkage mechanisms (Figure2.11 to Figure2.13) provide a significant rearward movement of slotted before the main rotation occurs. However, because the motion is normal to the hinge line, fairing will be difficult to arrange when high wing sweeps are combined with large flap displacement. Fairing sizes for these kinds of mechanisms vary and greatly depend on the linkage systems' complexity. They could be shallow on complex 4-bar linkages, but rather bulky on upside-down/upright 4-bar linkages. [8] Four-bar linkage systems are usually complicated because a series of bars and joints are needed to realize required flap motion track. Another potential problem of these mechanisms is that they are prone to jam under high aerodynamic load due to structure strain.

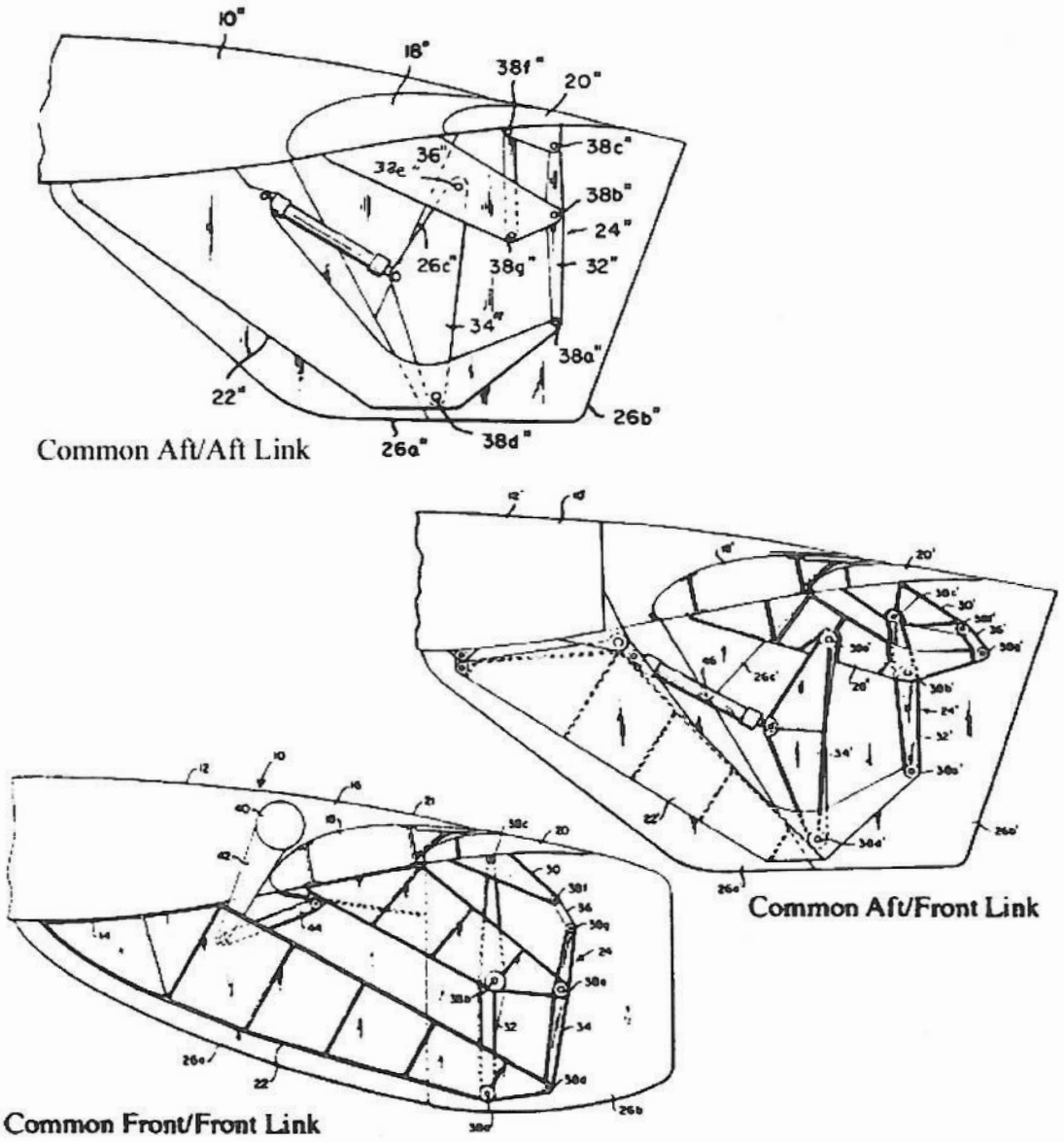

Figure 2.11 Upright, Four-bar Linkages [8]

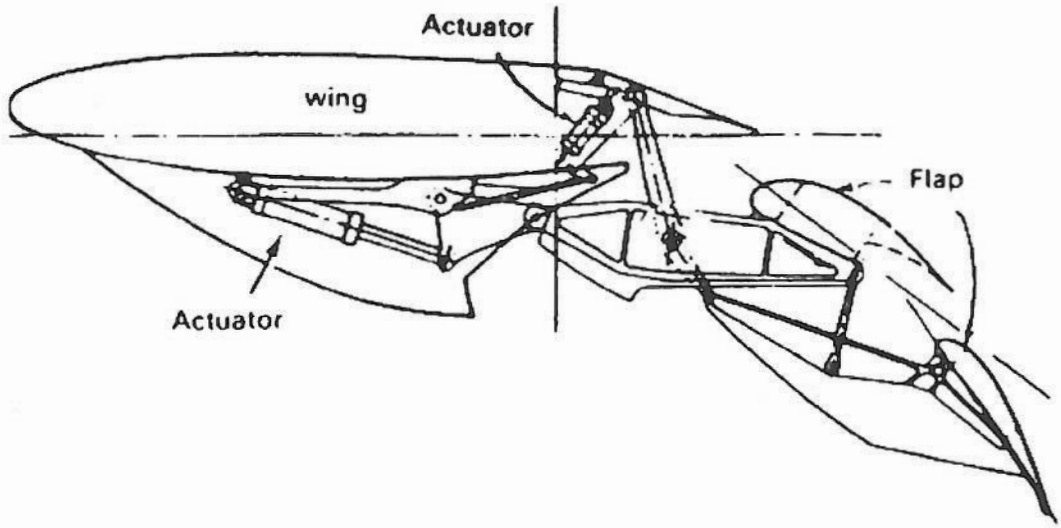

Figure 2.12 Upside-down, Four-bar Linkages [8]

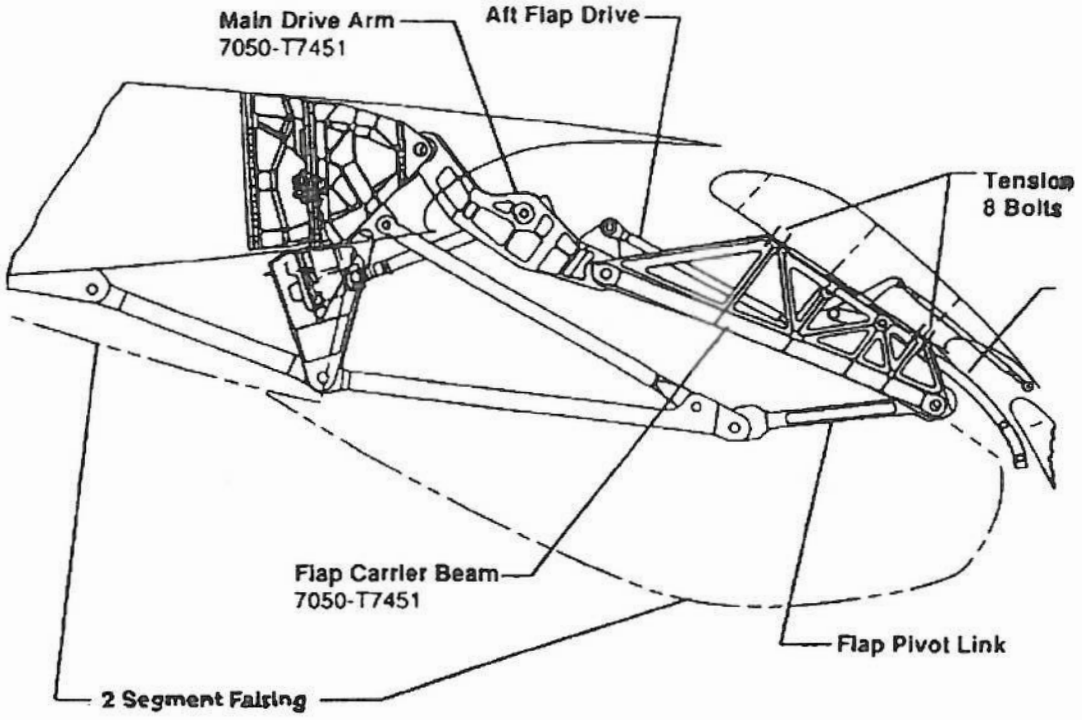

Figure 2.13 Upside-down/Upright, Four-bar Linkages [8]

2.3.3 Track systems

The flap deployment of track systems (Figure2.14) is controlled by tracks which are shaped for the required flap movement. When it is applied to high swept wings, the

track will be subjected to considerably side loads which make them fairly heavy and bulky to carry the side loads in bending if aligned with the flight. Fairing for these types of mechanisms are medium sized. [8] Track systems have better stiffness and usually are simpler than four-bar linkage systems. The drawback is heavier weight and wearing problem.

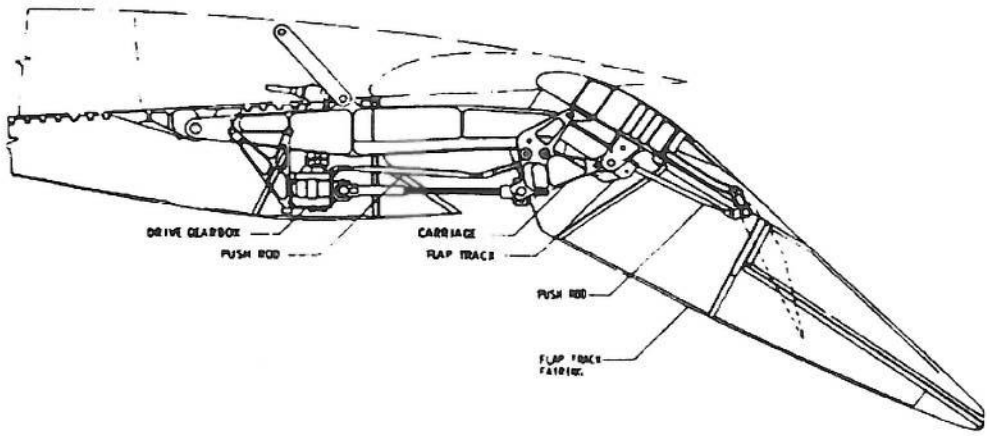

Figure 2.14 Hooked-track Supports [8]

2.3.4 Link/track mechanisms

Link/track mechanisms (Figure2.15 and Figure 2.16) consist of a straight track fixed on wing structure and a link arrangement. These types of mechanisms provide a better Fowler motion progression and shallower support fairings than those for linkages systems.

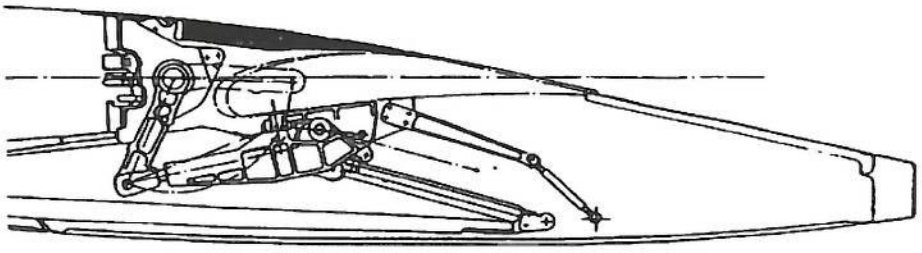

Figure 2.15 Link/Track Mechanisms on Airbus A320 [8]

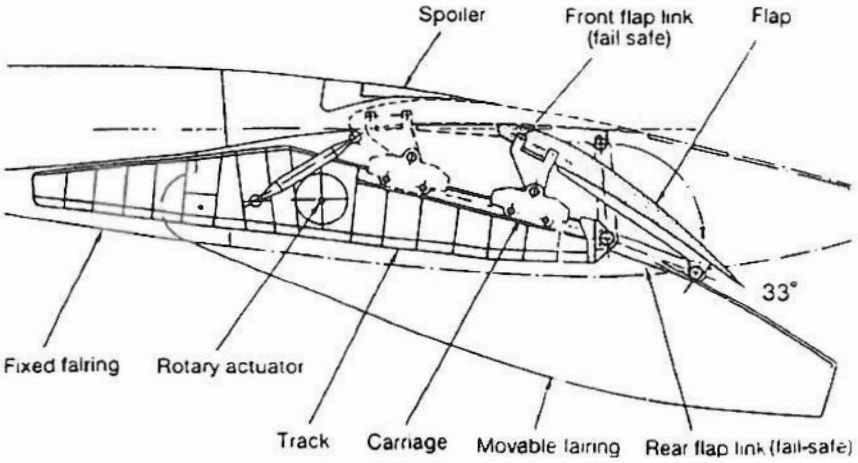

Figure 2.16 Link/Track Mechanisms on Airbus A330/A340 [8]

These several mechanism types have their own advantages and disadvantages. The simple hinge mechanisms were only applied on some earlier airliners due to its low lift capability and high drag. Four-bar linkage systems and track systems provide more efficient means for trailing edge flaps. On the other hand, both weight and complexity of the mechanisms ascend and this may weaken the benefit coming from aerodynamic performance. Link/track systems combine some advantages of both four-bar linkage systems and hooked track systems, i.e. relatively simple mechanism and better flap Fowler motion. But general speaking, it is still heavy mechanism. That is why the author try to develop a new mean of mechanism design for airliner's trailing edge flaps, which are supposed to have high efficiency, whilst be light and simple mechanism.

2.4 Application of swing arm mechanism on high lift devices

The application of swing arm mechanism on high lift devices is not a totally new idea. Leading edge and trailing edge high lift devices basing on swing arm principle were invented by F. H. Page [9] and H. Wagner [10] respectively, in 1921 and 1941. However, both of their design just stayed at conceptual stage and neither were applied to any real type aircraft. In 2005, Craig Broadbent disclosed his patent about deployment system for a moveable leading edge wing surface. This system also bases on swing arm mechanism concept and mitigates some disadvantages of previous systems.

2.4.1 Craig Broadbent's Swing Arm mechanism [3]

Figure2.17 presents the planform of a wing with three leading edge slats associated with Craig Broadbent's swing arm mechanisms. The port wing shown in below drawing consists of an inner slat (22a), a middle slat (22b) and an outer slat (22c). All these slats are attached to the wing leading edge (10) by means of swing arm assemblies (24 and 26). (24) is the first type of swing arm assembly which is located towards the inner end of the slat, and (26) is the second type located towards the center and outer end. (18) and (20) presents the engine and its pylon respectively.

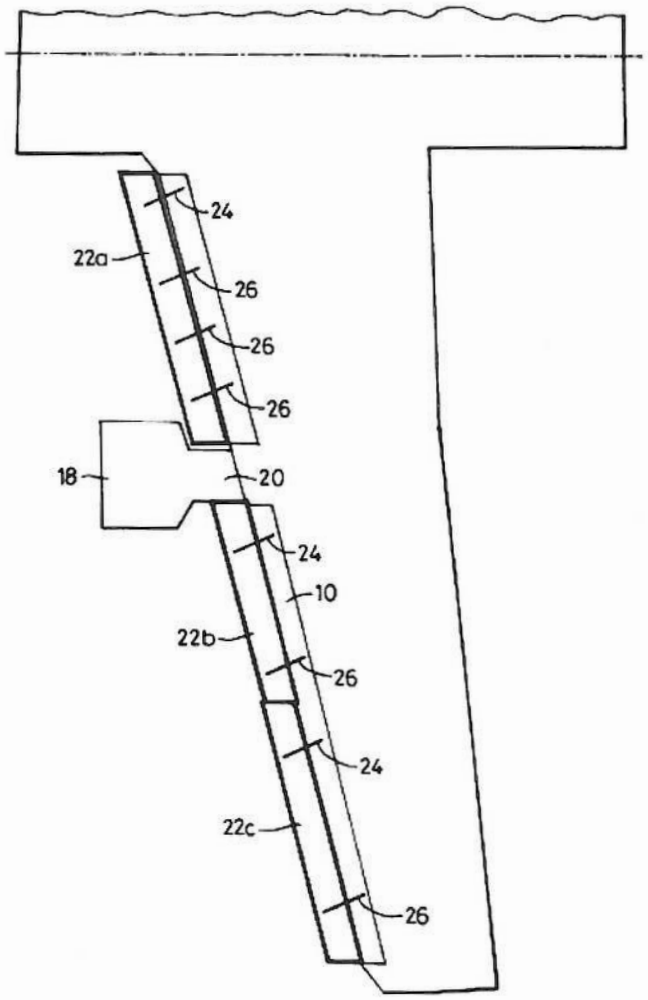

Figure 2.17 Planform of Craig Broadbent's Swing Arm Slat Mechanism [3]

The first swing arm assembly (Figure2.18) consists of a first swing arm (30) which is attached at one end by means of a first pivot joint (32) to a structural member (33)

within the leading edge envelope of the main wing section. The other end of the swing arm is attached to the slat (22) via a second pivot joint (34) and an orthogonal third pivot joint (36). The pivot axis of (32) is inclined forwards so that the slat will be translated forwards and downwards relative to the wing leading edge when it is deployed. The pivot axis of (34) extends substantially parallel to the longitudinal axis of the slat, and the slat can rotate or tilt about this axis between retracted and deployed positions. A control arm (38) is attached to the slat end of the swing arm by means of the third pivot joint (36), and to the slat by means of a fourth pivot joint (40). The control arm controls the angle of the slat relative to the main wing section. The axes of (32) and (36) are inclined relative to on another. So slat is tilted forwards whilst it is translated during the deploying process. A drive mechanism drives the swing arm rotating about axis (32).

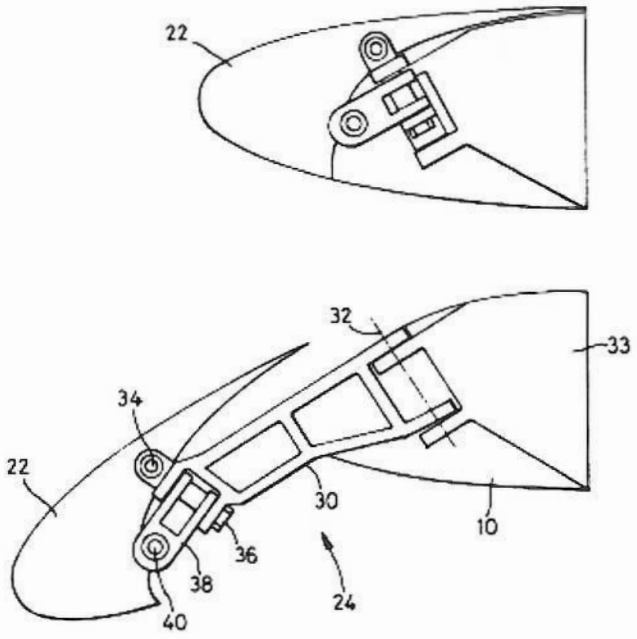

Figure 2.18 First Swing Arm Assembly [3]

The second swing arm assembly (Figure2.19) is mechanically similar to the first swing arm assembly. The difference is that the pivot joints (50) extending substantially parallel to the longitudinal axis of the slat includes a sliding joint mechanism that permits axial movement between the slat and the swing arm. This type of lost motion mechanism compensates for thermal expansion or contraction of the moveable wing surface without transmitting stresses to the main wing section and prevents jamming of the deployment

system. The sliding joint is mechanically simple and reliable.

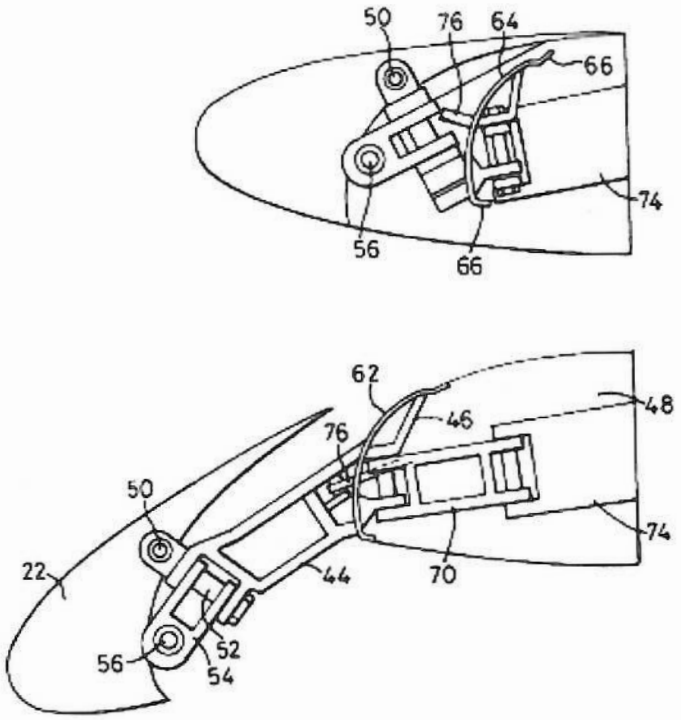

Figure 2.19 Second Swing Arm Assembly [3]

The advantages of Broadbent's system comparing with previous swing arm designs are listed below:

- Both the first and the second swing arm are driven. It provides close control over the slat movement and minimizes size of the gap between the slat and main wing section when slat is detracted.
- The first and the second swing arm are arranged to swing through an angle from 90 degrees to 120 degrees. The increment of rotating angle makes it possible to reduce swing arms' weight and length.

The sliding movement between the second swing arm and the slat in its longitudinal direction provided by the lost motion mechanism prevents jamming and stress concentration in this device.

2.4.2 Baxter's Achievements [4]

A previous MSc student of Cranfield University, Thomas Edward Baxter, worked out the kinematic model of Broadbent's 'swing arm mechanism' concept by CATIA and

provided this mechanism does work in thinker wing sections. The conclusions were also drawn that this kind of mechanism will have advantages than traditional high lift devices mechanisms in terms of weight and volume. However, some drawbacks were also discovered via Baxter's research. The main problem is the sideways translation. The spanwise incontinuity of slat may lead to aerodynamic efficiency loss. Another drawback is the clash problem between swing arm and low surface of the wing when this mechanism is applied in very thin wing sections.

2.4.3 Review Summary

Conclusions drawn from literature reviews of this chapter are listed below:

- Leading edge and trailing edge high lift devices are very important for modern commercial airliners. It allows their airfoils have both high efficiency in cruise phase and sufficient lift in low-speed conditions. High lift devices should be designed very carefully basing on multi-aspect consideration, such as aerodynamic performance, mass, complexity, reliability, maintainability and cost.
- Slot between flap leading edge and main wing section can enlarge increment of lift due to the deployment of trailing edge flap. However, the devices' complexity also rises as the increase of the slot number. And this may cause too much penalty which trade-off the improvement of aerodynamic performance. Statistical speaking, single slotted flap could achieve a significant lift increment as well as keeping relatively simple and light mechanism.
- For modern commercial airliners, the general means of mechanical arrangement are to utilize four-bar linkage systems or track systems or mix systems of the previous two. They can fulfil the design requirements of high lift devices and are applied in practice comprehensively. But designers never give up attempt to seek better compromise between the devices' performance and other aspects, like their weight and complexity.

Mr. Broadbent put the 'swing arm mechanism' concept forward. Mr. Baxter validated the new mechanism's feasibility and proved that it has a good possibility of showing competition to existing mechanisms, in the case of a commercial airliner's leading edge slats. This also pointed out a direction for the application of swing arm mechanism to an airliner's trailing edge flaps, which is this research study supposed to do.

3 Mechanism Design

3.1 Wing planform parameters

The airfoil was determined in conceptual design phase of Flying Crane aircraft. For consideration of appropriate lift and drag properties, NASA SC(2)-0612 airfoil was chosen as the baseline airfoil [2]. Detailed wing parameters and estimation of clean airfoil lift coefficient are presented in appendix B.

According to the method based on procedures derived in Engineering Sciences Data Unit (ESDU) (reference [12] to [16]), the maximum lift coefficient of Flying Crane's basic clean wing is 1.5. And the field performance requires this aircraft to achieve maximum lift coefficient about 3.0 at landing phase. So the lift coefficient increment about 1.5 is supposed to be provided by deployment of leading edge slats and trailing edge flaps.

3.2 Flap airfoil design

Flap type was defined as single slotted Fowler flap and flaps' chord takes 30 percent proportion in local wing chord in initial design. It is supposed to deploy 25° and 45° in take-off and landing position respectively. [2] High lift capability of this flap type and proportion is validated through the calculations presented in appendix B. In spanwise, flaps on each side of wing are divided into two parts, inboard flap and outboard flap, by the single crank on wing's trailing edge. In planform, inboard flap is square and outboard is tapered.

The shape of wing's trailing edge is formed by upper and lower surface of trailing edge flaps. Thus, the airfoil of flap could be drafted in CATIA sketch according to the trailing edge of NASA SC(2)-0612 section. Other constraints for the flap airfoil are its 30 percent proportion in local wing chord and its leading edge shape should be smooth. Coordinates of Flying Crane's flap airfoil at kink section are presented in TableB.3 of Appendix B. Data at other sections could be obtained by scaling values in TableB.3 with ratio of local wing chord.

As conclusion of Appendix B, the increment due to deployment of the single slotted Fowler flaps is 1.202 and 0.867 when they are landing and take-off position respectively. By cooperation of trailing edge and leading edge high-lift devices, Flying Crane's wing could achieve the design lift coefficient.

3.3 Principle of swing arm flap mechanism

T. E. Baxter developed a set of deploying mechanism basing on swing arm concept [4]. It consists of two swing arms, one control arm and one slide block on slat fitting. Lengths of the two swing arms are different due to the taper ratio of the wing. And both of the two swing arms are driven at a same time in order to control panel motion close. Figure3.1 demonstrates this mechanism in fully deployed position briefly. The two green racks (1) are fixed on structure of main wing section, and two swing arms (2 and 3) are pivoted at a rotation axis on two racks respectively. At another end of the swing arm, a control arm (4) is pivoted at a rotation axis on swing arm. Control arm's rotation axis leans forwards relative to swing arm's axis. Therefore, when swing-arm swings from stowed position to deployed position, certain mount of deflection also occurs on slat (6). The shorter swing arm (3) and its control arm are connected to slat through a sliding joint (5) which is used to compensate the extra travel due to different swing arm length.

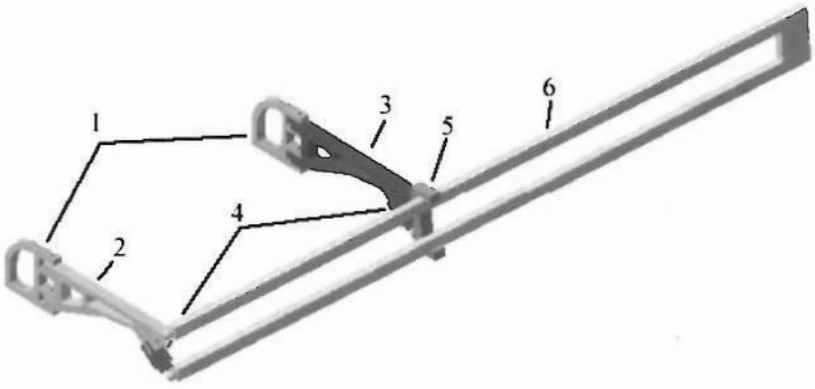

Figure 3.1 Baxter's swing arm mechanism

One major disadvantage of Baxter's mechanism is that a considerable spanwise displacement occurs on slat panel when it is deployed and retracted. This will incur loss of percentage taken by slat on spanwise direction of wing's leading edge, and leads to

reduction of slats' aerodynamic efficiency consequently. This issue will be more serious in trailing edge than in leading edge because that the trailing edge flaps have bigger chordwise movement than leading edge slats.

To mitigate this spanwise displacement mentioned above, a pair of levers is introduced. It is pivoted on a hinge which is fixed on wing rear spar, and it is attached to a point on flap panel through a spherical joint at the other end. Those two levers are pivoted to each other via a spanwise axis. Thus, that point on flap can only move in a plan which is parallel to the symmetrical plan of the aircraft. The spanwise displacement occurring on panel in previous design is mitigated greatly now because of the new constraint on spanwise. In fact, only a little spanwise displacement remains due to the different amount of Fowler motion at the inboard and outboard end of the flap.

Since a new spanwise constraint was introduced, the original mechanism becomes over-constrained. To resolve this problem, an extra lost motion mechanism was introduced which allows a degree of spanwise movement between the outboard swing arm and structure of main wing section.

Meanwhile, the control arm on inboard swing arm in original design is cancelled so that the flap deflection is provided only by outboard control arm now. This makes the sliding joint at the flap end of inboard swing arm more simple and alleviates potential jam problem.

Another difference between the swing arm mechanism on trailing edge and leading edge is that the swing arms are longer for the former one. The reason is that trailing edge flaps take more percentage of local wing chord than leading edge slats.

Thus, kinematic model of the developed mechanism has 2 sliding joints, 3 pivoted joints, 3 spherical joints and a spanwise-constraint lever pair. Figure3.2 presents this model in retracted position, take-off position and landing position separately.

The inboard swing arm is pivoted on a fixed rack, while the outboard one is pivoted on a rack which can slide along a spanwise-direction track. At the flap end of inboard swing arm, a spherical joint connects the arm to a lost motion mechanism which allows relative spanwise motion between the spherical joint and flap panel. This mechanism is just similar to the one used in Baxter's mechanism. In case of outboard side, the swing arm is linked to flap through two spherical joints and a control arm which is structurally similar to Baxter's mechanism.

Figure 3.2 Swing arm mechanism on trailing edge flap device

At retracted position, inboard and outboard swing arm are both approximately parallel to wing's rear spar. When those two arms swing rearward, the flap panel is pushed backwards as well as being deflected downwards due to the rotation of the control arm relative to outside swing arm. And when the flap is deployed, there is only very little displacement yielded on spanwise because of the lever pair which connects to middle section of the flap and constrains its spanwise movement. The motion trail of outboard flap is conical due to the panel is tapered, while that of inboard flap is columned, because flap is not tapered any more in the inboard section.

Details about flap end of the outboard swing arm and the control arm are shown in Figure3.3. The control arm is pivoted at a lug on swing arm and its rotation axis (C-D) leans forwards with respect to swing arm's rotation axis (E-F). When the mechanism is in retracted position, the swing arm is approximately parallel to wing's rear spar, and the leaning angle of control arm's rotation axis only contributes a little to the angle between the line connecting centers of two spherical joints (A-B) and horizontal plan. As the mechanism is deployed, the swing arm swings backwards around axis E-F, and angle between C-D and E-F contributes more and more to angle between A-B and horizontal plan because the flap panel is constrained on spanwise by the lever pair. In another words, line A-B was 'twisted' downwards during the deployment process. This also leads to the deflection of the flap because flap panel is connected to those two spherical joints.

According to description above, theoretically, this new mechanism could provide desired motion for trailing edge flaps, which means backwards movement and downwards deflection occur on flap panel at same time. Meanwhile, only very slight spanwise displacement will be yielded on flap panel when it is deployed.

One remarkable specification of this mechanism is that it utilizes spanwise space effectively to stow sliding tracks and swing arms when the flap is retracted. Hence, this mechanism needs less space on chordwise to arrange its components than traditional four-bar linkage and track mechanisms.

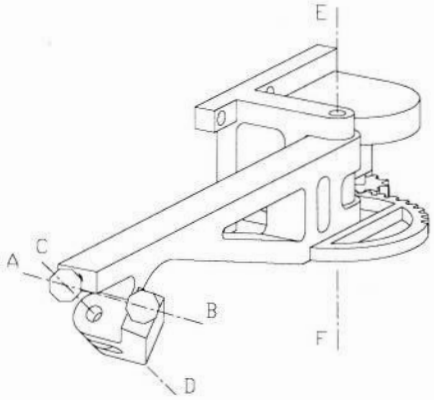

Retracted position

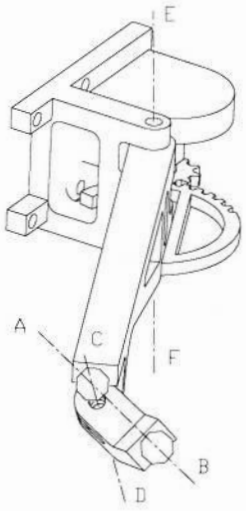

Take-off position

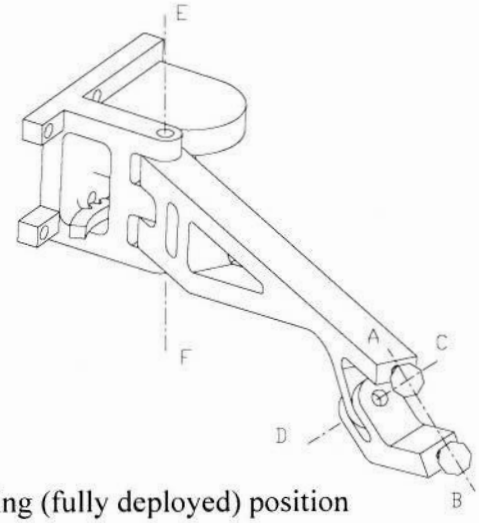

Landing (fully deployed) position

Figure 3.3 Control Arm Details

3.4 Initial sizes of components

3.4.1 Spanwise location

The first thing should be determined is the spanwise location of swing arms. There are two swing arms for each inboard and outboard flap. As the initial design, two arms for each flap are located at its inboard and outboard end respectively. Figure3.4 is planform of the port wing with the trailing edge flaps at deployed position and demonstrates their four swing arms' location from Station1 to Station4. Reason for such arrangement is that it will incur less aerodynamic penalty to cut out part of the flap panel to provide space for the spherical joints and swing arm when it is retracted at end section.

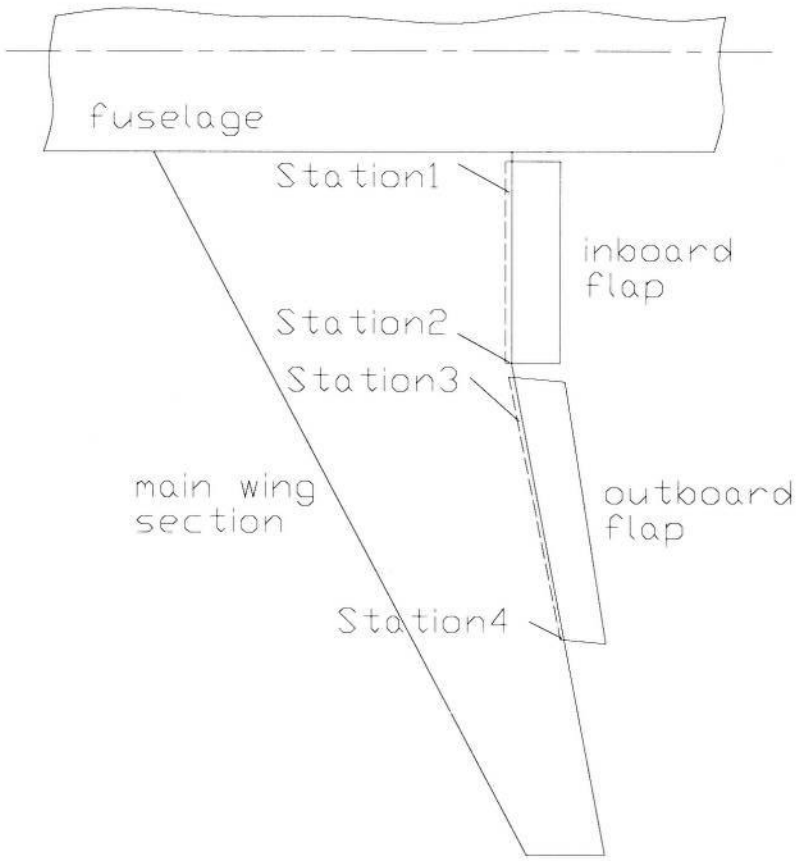

Figure 3.4 Spanwise locations for swing arms

3.4.2 Swing angle

At retracted position, four swing arms are all on the way of flaps hinge lines, which are approximately parallel to rear spar of the wing. This transfers stowed space for swing arms mostly to wing spanwise, and thus, the mechanism only needs small space to stow itself comparing with traditional flap mechanisms. And at fully deployed position, swing arms are supposed to be parallel to airflow direction so that desirable backward displacement could be achieved by relatively shorter arms.

In the case of Flying Crane aircraft, the sweepback of wing's rear spar approximately equals 65 degree. Hence, swing angle of swing arms for outboard flap is 65 degree from retracted position to fully deployed position. At the inboard section, wing's trailing edge is turned to perpendicular to airflow direction for purpose of accommodating landing gears. Hence, swing angle of swing arms for inboard flap is 90 degree from retracted position to fully deployed position.

3.4.3 Swing arm length

Flaps' Fowler motion is yielded totally by swing of swing-arms. Hence, length of flap swing-arms could be retrieved basing on their swing angle and flaps' Fowler motion. A NASA contract report (Reference [18]) pointed out that the ratio of flap Fowler motion to local wing chord is 17.4% at 35 degree flap deflection angle basing on statistic data about 12 existing trailing edge flap mechanisms for airliner. Considering to the fact that flap angle is 45 degree for Flying Crane in landing phase [2], the maximum flap Fowler motion is defined as 20% of local wing chord initially. At retracted position, hinge line of flap passes through two ends of both inboard and outboard swing-arms. And at fully deployed position, swing-arms are approximately parallel to streamwise. Moreover, hinge line of flap superposes with flap leading edge approximately. Therefore, the length of swing arm could be regarded as equal to flap Fowler motion in local wing cross-section, which is 20 percent of local wing chord.

In the case of inboard flap, two swing arms have same length to provide columned motion for flap panel. Thus the value of wing chord is measured from the wing section where outside end of inboard flap is located, because of the turning of inboard wing

trailing edge. In case of outboard flap, outside end swing arm is shorter than inside end one because of the flap panel is tapered. Hence, outside flap panel has a conical motion trail when it is deployed.

The length of four swing arms are tabulated in Table3.1, and station1 to station4 are defined as Figure3.4.

	Station1	Station2	Station3	Station4
local wing chord (mm)	5330	3135.8	3061.1	2169.2
Fowler motion (mm)	627.2	627.2	612.2	433.8
Fowler motion / c_w	0.12	0.2	0.2	0.2
swing arm length (mm)	627.2	627.2	612.2	433.8

Table 3.1 Swing arm length

3.4.4 Vertical location of mechanisms

Two constraints should be considered when the mechanisms are arranged on vertical direction:

- The mechanisms should lie in the scope of wing rear spar on vertical direction. This could help to reduce bulk of fairing for flap mechanism which would impact flap aerodynamic performance and weight significantly.
- The hinge line of flap should be close to the leading edge of flap as more as possible. This gave a base line for the flap displacement on vertical direction when it is deployed, which would impact the size of the gap between overlap and flap panel, and makes it become simpler when further improvement is carried on.

3.4.5 Dimensions of control arm

The relationship between flap motion and dimensions of control arm, e.g. its length and lean angle of its rotation axis, is not clear before the kinematic model is worked out. So data coming from Baxter's mechanism [4] was used as the initial dimensions for the control arm. Figure3.5 illustrates details of this component.

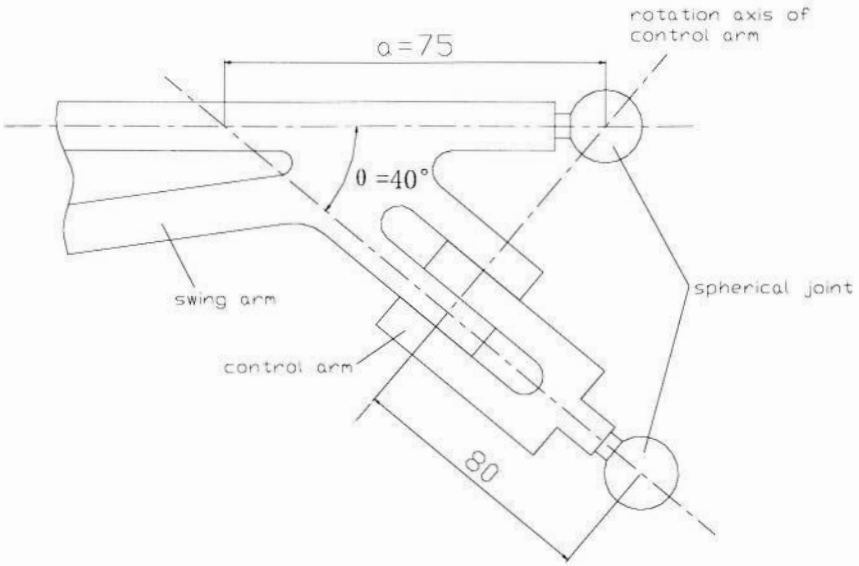

Figure 3.5 Details about control arm

According to description in paragraph 3.3 and 3.4, an initial kinematic model could be built up as shown in Figure3.6 (only outboard flap).

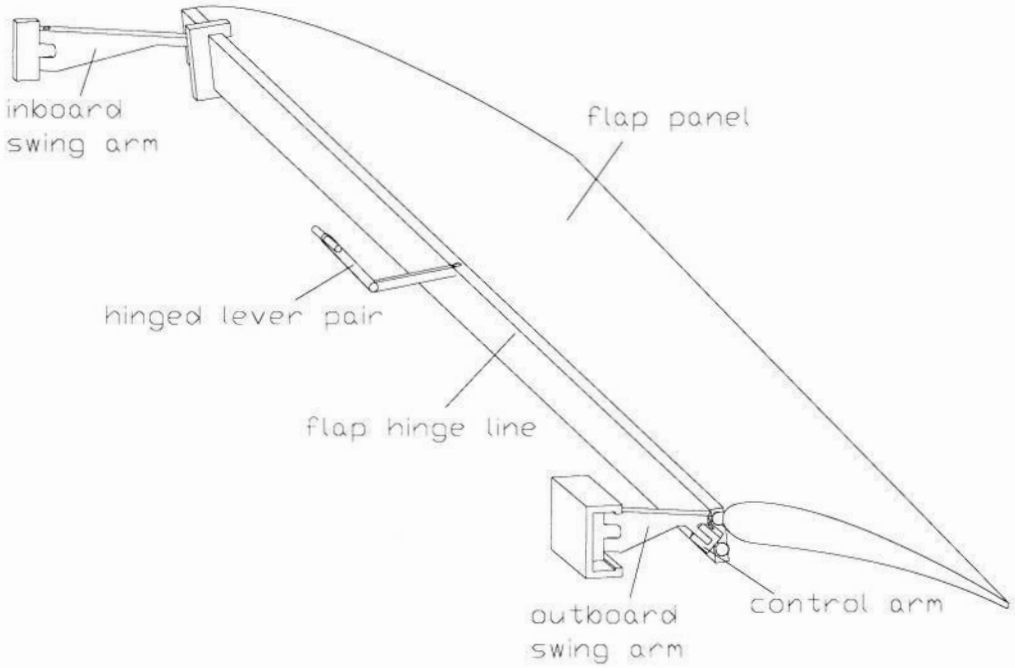

Figure 3.6 Initial kinematic model

After the kinematic model was built up, motion trail of the flap panel could be retrieved. However, one major problem is that the deflection of flap was too low to meet design

requirement. This could be improved in next design stage by means of adjusting dimensions of control arm.

3.5 Improvement procedure and final design

3.5.1 Modification about control arm

The first problem should be resolved is the insufficient deflection of flap in initial kinematic model. It was found that flap deflection is relevant to two parameters close: a and θ as presented in Figure3.7. Table3.2 lists change of flap deflection (δ) with adjustment of these two parameters.

Step	a (mm)	θ (degree)	δ (degree)
1	75	40	18. 466
2	5	40	36. 917
3	5	50	46. 11

Table 3.2 Change of flap deflection

As a disadvantageous result of the modification mentioned above, the lug which the control arm is pivoted on becomes too short because its turning is too close to flap end of the swing arm, and there is no plenty place to accommodate the control arm. Thus, the control arm was made cranked to fix this problem, which is shown in Figure3.7. The pivot point of control arm moves downward along its rotation axis and another end attached to spherical joint is tilted upwards. In this way, the control arm gets enough space to be installed whilst guarantees sufficient flap deflection.

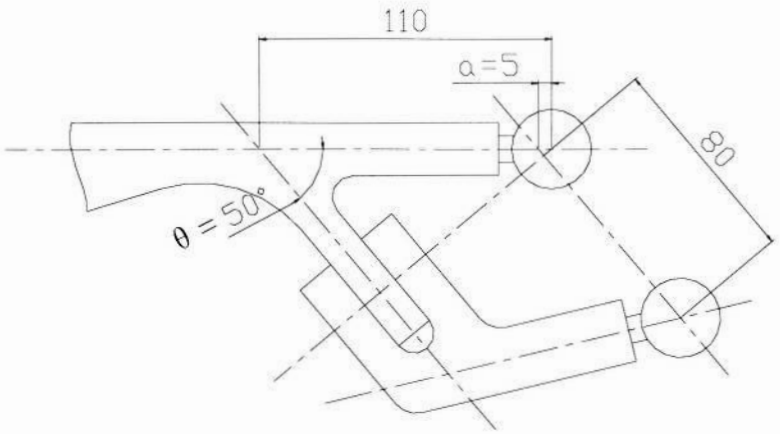

Figure 3.7Cranked control arm

3.5.2 Modification about spanwise constraint

In the design of new mechanism, the spanwise motion of flap panel is constrained by a lever pair assembly which is hinged on wing rear spar. The flap panel and lever pair connects each other through a spherical joint, and spanwise force on the spherical joint is yielded by actuation of the electric motor mainly and component force of aerodynamic loading due to wing's dihedral angle. The lever pair consists of two simple thin levers pivoted to each other which are shown in Figure3.8. This kind of cantilever structure is not very good to bear loading. Quite large deformation will occur on flap end of the lever pair when loading acts on it. This might incur undesirable vibration on flap panel. To avoid this situation, the lever pair should be reinforced.

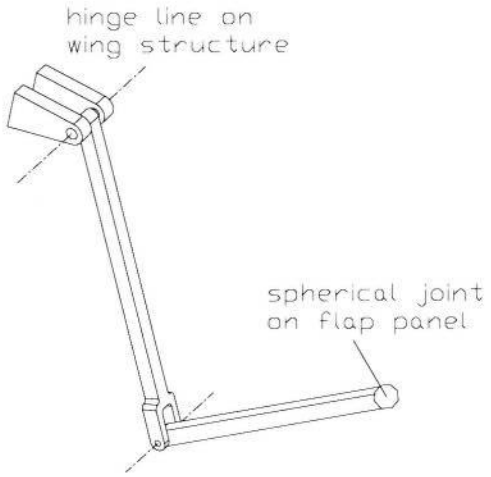

Figure 3.8 Reinforcement of lever pair

Two reinforced designs are demonstrated in Figure3.9. The hinge numbers of both levers are all increased. Meanwhile, spanwise cross-section area and moment of inertia of the two levers also rose greatly. Thus, the lever pair could bear more loading with less stress and deformation. In design A, the first and second levers are linked by a pivot gemel, and the second lever is connected to flap panel through a spherical joint. While in design B, the spherical joint is arranged between two levers, and the second lever is connected to flap panel through pivoted means. The bending moment on pivot of the first lever on wing structure in design B is much smaller than that in design A because that the spherical joint will not carry moment on any direction. However, in design B, the hinge line of second lever on flap panel is not always parallel to the hinge line of

flap. Hence when flap is deployed, the centers of spherical joints on two levers will not superpose to each other. This means the mechanism would be jammed probably. According to this reason, design A was chosen as reinforcement of the lever pair. Detailed stress analysis about lever pair was presented in Appendix D.

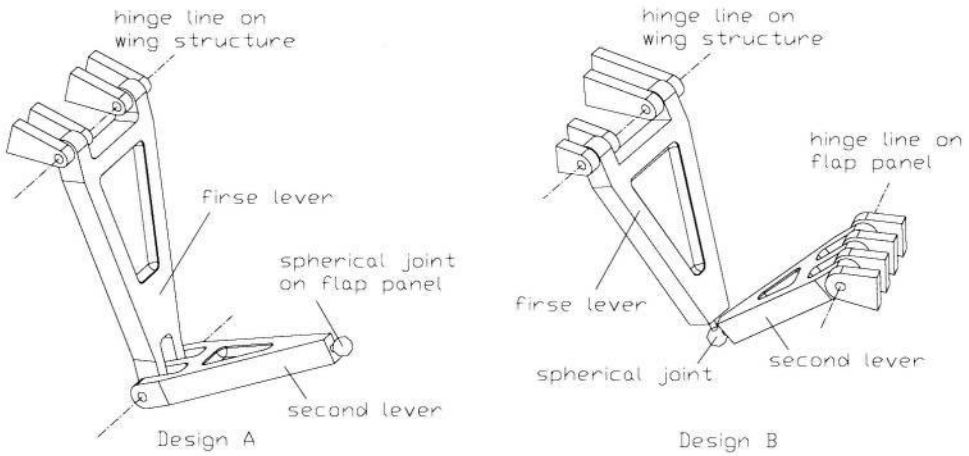

Figure 3.9 Reinforced designs of lever pair

3.5.3 Modification about swing arm length

When the mechanism is deployed from its retracted position, a certain extent of outward spanwise displacement still occurs on the trailing edge of outboard flap panel in spite of the spanwise-constraint lever pair, and this displacement will cause some clash issue in initial model. This is due to the different Fowler motion between inboard and outboard end of flap panel and derivative rotation around a vertical axis through the spherical joint point between lever pair and flap panel. Therefore, the length difference between outboard flap's inside and outside end swing-arms should be minished to alleviate this spanwise displacement. Through adjustment and simulation on kinematic model, length of inside and outside end swing-arm was modified to 518mm and 450mm respectively, and the spanwise displacement is reduced in an acceptable scope which means no clash happens between flap panel and adjacent wing structure.

This modification will also influence flap's Fowler motion. As measured result, the Fowler motion in inside end section dropped to 17% of local wing chord from initial 20%. Figure3.10 presents the different flap planform before and after this modification.

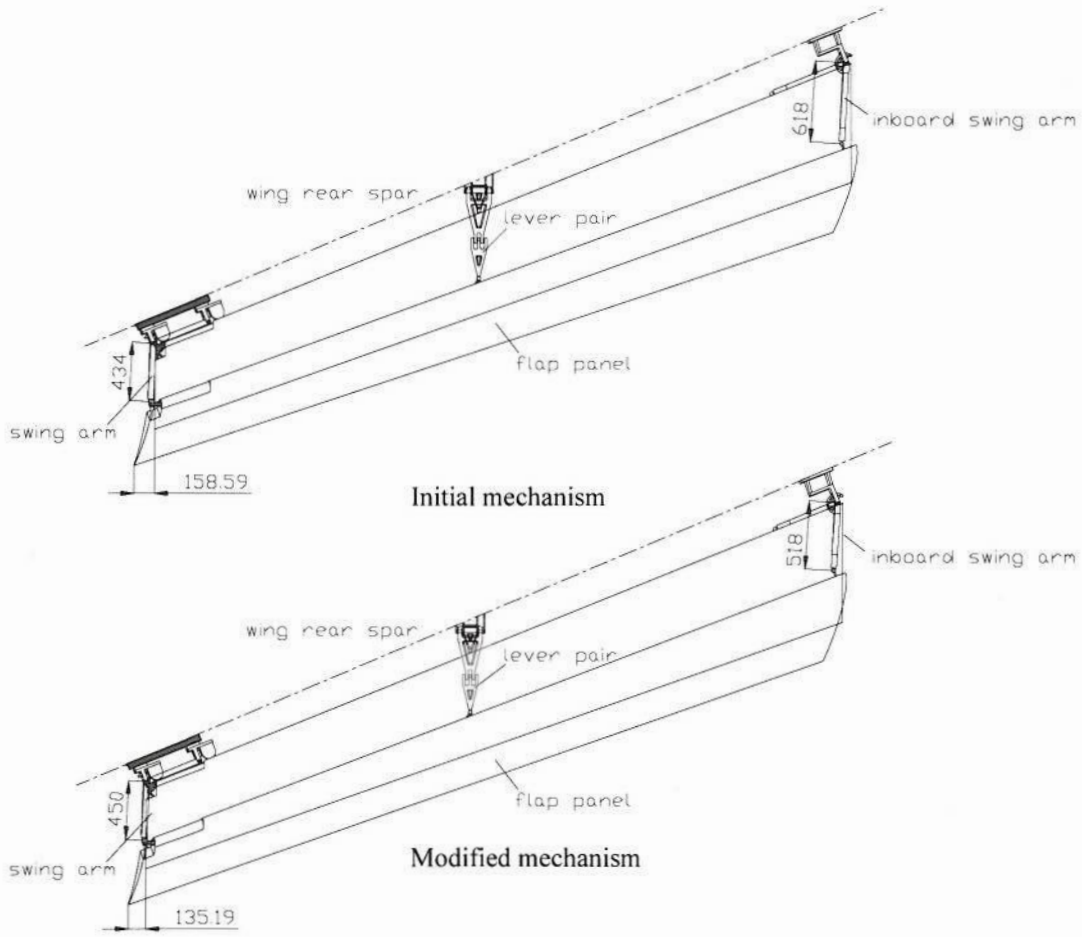

Figure 3.10 Modification about outboard flap's swing-arm length

3.5.4 Modification about vertical location

The vertical location of mechanism will affect the gap size between leading edge of flap and trailing edge of main wing section when flap panel is deployed. This gap size is recommended to be around 0.02c in reference [19] as plotted in Figure3.11. In this figure, flap deflection angle is constant at fully deployed position. This proportion between flap gap and local chord is an approximate recommending value and flaps are supposed to achieve best efficiency around this figure. Hence, 0.02 was applied in the Flying Crane case directly in spite of slight difference in terms of flight conditions.

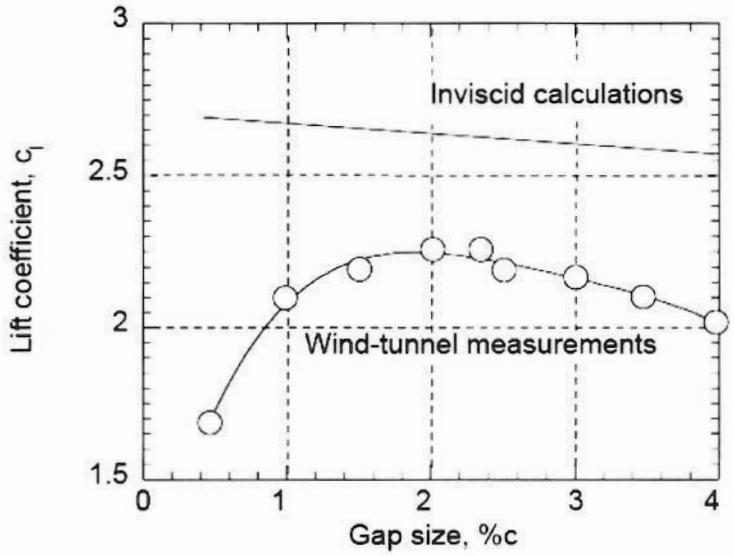

Figure 3.11 Effect of flap gap on lift coefficient of a two-element airfoil at α =0° , Re=3.7 million, M∞=0.2 [19]

The initial mechanisms were arranged to keep flap hinge line, which connects spherical joints on inside and outside end swing arms, superposing on flap trailing edge. However, the result of this arrangement about the gap size is not ideal. Gap of inboard flap is too wide, while the one of outboard is too narrow. Hence, the mechanisms need to be moved vertically to adjust the gap size. Value and direction of the movement is determined by measuring data coming from kinematic model, and the results are tabulated in Table3.3.

	gap size / Cw			
	Station1	Station2	Station3	Station4
Initial position	0.024	0.036	0.012	0.018
Mechanism moves 30mm upwards	0.022	0.032	0.012	0.012
Mechanism moves 30mm downwards	0.028	0.043	0.016	0.027

Table 3.3 Relationship between gap size and mechanism vertical location

3.5.5 Final design and validation

The final arrangement of swing-arm mechanisms for inboard and outboard trailing edge flaps is shown in Figure3.12 (only port wing). More detailed figures about flap motion trail are presented in Appendix C. It could be seen that most part of the mechanism is in

the scope of wing rear spar and utilizes stowed space very efficiently in retracted position. Fairings are used only for the two lever pairs which will stretch out low surface of airfoil when flaps are stowed. Figure3.13 presents the wing cross-sections where the two lever pairs locate. Table3.5 tabulates the fairing parameters of swing-arm mechanism and some other types of mechanisms (reference [18]). Apparently, fairing for swing-arm mechanism is much smaller than other current flap mechanisms both in depth and in length. Meanwhile, width of fairing for swing-arm mechanism is also quiet small because the lever pairs are simple hinged 2-bar linkages and take a little space in spanwise, which is presented in Figure3.14.

mechanism type		depth	length	fairing depth/ max. Fowler motion	fairing length/ max. Fowler motion
swing-arm linkage mechanism	inboard	154.32	673.72	0.27	1.18
	outboard	130.52	646.99	0.28	1.38
777 outbd. flap 4-bar linkage (conservative)				1.11	3.76
777 outbd. flap 4-bar linkage (aggressive)				0.95	3.6
YC-15 4-bar linkage				0.95	3.18
Short Brothers 4-bar linkage				0.85	3.99
747 SP 4-bar linkage				0.62	3.68
A330/340 link/track				0.83	4.32
A320 link/track (2 supports)				0.76	4.2
A320 link/track (end plus aux. supports)				0.55	3.26
Boeing link/track (2 supports)				0.66	3.7
Boeing link/track (end plus aux. supports)				0.53	3.06
767/777 inbd. flap linkage				0.55	3.41

Table 3.4 Fairing size comparison

The maximum swing angles of four swing-arms are all reduced to 61° because the flap deflection has already reached desirable value. At this swing angle, the flap Fowler motion to wing chord ratio of airfoil section at station2, station3 and station4 is 18.3%, 16.9% and 19.3% respectively. This value at station1 is only 10.7% because of the cranked trailing edge in inboard section. Thus, Fowler motion for inboard and outboard flap is 18.3% and 17% respectively, and these values are applied in calculations of Appendix B which proved this kind of mechanism can provide sufficient lift increment for Flying Crane aircraft in take-off and landing phase.

It could be seen from diagrams presented in Appendix C that flap deflection increases more rapidly with swing of swing-arms from retracted position (0°) to take-off position (25°) than that from take-off position to landing position (45°), while the Fowler motion curves are approximately linear. It means that Fowler motion at take-off position is relatively low and flaps could provide less lift increment than expected. This issue could be improved by rearranging swing-arms hopefully, e.g. swinging the arms from a minus angle with respect to flap hinge line. More research should be done about this in future work. However, it will not be contained in this thesis because of time constraint. Fortunately, the existing arrangement could also fulfil aerodynamic requirements in terms of flap deflection and Fowler motion, although it is not the optimum solution.

The gap between trailing edge of wing upper surface and flap panel when it is at landing position also changed due to reduction of swing angle. The final sizes of the gap are listed in Table3.4. These data are in reasonable range according to description in reference [19] and [20]. More detailed research about relationship between mechanism arrangement and gap size should be done in future work because this size will impact aerodynamic performance of flap remarkably.

	station1	station2	station3	station4
gap size (mm)	70.612	70.612	39.132	30.108
gap / cw	0.013248	0.022518	0.012784	0.013879

Table 3.5 Gap size in landing position

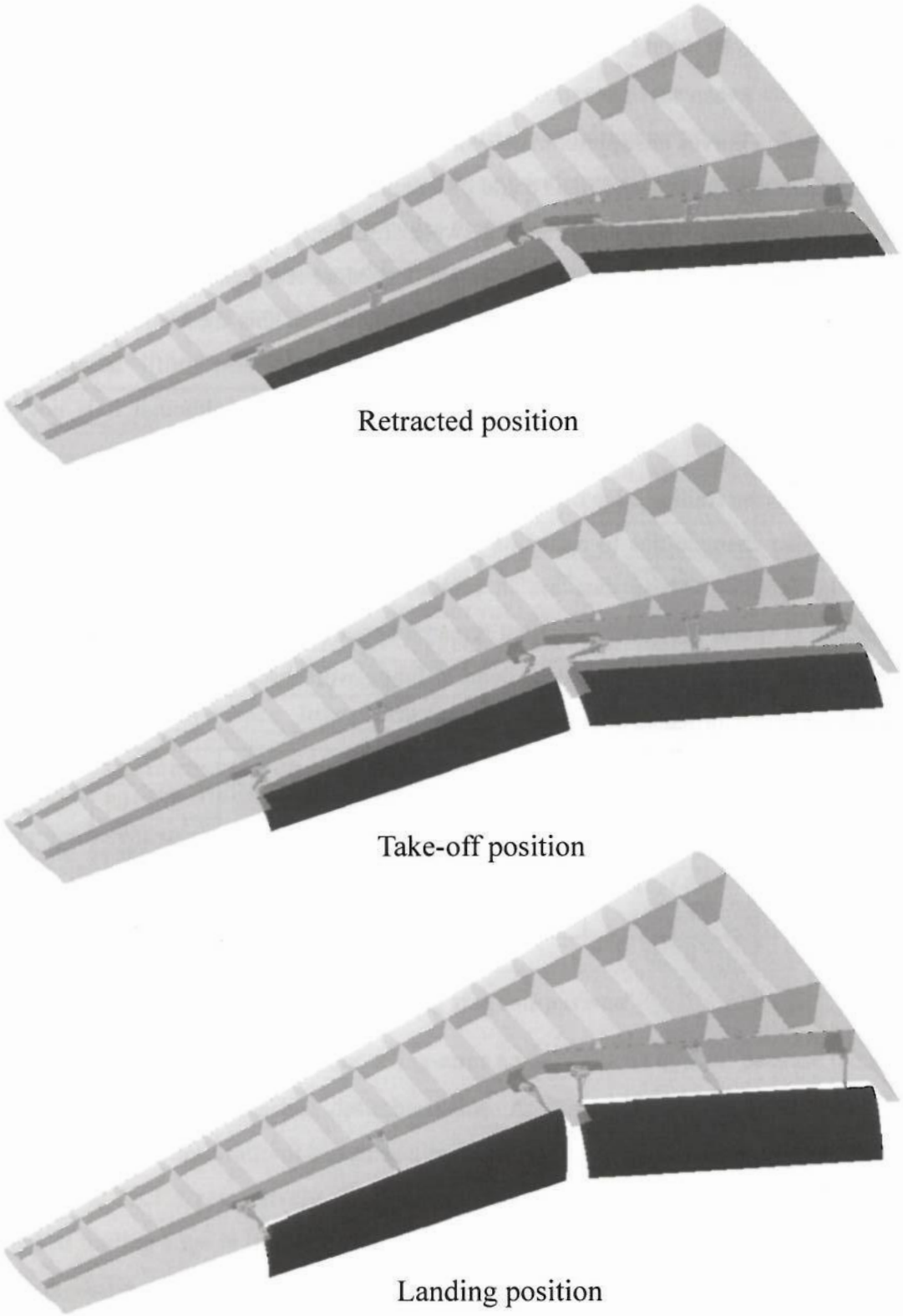

Figure 3.12 Arrangement of swing-arm mechanisms for trailing edge flaps

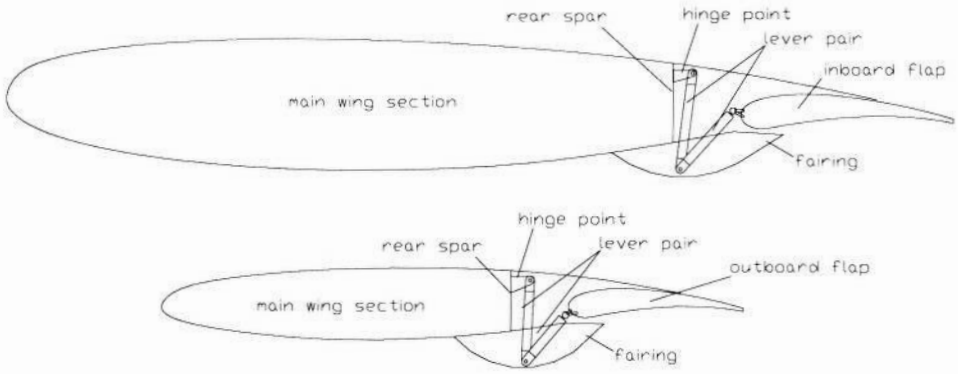

Figure 3.13 Fairings for lever pairs

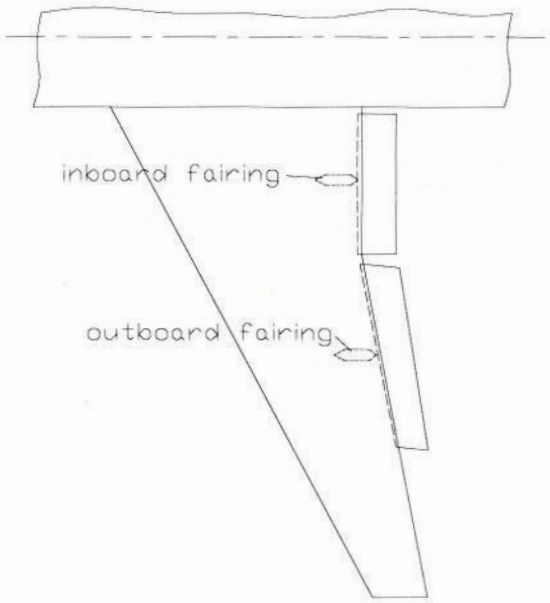

Figure 3.14 Spanwise position of fairings

3.6 Flap loading calculation

Mr. Ammoo deducted equations of aerodynamic loading on flap panels as function of airfoil sections' spanwise location for ATRA project [5]. The role and size of ATRA are similar to Flying Crane. They are both modern transport airliners and have maximum passenger capacity of 138 and 150 respectively. Therefore, these equations were adopted in the case of Flying Crane aircraft to determine aerodynamic loading on its trailing edge flaps after consultations with the supervisor. This method is not very accurate for the research of this thesis but it is the only available method which could provide flap loading conveniently for further analysis procedure.

Equations are listed below:

Take-off phase: $L = -106.97x^2 + 1265.1x + 6581.3$ (N/m)

Landing phase: $L = -63.095x^2 + 591.2x + 8055.8$ (N/m)

Cruise phase: $L = -36.063x^2 + 435.22x + 2527.2$ (N/m)

Where x is spanwise location of flap section

The curves of loading in these three phases are plotted in Figure3.15. Total loading overall flap span could be obtained by integrating loading equations. The flap loading is assumed constant over the flap span in order to avoid mathematical complexity. The values of mean load are tabulated in Table3.6. Loading on inboard flap is higher than that on outboard flap in both take-off and landing phases.

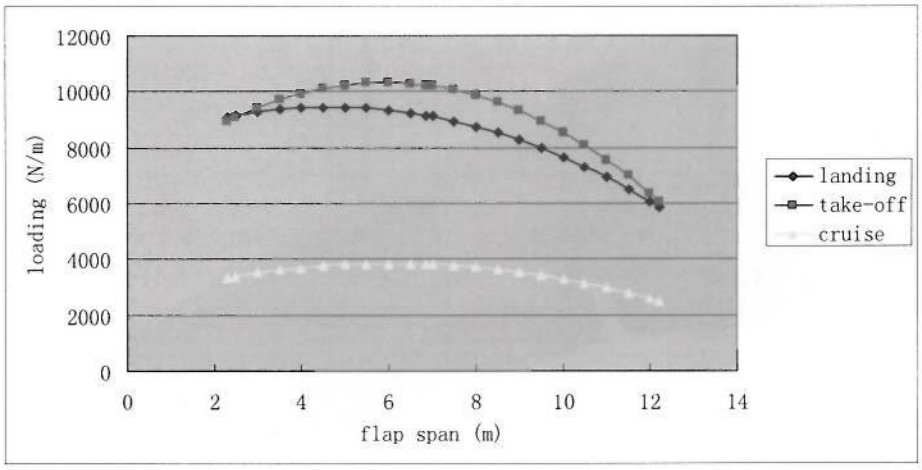

Figure 3.15 Spanwise flap loading distribution

		take-off	Landing
total loading	Inboard flap	41662.1 N	39239.8 N
	Outboard flap	46335.1 N	41753.7 N
flap span	Inboard flap	4.2 m	
	Outboard flap	5.353 m	
mean loading	Inboard flap	9919.6 N/m	9342.8 N/m
	Outboard flap	8655.9 N/m	7800.0 N/m

Table 3.6 Mean loading on flap

On chordwise, load distribution is plotted in Figure3.16. The method to determine chordwise load distribution also comes from reference [5] and is commonly used by structure engineers in aviation industry. Lines were drawn to represent the approximate Cp curve. The line above represents Cp applied on flap upper surface and the lower one represents Cp applied on flap lower surface. The loading is assumed to vary linearly

from flap trailing edge to its hinge line, which results in a trapezoidal pressure distribution.

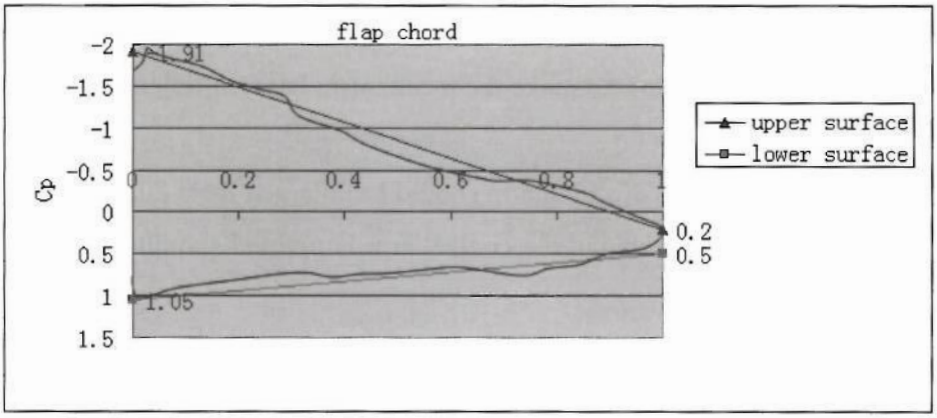

Figure 3.16 Chordwise flap loading distribution

Therefore, curve equations of pressure coefficient on upper and lower surface along flap chordwise could be retrieved and presented below:

Upper surface: $y = 2.11x - 1.91$

Lower surface: $y = -0.55x + 1.05$

Where x is flap chord proportion and y is pressure coefficient

Total pressure coefficient C_p is given by

$$C_p = y_l - y_u = (-0.55x + 1.05) - (2.11x - 1.91) = -2.66x + 2.96$$

The percentage taken by pressure center chordwise location in flap chord is given by

$$p_c / c_f = \frac{\int_0^1 (C_p x)dx}{\int_0^1 C_p dx} = \frac{\int_0^1 (-2.66x^2 + 2.96x)dx}{\int_0^1 (-2.66x + 2.96)dx} = 0.364$$

3.7 Mechanical stress analysis

According to loading calculation carried out in previous paragraph, stress on each component in the mechanism could be gotten. Material of all components (not including flap panel) are assumed to be steel initially, its mechanical properties could be found in reference [6]. Material had been considered to change into lighter material such as aluminum or titanium in order to save weight. However, the reserve factor of swing arm has low redundancy so that material changing is not available for swing arms. The control arms and lever pairs could be changed into titanium because of their high

reserve factor redundancy. Details about stress analysis are presented in Appendix D.

The calculation results illuminated that the most critical situation occurred at outside arm assembly of inboard flap in take-off position. Two dimensions of swing arm need to be modified as described below to make the mechanism have sufficient strength to carry design loading:

- The thickness of top bar of swing arm should be enlarged from 20mm to 30mm.
- The thickness of lug on which the control arm is pivoted should be enlarged from 15mm to 20mm.

The mechanisms are validated being capable to carry design loading after being modified as mentioned above. One thing should be mentioned is that reserve factors of some parts are much higher than design target which is equal to 1.5. This means that these parts were over designed and more optimization about these parts should be done in order to make the design more effective in future works.

3.8 Actuation system arrangement

3.8.1 Actuating method and actuator type

There are two methods to actuate the swing arms to swing around their pivots:

- To rotate the swing arms around their pivots directly by rotating actuation systems, which is shown in Figure3.17.
- To push or pull the swing arms to swing around their pivots by linear actuation systems, which is shown in Figure3.18.

In the second actuating method, the required actuating loading might become quite high at high deployed position due to the reduction of distance between actuator's stroke and swing arm's pivot. Moreover, the size of linear actuator might be much bigger than that demonstrated in Figure3.18, which is based on actuating loading and type of the linear actuator. Another consideration about the choice of actuating method is that the outside end actuator is supposed to move together with swing arm along spanwise on the slide track, and electric wire has more flexibility than hydraulic pipe in this case. Summing up reasons mentioned above, the first actuating method was chosen for the mechanisms. And brushless direct current motor (BDCM) was chosen as the actuator because of its outstanding power density and reliability properties [22]. A reducing gearbox was

introduced to connect motor and rack in order to match output torque and speed of the motor to actuating requirements.

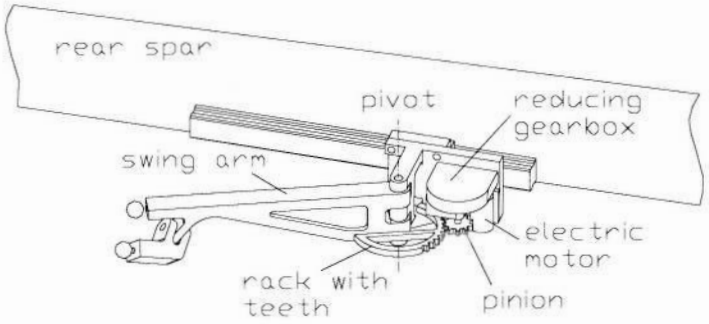

Figure 3.17 Rotating actuating method

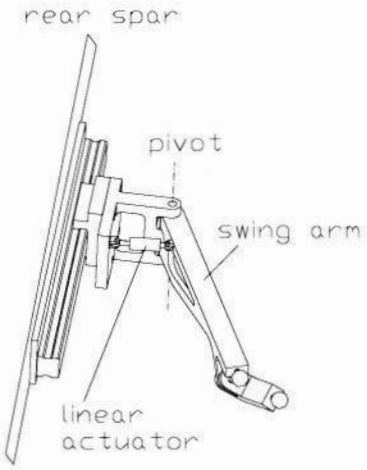

Figure 3.18 Linear actuating method

Advantages and disadvantages of the rotating actuating method are listed below.

Advantages:

1. It can control movement of swing arms with a high degree of controllability.
2. The drive system is irreversible. Thus it is unnecessary to arrange extra locking devices.
3. Only small stowed space is required to accommodate actuators and their attachment.
4. Sensors could be installed conveniently on the teeth rack, which provide an accurate indication of the swing arm position.
5. Electric motors are commanded by control circuit. Therefore synchronization could be realized by electrical means.
6. Electric wires are more flexible and light than hydraulic pipes.

Disadvantages:

1. The teeth rack requires high precision.
2. The rack and pinion needs protection from jam issue incurred by intrusion of foreign objects.
3. The rack and pinion is prone to be worn after a work period. Thus inspection and maintenance need to be done termly on this area.
4. Introduction of reducing gearbox incurs rise of mechanism mass.

3.8.2 Power calculation

Basing on analysis about forces acting on swing arms which was presented in Appendix C, the torque of swing arms around their pivots yielded by aerodynamic loading could be calculated. Calculation results are listed in Table3.7. It could be seen that maximum torque occurred on inside end swing arm of inboard flap at landing position.

	take-off	landing
P1s (N)	-125646	-62327.8
P1c (N)	43710.71	101041.7
P4c (N)	-7982.63	-23962.5
θ (deg)	23	61
L (m)	0.655	
Mi (N m)	4812.975	7609.301
Mo (N m)	5801.968	3620.261

Table 3.7 Torque on swing arm pivot

Total time that flap was deployed from retracted position to landing position is assumed to be 15 seconds according to data of other existing airliners. And the swing arms are regarded as moving at an even speed through the whole deploying process. Thus, rotating speed of swing arm is given by

$$n = \frac{\pi/3}{15} = 0.07 rad/s$$

Output power of the electric motor is given by

$$P = M \cdot n / \eta$$

Where η is the efficiency of reducer, which is assumed to be 0.9.

Thus

$$P = 7609.3 \times 0.07 / 0.9 = 590.3w$$

An approximate power density of BDCM is suggested to be 2kg/kw by reference [22].

Hence, mass of the motor is given by

$m = P \cdot \rho_p = 1.18kg$

This mass is gotten basing on the maximum torque might occur on swing arms pivot. Actually, this torque should be smaller when flap was being deployed. This means that actuators' real weight might be less than the calculating value. This difference could be regarded as a margin to compensate tolerance of the estimating method.

3.8.3 Assemble attachment and reducing gearbox

A semi circular rack with teeth on its outside surface is rigidly fixed on each swing arm, and a pinion installed on output axis of a reducing gearbox meshes these teeth. The rotation output by electric motor is transferred to the rack by the reducing gearbox. No more detail design was involved into this thesis due to time constraint. And further researches about size and reducing ratio configuration are recommended to be done in future works.

3.8.4 Synchronization

Each swing arm has their own actuator, and all the swing arms are supposed to swing at a same rate. Therefore there should be some kind of synchronous devices to make sure the correspondence of their motion. Considering to the fact that the outside actuators move along spanwise when they work while the inside actuators are fixed all the time, mechanical synchronization means are quite difficult to be realized in this mechanism. The information of flap position is send to flight control computers (FFCs) by flap position sensors, and then FFCs send command to control circuit collaborating with pilot command. The control circuit will control flap actuators basing on the command to work, or to stop to wait others. The control logic is demonstrated in Figure3.19.

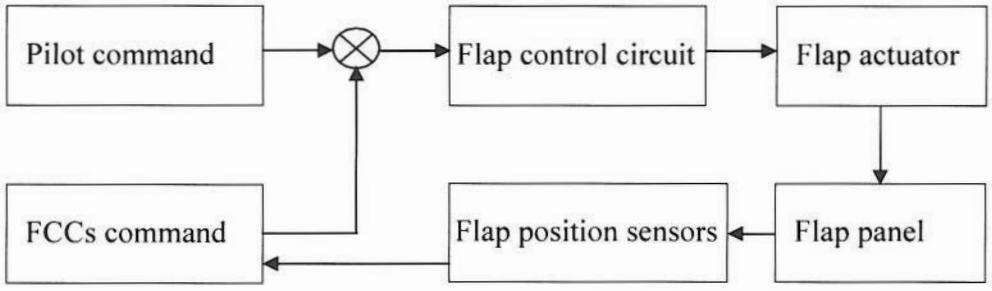

Figure 3.19 Flap control logic

3.9 Discussion

3.9.1 Spanwise location of swing arms

In the beginning of the design procedure, the spherical joints linking swing arms and control arm with flap panel are arranged at inside and outside end of the panel due to consideration about impact to aerodynamic characteristics caused by cutout on panel. However, this arrangement leads to poor stiffness of support for flap panel and large quantity of deformation might occur on middle section of the panel. This problem could be resolved through stiffer structural design for flap panel, or by rearrangement of the spanwise location of swing arms. It could improve flap panel stiffness to move swing arms from panel ends to its middle section. It is a recommendation from the author for future works to optimize swing arms' spanwise locations.

3.9.2 Application of monorail guidance systems

A four-row ball monorail guidance system was introduced into the outside swing arm assembly to provide spanwise slide motion for the support bracket. This kind of system provides advantages such as high loading ratings, small mounting space, low mass, long-term running quality, minimum maintenance and high reliability [25]. Effective methods such as upper sealing strips and end wipers provide good seal for the balls in sliding block. Figure3.20 presents sketch of the monorail guidance system.

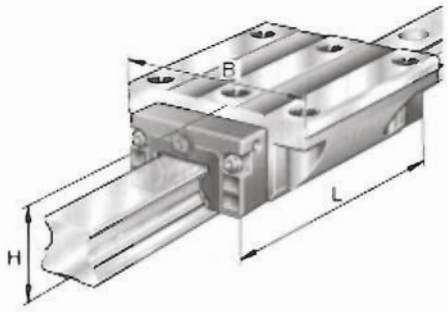

Figure 3.20 Monorail guidance system

*resource: http://medias.ina.de/

Schaeffler (UK) Ltd. is a professional company providing rolling bearing products. Detailed data about monorail guidance system produced by this company could be

found on its website (reference [25]). KEUV55-B type product was chosen according to its size and stowed space in the wing. Data about loading capability of this product are shown in Figure3.21.

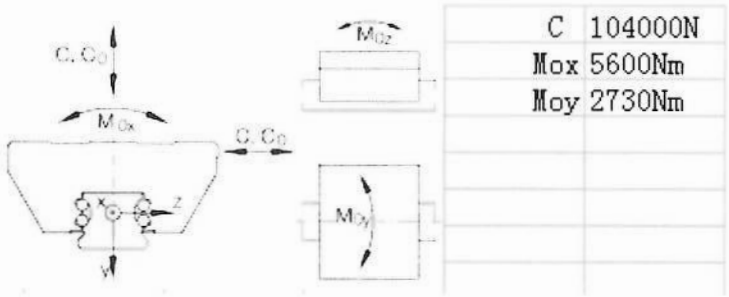

Figure 3.21 Loading capability of KEUV55-B

*resource: http://medias.ina.de/

According to the force analysis carried out in Appendix D, loading on the sliding block could be gotten. And the results are tabulated in Table3.8. It could be seen that values of loading are all smaller than the maximum allowable load ratings and moment ratings of KEUV55-B. Hence, this type of product is regarded as having the capability to carry the design loading.

Mox (Nm)	inboard	4235.2	3719
	outboard	1815.7	1551.6
Moy (Nm)	inboard	920.5	332.2
	outboard	806.9	317.6
Pv (N)	inboard	1528.1	1054.5
	outboard	1943.3	1443.1
Pc (N)	inboard	9704.6	21348.5
	outboard	4410.1	9166.8

Table 3.8 Loading and moments on sliding block

3.9.3 Details of spherical joints

Four spherical joints were used to connect each flap panel to two swing arms, one control arm and one lever pair. Detailed design about the spherical joint was not involved into this thesis due to time constraint and lack of relevant information. General speaking, the spherical joints would be prone to suffer from dirt accumulation and wearing issue. Replacement of these components could potentially be very expensive and complicated, which would lead to the rise of direct operating cost (DOC). Another

remained problem is whether the spherical joints are tough enough to bear design loading. The author suggested that more careful and deeper research about the spherical joint should be done in future works.

3.9.4 Jam issue

It is necessary to consider the possibility of jam that could happened in the mechanism. The jam might occur on the inside sliding joint or on the mesh part between driven racks and pinions of both inside and outside swing arm assemblies. Outside sliding joint can avoid jam issue effectively due to the introduction of monorail guidance system. If jam occurs on inside swing arm assembly, the flap panel can still be deflected and pushed backward at outside section by outside swing arm assembly. This could provide nearly whole flap deflection and part Fowler motion. However, if jam occurs on outside assembly, there will be not any deflection on flap panel. This may lead to insufficient lift on wing during take-off and landing phase and incur premature stall consequently. Therefore some measures should be done to prevent jam occurring on outside rack and pinion. Those measures could be termly inspection and maintenance, or to add a protective shell for outside rack and pinion.

3.9.5 Stiffness of flap panels

The flap panels are considered as rigid body in the stress analysis procedure. Actually, the panels are not absolutely rigid and will experience deformation under action of aerodynamic loading. This deformation might reduce flap deflection and efficiency, or even cause jam in mechanism. Thus, more researches about the influence of flap flexible deformation on efficiency of flap mechanisms are recommended for future works.

3.9.6 Locking and motion limiting devices

It is unnecessary to set extra locking devices because the actuating system is irreversible. Some blocks are located on the sliding rail and support brackets to stop the sliding block or swing arms physically when they move beyond their expected motion scope due to inappropriate work of actuators.

3.9.7 Maintenance

Several key parts of the maintenance are listed below:

- The spherical joints
- The inside sliding joints
- The mesh part of racks and pinions

Inspection and maintenance works should be operated on these areas termly to guarantee appropriate work of the mechanisms.

3.10 Summary of mechanism design

To apply the swing arm mechanism concept to trailing edge flap of the Flying Crane aircraft, three major modifications were carried out basing on the Baxter's design for leading edge devices:

1 A spanwise constraint lever pair was introduced and connected to a spherical joint on middle section of flap panel. This device guarantees the panel moving along airflow direction with only slight spanwise displacement caused by different Fowler motion between inside and outside sections.

2 A monorail guidance system was introduced into the outside end swing arm assembly to provide spanwise degree of freedom. This kind of guidance system has superiorities in terms of high loading ratings and high reliability.

3 Detailed dimensions of control arm were improved to compromise the confliction between flap deflection angle and install space for control arm.

According to the kinematic model and stress analysis had been done in previous steps, it was proved that the concept of swing arm mechanism does work for trailing edge flaps of thicker wing sections. Desirable flap motion trail could be achieved by deployment of the mechanisms. These new mechanisms also show significant competitive potential in terms of fairing size and actuating requirement.

However, still many problems are not solved in the new design because of time constraints, including details design about spherical joints, relatively low Fowler motion in low flap deflection, stiffness consideration about flap panel, and maintenance and cost details prediction. The author gave brief suggestions about those problems and recommended them for future works.

4 Mass Comparison

This chapter gives detailed estimation about mass of the swing arm flap mechanisms. Kinematic model of the mechanisms has been established in CATIA. So volumes and masses could be retrieved directly from the CAD software by its measure function. As a comparison, masses of traditional flap mechanisms were also estimated with the method provided by reference [21]. The estimation covers all the driving and attaching components, whereas the flap panel was not involved.

4.1 Mass estimation for conventional flap mechanisms

The empirical method for estimating mass of flap mechanism comes from a NASA contract report (reference [21]) and is based on flap's stowed area and Fowler motion. It covers three traditional trailing edge flap mechanism types: hooked track supports, link/track supports and external hinge supports. Total weight of trailing edge flap is broken down into four parts: panel weight, support weight, fairing weight and actuation weight. The objective of this thesis is only to discuss the improvement of novel swing arm mechanism for trailing edge flap, and the flap panel used in this thesis has no difference with traditional ones. Therefore, the panel weight was ignored in following calculation.

Calculating equations are listed below:

$$W_{\text{sup port}} = a_2 \cdot f_{fow} \cdot S_{TE}$$

Where f_{fow} is function of Fowler motion and is used to scale the masses of supports and fairings.

For track supports, $f_{fow} = 1$;

For external hinge and linkage supports, $f_{fow} = 0.47 + 0.53\dfrac{R_{fow}}{0.5}$

Where R_{fow} is ratio of Fowler area to area of trailing edge flap

$$R_{fow} = \frac{\Delta S_{Fowler}}{S_{TE}}$$

$$W_{fairing} = a_3 \cdot f_{fow} \cdot S_{TE}$$

$$W_{actuation} = a_4 \cdot S_{TE}$$

Data of Flying Crane flaps are tabulated in Table4.1. Factors and calculation results are tabulated in Table4.2. All the data are on one wing.

	inboard	outboard
STE (m2)	3.95	4.20
SFowler	2.41	2.50
Rfow	0.61	0.60

Table 4.1 Data of Flying Crane Flaps

		hooked track	link/track	external hinge
a1 (lb/ft2)		2.7	2.7	2.7
a2 (lb/ft2)		3	1.5	1.1
a3 (lb/ft2)		1	0.11	0.28
a4 (lb/ft2)		2.2	2	0.9
ffow	inboard	1	1.12	
	outboard		1.10	
Wsupport (kg)	inboard	57.9	32.3	23.7
	outboard	61.5	34.3	24.8
	Σ	119.4	66.6	48.5
Wfairing (kg)	inboard	19.3	2.37	5.95
	outboard	20.5	2.52	6.32
	Σ	39.8	4.88	12.3
Wactuation (kg)	inboard	42.4	38.6	17.4
	outboard	45.1	41.0	18.5
	Σ	87.6	79.6	35.8
tatol mass not including panel (kg)		246.7	151.1	96.6

Table 4.2 Mass Estimation for traditional flap mechanisms

4.2 Mass of the swing arm mechanism

Mass of the swing arm mechanism could be measured directly from its CATIA model. Material of all components are assumed to be steel ($\rho = 7.85kg/mm^3$) except that of fairings which is assumed to be aluminium ($\rho = 2.78kg/mm^3$). Actually, according to the stress analysis presented in appendix D, materials of control arm and lever pair have

been changed into aluminium alloy, and material of swing arm has been changed into titanium alloy. But in this chapter, these components were still regarded as being made by steel in order to find out weight change due to the new mechanism instead of utilization of new materials. Data on one wing are presented in Table4.3.

Item	volume (mm^3)	density (kg/mm^3)	mass (kg)	quantity
outboard track and hinges			9.35	1
outboard slide support			8.95	1
swinging arm station 4	0.910	7.85	7.15	1
control arms	0.152	7.85	1.20	2
outboard hinge arm 1	1.331	7.85	10.45	1
outboard hinge arm 2	0.616	7.85	4.84	1
swinging arm station 3	0.989	7.85	7.76	1
outboard flap slide block			0.13	1
inboard track and hinges			10.67	1
inboard slide support			8.95	1
swinging arm station 2	1.30	7.85	10.19	1
inboard hinge arm 1	1.632	7.85	12.81	1
inboard hinge arm 2	0.783	7.85	6.15	1
swinging arm station 1	1.247	7.85	9.79	1
inboard flap slide block	0.013	7.85	0.10	1
electric motor actuators			1.18	4
reducing gearboxes			5	4
outboard fairing	0.873	2.78	2.43	1
inboard fairing	0.978	2.78	2.72	1
	total mass (kg)		139.56	

Table 4.3 Mass data of swing arm flap mechanisms

4.3 Comparison result

Results coming from previous two paragraphs indicated that swing arm mechanism provides approximately 40% and 7% weight saving comparing to hooked track and link/track mechanisms respectively. Comparing to external hinge mechanism, swing arm mechanism is much heavier. One thing should be mentioned is that the estimation about mass of reducers has poor accuracy. The practical weight of them is probably higher than it has been calculated. Even though, swing arm mechanism still shows great superiority in terms of weight comparing with traditional mechanisms.

Weight data about trailing edge flaps of Boeing737-200 is given by reference [21]. Comparison has been done between Weight/S_{TE} of Boeing737-200 and Flying Crane. Result is presented in Table4.4, and the weight data are neither including weight of flap panels. It could be seen that Flying Crane has great advantage on this ratio than the other competitor. However, it should be noticed that Boeing 737-200 trailing edge flaps are triple-slotted type and Flying Crane ones are single-slotted. This difference would incur great deal of weight increase.

	Boeing737-200	Flying Crane
Weight (kg)	401.43	139.54
S_{TE} (m^2)	8.129	8.151
Weight/S_{TE}	49.38	17.12

Table 4.4 TE flap weight comparison between Boeing737-200 and Flying Crane

5 Conclusion and Future Works

5.1 Conclusion

Though the whole design and refinement procedure of the novel swing arm mechanism for trailing edge flaps, this mechanism was validated to have capability to provide desirable flap motion trail for Flying Crane concept. Stress analysis about components in this mechanism proves that it could carry design loadings. Advantages and disadvantages of this mechanism are listed below.

Advantages:

1 The fairings required by swing arm mechanisms are shallower and shorter comparing with those for traditional flap mechanisms. The ratio of swing arm mechanism fairing length and depth to flap maximum Fowler motion is 0.28 and 1.38 respectively. While these two ratios of most existing trailing edge flap mechanisms are higher than 0.5 and 3 (seen in page 41). Swing arm mechanisms have more effective flat packed characteristic at stowed position and fairings are required only to cover part of lever pairs stretching beyond wing lower surface. The reduction of fairing size and number leads to saving of weight and decline of drag on wing.

2 The power of each actuator which is used to drive swing arms is just 590w for each electric motor because only small extending force is needed (seen in page 49). This permits light and small electric motor was chosen as actuator.

3 Weight of swing arm mechanism is 40% and 7% lower than traditional track and link/track mechanisms for trailing edge flap respectively on the assumption that having same flap area (seen in page 57). Low weight could bring much superiority in terms of efficiency and cost.

Disadvantages:

1 Potential jam may occur on the rack teeth and pinion meshes, the spherical joints, and the inside end sliding joint.

2 Potential vibration and flutter may occur on the flap panel due to the mechanism

provides not stiff enough support for the panel.

As a conclusion, swing arm mechanism broke a new path for high-lift device mechanism design. It was also validated has great potential in terms of weight and volume saving. However, there are still many issues need to be researched more carefully before it can be applied to practical aircraft.

5.2 Future works

- More accurate calculation about flap aerodynamic efficiency at take-off and landing position should be done by CFD means to get reliable data about the relationship between flap deflection, Fowler motion, gap size and its aerodynamic performance.
- Rearrangement about swing-arms, for example swinging the arms from a minus angle with respect to the hinge line instead of from position being parallel to hinge line in current design, should be investigated in order to develop potential of swing arm mechanisms in terms of flap Fowler motion in low flap deflection hopefully.
- Moving attaching points between swing arms, control arm and flap panel from panel's end part to its middle section to obtain better stiffness for flap panel should be investigated in more details.
- More comprehensive and deeper research about the spherical joint should be done, including structural details, strength validation, wearing issue and potential jam may occur on this component.
- Deformation and vibration occurring on flap panel should be analyzed carefully to find out how seriously they jeopardise flap structure and performance. Only maximum static loading was considered to validate static strength of the mechanism in this thesis. Dynamic loading also needs to be considered to validate fatigue strength of the mechanism in future works.
- More accurate calculation about mass and bulk of the electric motor and reducing gearbox should be carried out. And the gearbox should be designed in more details. More works about the failure modes of the actuators also should be done to analyze redundancy of the actuating system.
- Detailed maintenance and cost estimation about the swing arm mechanism should be carried out to check whether it will be too expensive to develop, manufacture or maintain. Cost comparison between swing arm mechanism and traditional flap

mechanisms could give more solid evidence of the novel mechanism's competitive ability.

- More optimization about these parts which have too high reserve factors should be done in order to make the design more effective in future works.

6 References

[1] Egbert, Torenbeek, *"Synthesis of subsonic airplane design"*. Delft University Press, 1982.

[2] AVIC 1 Aerospace Vehicle Design Group, *"Flying Crane Specification"*. 2008.

[3] Broadbent, Michael Craig, *"DEPLOYMENT SYSTEM FOR A MOVEABLE WING SURFACE"*. United Kingdom Patent, GB 2,362,363 B, 2003.

[4] Baxter, Thomas Edward, *"Investigation into a Novel Flap and Slat Mechanism Concept"*. MSc thesis, Cranfield University, 2001.

[5] Ammoo, M. S., *"Development of a Design Methodology for Transport Aircraft Variable Camber Flaps Suitable for Cruise and Low-Speed Operations"*. PhD thesis, Cranfield University, 2001.

[6] *"STRESSING DATA SHEETS"*. AVT-AVD 9632 lecture notes. Air Vehicle Technology, Cranfield College of Aeronautics, 1999.

[7] HOWE, D., *"Aircraft conceptual design synthesis"*. Professional Engineering Publishing, London, 2000.

[8] Rudolph, P. K. C., *"High-Lift Systems on Commercial Subsonic Airliners"*. NASA/CR 4746, 1996.

[9] Page, F. H., *"WING AND SIMILAR MEMBER OF AIRCRAFT"*. United States Patent, US 1,394,344, 1921.

[10] Wagner, H., *"AIRPLANE WING STRUCTURE"*. United States Patent, US 2,246,116, 1941.

[11] Gilbey, R. W., *"Geometrical properties of cranked and straight tapered wing planforms"*. ESDU-76003, London, 1976.

[12] Greenman, D. C., *"Method for rapid estimation of spanwise loading of wings with camber and twist in subsonic attached flow"*. ESDU-83040, London, 1983.

[13] Dovey, J. R. J., *"The maximum lift coefficient of plain wings at subsonic speeds"*. ESDU-89034, London, 1989.

[14] Hollis, C. D., Williams, R. G., *"Airfoil maximum lift coefficient for Mach number up to 0.4"*. ESDU-84026, London, 1984.

[15] Dovey, J. R. J., *"Increments in airfoil lift coefficient at zero angle of attack and in maximum lift coefficient due to deployment of a single-slotted trailing-edge flap, with or without a leading-edge high-lift devices, at low speeds"*. ESDU-94030, London, 1995.

[16] Dovey, J. R. J., *"Maximum lift of wings with trailing-edge flaps at low speeds"*. ESDU-91014, London, 1991.

[17] *"SLOPE OF LIFT CURVE FOR TWO-DIMENSIONAL FLOW"*. ESDU Wings 01.01.05.

[18] Rudolph, Peter K. C., *"Mechanical Design of High Lift Systems for High Aspect Ratio Swept Wings"*. NASA/CR-1998-196709.

[19] Van Dam, C. P., *"The aerodynamic design of multi-element high-lift systems for transport airplanes"*. Progress in Aerospace Sciences 38 (2002) 101-144, Elsevier Science Ltd., 2002.

[20] Lin, J., Dominik, C., *"PARAMETRIC INVESTIGATION OF A HIGH-LIFT AIRFOIL AT HIGH REYNOLDS NUMBERS"*. Journal of Aircraft 0021-8669 vol.34 no.4, pp485-491, 1997.

[21] Pepper, R. S., Van Dam, C. P., "Design Methodology for Multi-Element High-lift Systems on Subsonic Civil Transport Aircraft". NASA-CR-202365, 1996.

[22] Fitzgerald, A. E., Kingsley, C., Umans, S. D., *"Electric Machinery"*, Sixth Edition, McGrwa-Hill Higher Education, 2003.

[25] Official website of Schaeffler (UK) Ltd., http://www.schaeffler.co.uk/

[24] CS 25.393, Loads parallel to hinge line. European Aviation Safety Agency, 2007.

[25] FAR 25.393, Loads parallel to hinge line. Federal Aviation Administration, 1996.

7 Bibliographies

[1] Edi, P., *"Investigation of the Application of Hybrid Laminar Flow Control and Variable Camber Wing Design for Regional Aircraft"*. PhD thesis, Cranfield University, 1998.

[2] Fielding, J. P., *"Introduction to Aircraft Design"*. Cambridge University Press, 2000.

[3] Hughes, N. F., *"Investigation of Novel Slat Swing Arm Mechanism Design"*. MSc thesis, Cranfield University, 2001.

[4] Lajux, V., Fielding, J. P., *"Development of the SYNAMEC – A Design Tool for Aeronautical Mechanisms Applied to Leading Edge Devices"*. ICSA, 2004.

[5] Lajux, V., *"Methodology for the design of leading edge devices applied to variable camber"*. PhD thesis, Cranfield University, 2007.

[6] Macci, S. H. M., *"Structural and Mechanical Feasibility Study of a Variable Camber Wing (VCW) for a Transport Aircraft"*. PhD thesis, Cranfield University, 1992.

[7] Niu, M. C., *"Airframe Structural Design"*. Hong Kong: CONMILIT PRESS Ltd., 1991.

[8] Pires, R. M. M., Lajux, V., Fielding, J. P., *"Methodology for the Design and Evaluation of Wing Leading and Trailing Edge Devices"*. ICAS, 2006.

[9] Pires, R. M. M., *"Design Methodology for Wing Trailing Edge Devices Mechanisms"*. PhD thesis, Cranfield University, 2007.

[10] Rao, A. J., *"Variable Camber Wings for Transport Aircraft"*. PhD thesis, Cranfield University, 1989.

[11] Roskam, J., *"Airplane Design"*. University of Kansas, 1986.

Appendix A
Group Design Project Report

A.1 Introduction

This project is conducted by China Aviation Industry Corporation I and Cranfield University and named as Flying Crane. Meanwhile, it is the maiden co-operation of MSc training program in aircraft design field between China Aviation Industry Corporation I and Cranfield University.

The major objective of this group design project is to develop an imaginary commercial aircraft which may come into both Chinese domestic market and global market in 10 to 15 years. Three different groups, near 25 delegates of each, will be involved in this project separately from 2008 to 2010 to fulfill the project objective and each of the groups will accomplish the conceptual design, preliminary design and detail design of Flying Crane aircraft respectively. It is a maiden attempt for AVIC1 and Cranfield University to utilize three different groups to go through the overall civil aircraft design process and finalize this imaginary aircraft design within the following three years.

This year, 2008, is the first design stage - conceptual design phase of Flying Crane aircraft which all the delegates here participate. During this phase, all the design work focus on applying civil aircraft design technology, such as aerodynamics, performance, aero-structure, material, to determine a set of final key parameters, configuration, sizing, propulsion and so forth. Simultaneously, all the above results will be incorporated in Flying Crane aircraft specification which will be delivered to the next design group to act as the top level requirement and design input.

A.2 Design Phases

A.2.1 Phase One: Derivation of Requirements

A.2.1.1 Phase One (i): Data Collection

Task of this stage is to collect data and information about existing 80 to 150 seat aircraft on terms of all aspects. We were divided into 6 sub-teams and I was in general characteristics team.

The assignments of our sub-team consisted of 5 main tasks. Firstly, we needed to survey the general characteristics of existing 80 to 150 seat aircraft comprehensively and to produce a rigorous and extensive data set, including payload/range curve, Mach number capability, etc. Secondly, we were supposed to figure out principle mass characteristics of all aircraft involved and attempt to assemble component mass breakdowns for aircraft where possible. Thirdly, we needed to determine flight and ground cg ranges of all aircraft. Fourthly, we needed to collate information on capacities e.g. cabin, baggage hold, doors and exits, etc. Lastly, we needed to review operational reliability and other operational aspects of all aircraft in our survey.

The first step of our work is to make out the scope about aircraft prototypes which we will investigate and data we will collect.

There are more than 40 kinds of aircraft prototype being investigated. The list of these aircraft is shown in the following TableA.1.

TableA.1 The List of Most 80-150 seat aircraft in the world

Nation	Company	The Type of Aircraft
America	Boeing	Boeing 707-120 Boeing 707-320 Boeing 737-100 Boeing 737-200 Boeing 737-300 Boeing 737-400 Boeing 737-500 Boeing 737-600 Boeing 737-700

TableA.1 The List of Most 80-150 seat aircraft in the world (continue)

Nation	Company	The Type of Aircraft
America	McDonnell Douglas	DC-9-10/21/30/40/50 MD-88/88shuttle/90
	Lockheed	Lockheed L-1049C Lockheed L188 Electra
International	Airbus	Airbus A318 Airbus A319 Airbus A320
	Avions	ATR72
	Sud Aviation- BAC	Concorde
United Kingdom	Hawker Siddeley	Trident 1C Comet 4C
	BAe	BAe 146 series 200
	Antonov	An-10 An-148-100/-200
	Ilyushin	Il-18/18B/18D
	Yakovlev	Yak-42
	Sukhoi	Superjet 100-75/-95
	Ilyushin&Irkut&Sukhoi	MS-21-100/-200
	HAL & Ilyushin&Irkut	IRTA-21
China	Shanghai	Y-10
	Xi'an	ARJ-21-700/900

These aircraft listed above covers most prototypes produced by Europe, U.S.A, Russian Federation and other countries like Canada, Brazil and China since WWII. I took response of to collect all information relating to our tasks of aircraft produced by Europe, and to analysis performance data collected by us about all of the 45 types of aircraft.

In the term of general performance data, we involved Payload/range and Mach number capabilities. And we divided our survey results into three groups by number of seats to compare these data: 80-100 seat aircrafts, 100-130 seat aircrafts and 130-150 aircrafts.

In the first group, 80-100 seat aircrafts, the data of Max Payload change from 7,050kg to 13,500kg. Basically, the more seats are allocated in an airplane, the more maximal payload capacity it has. For example, Boeing 737-100 which can accommodate 101 passengers has the maximal payload capacity of 13,196kg. Whereas, ATR 72, an airplane can contain 72 seats max, only provides 7,050kg on the aspect of maximal payload. There are three types of aircraft in this group demonstrating Fuel Capacity and Range: Boeing 737-100, Superjet 100-95 and ARJ21-700. Fuel capacity is 14,140kg, 9,550kg and 10,386kg respectively, while range with maximal payload is 2,960km, 3,279km and 2,222km respectively. We can draw a conclusion from above data that Superjet 100-95 has an excellent economical speciality, meaning flight longer range with less fuel. Max Mach Number of aircrafts in this group is around 0.8-0.9, and Max Certificated Altitude is around 10,000m to 12,500m, except ATR72, whose Max Mach Number is 0.415 and Max Certificated Altitude is 7,620m. It's because that ATR72 is propelled by turboprop engines and others by turbofan or turbojet engines.

The second group is aircrafts have range of seat from 100 to 130. We involved 13 types of aircraft into this group, and it is the group containing most types, so far. In this group, the highest Max Payload type is 15,645kg achieved by Boeing 737-200, whose accommodation is up to 130 seats. And the lowest is 9,000kg carried out by An-148-200, a Ukrainian airplane, which can accommodate 100 passengers. Max Payload of most aircrafts in this group varies from 10,000kg to 13,000kg. The data of fuel capacity vary in a broad range from Fokker 100's 13,365 liters to Boeing 737-200's 23,830 liters and Tu-140B's 33,150 liters. It increases more than double. And the supersonic civil airplane named Concorde can carry fuel up to 95,680 liters because its high flight Mach number needs more fuel supply. The flight range under maximal payload can divide aircrafts in this group into two sub-groups. Shorter range is from BAe 146 series 200's 2,094km to Tu-334-100D's 3,020km, and longer range is from IRTA-21's 3,500km to An-10's 4,000km. However, Boeing 737-600's range increases from 2,482km to 5,648km after changing engines from CFM56-7B18 into CFM56-7B22S. The exception is Yak-42 which propelled by 3 turboprops and only has a range of 1,380km with maximal payload. On the other hand, the design range of Concorde is 6,230km with maximal payload at 2.02 Mach number. The Max Operating Mach contains 3 levels. The low speed level is old types such as An-10, BAC One-Eleven Series 500, Fokker 100 and so

on, whose Max Operating Mach are in the range of 0.59-0.77. The middle level is Boeing 737 series and their Max Mach are from 0.82-0.84. Concorde is delegate of the high speed level and it can achieve 2.2 Mach number max. The data of Max Certificated Altitude are generally approximate and around 12,000m, except the lowest type (9,600m) occupied by Yak-42 and the highest type (20,000m) recorded by Concorde.

The third group is aircrafts with seat number from 130 to 150 and involved 10 types in our survey, including the most successful civil airliner in the world such as A320 and Boeing 737-300. Max Payload of aircrafts in this group changes from 12,540kg (MS-21-100) to 34,827kg (Boeing 737-400). And most of these parameters are in the range of 16,000kg to 25,000kg. There is a close relationship between fuel capacity and flight range. For most short range airplanes (less than 5,000km), 26,000 liter fuel is enough. Y-10 is an example of middle range airplanes, which needs 63,750 liter fuel to support his design range of 5,560km. In the term of long range airplanes, there are two examples: Vickers VC10 and Boeing 707-320B. Their fuel capacities are 81,554 liter and 90,160 liter and ranges with maximal payload are 8,900km and 10,654km separately. There are two things should be pointed out. Firstly, as the only two kinds of successful airliner, Tu-144 needs more fuel (118,750 liter) than regular types, and has a relatively longer range which can reach 6,500km. Secondly, Boeing 737-700 gets a great improvement on the aspect of flight range which increased from 2,852km to 6,037km after mounted with winglets and changed engines from CFM56-7B20S to CFM56-7B24S. Two out-service types, MS-21-100 and Y-10, carry out Max Operating Mach of 0.69 and 0.79 respectively. Most in-service types, such as A320 family and Boeing 737 series, achieve Max Operating Mach from 0.82 to 0.95. Tu-144 achieves an extremely high speed whose Mach number is 2.35. The data of Max Certificated Altitude of aircraft in group three are around 12,500m. However, Tu-144's ceiling reaches 18,000m.

A.2.1.2 Phase One (ii): Data Validation

In this phase, our main tasks are to validate data we got from the previous phase and generate a full set of database. We were suggested to make analytical models for the various aircraft to check against quoted data and match estimated data to give consistency with known data.

The 6 sub-teams had done comprehensive investigation about 80 to 150 seat airliners,

and they all had their own prototype list which were not exactly same to each other. So, before we validated data from previous stage, we needed to decide which aircraft should be remained in the list, and which should be removed. After discussion between members of our sub-team, we chose 30 prototypes as our final investigating objects. And my assignments were to validate data about 4 prototypes: A320-200, Boeing737-500, DC-9-30 and FOKKER-100.

A320-200 is a member of A320 family and now is called A320 simply. It differs from initial A320-100 in having wingtip fences, wing centre-section fuel tank and higher maximum T-O weights. A320-200 can accommodate 150 seats in mix-classes (12 first class seats plus 138 economy class seats) or 180 seats in all-economy class.

737-500 is a member of 737 family and initially known as 737-1000. It is short-body version of 737-300 and placing 737-200. 737-500 incorporates advanced technology of 737-300 and -400, but fuselage shortened. 737-500 can accommodate 108 seats in mix-classes or 130 seats in all-economy class.

DC9-30 is a developed version of DC9-10 and initially with 62.3KN JT8D-7s engine, increased wing span, longer fuselage and new high-lift devices including full-span leading-edge slats and double-slotted flaps. DC9-30 can accommodate 97 passengers in mix-classes or 119 seats in all-economy class.

Fokker 100 is announced simultaneously with Fokker 50 and derived from F28 MK 4000, which it superseded in production. It is built in collaboration with Deutsche Aerospace Airbus and shorts. New main landing gear is introduced, and large upward opening cargo doors and forward opening passenger door become standard, by end of 1993. Fokker 100 can accommodate 107 passengers in mix-classes or 119 passengers in all-economy seats.

We picked up most of the data listed in our database from the website of Civil Jet Aircraft Design. And we also debated all these existing data by variant resources, such as Jane's all the world's aircraft, Airbus' official website and published documents. Some missing data in term of dimensions, e.g. area of control surfaces, are estimated by measuring three view drawings.

The whole series data in term of mass come from Civil Jet Aircraft Design. And they are proofed being reasonable by checking their inner relationship and comparing to terms in same names coming from other sources. The term of maximum taxi weight (MTW) and

maximum ramp weight (MRW) appear in different place and they are always same or have slight difference to each other. So we can tell that they are two different names with a same definition.

There are many data source about dimensions of fuselage and wings, such as the fuselage length, the wings area and aspect ratio. And data from different ways are approximately equal, so we consider they are reliable. Some detailed data like the area of control surfaces are missing. We measure these values in three view drawings by regarding those control surfaces are approximate parallelograms. And the measuring values are reasonable by comparing with same kinds of data of other types aircraft which are attainable. Dimensions of doors and exits can be found via official publications of Airbus.

Payload-range diagrams of these four types of aircraft are shown in FigureA.1 to FigureA.4. In these diagrams, we can get the information about maximum payload, Max payload range, Max economic range and ferry range. We can also estimate an approximate value of range by known payload or vice versa.

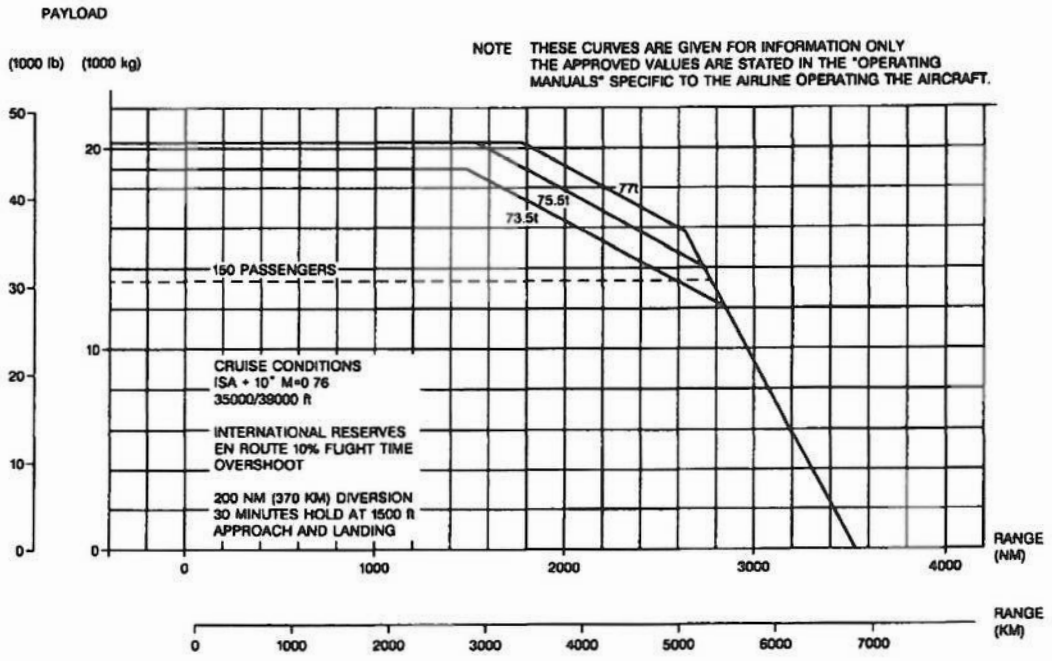

FigureA.1 Payload-range diagram of A320-200

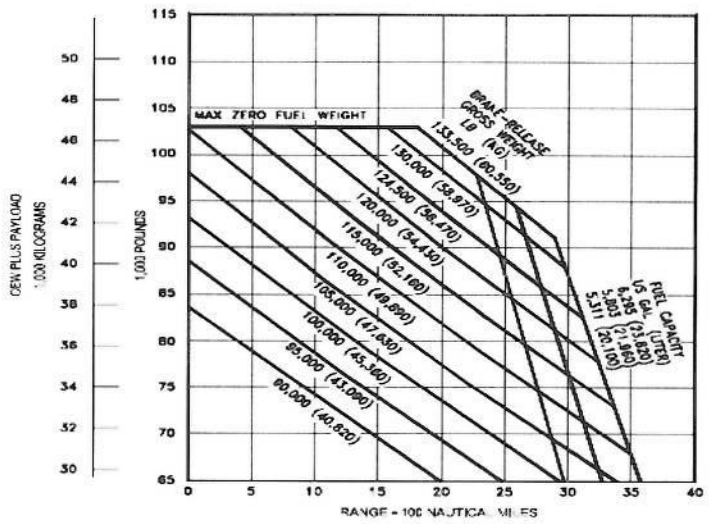

FigureA.2 Payload-range diagram of 737-500

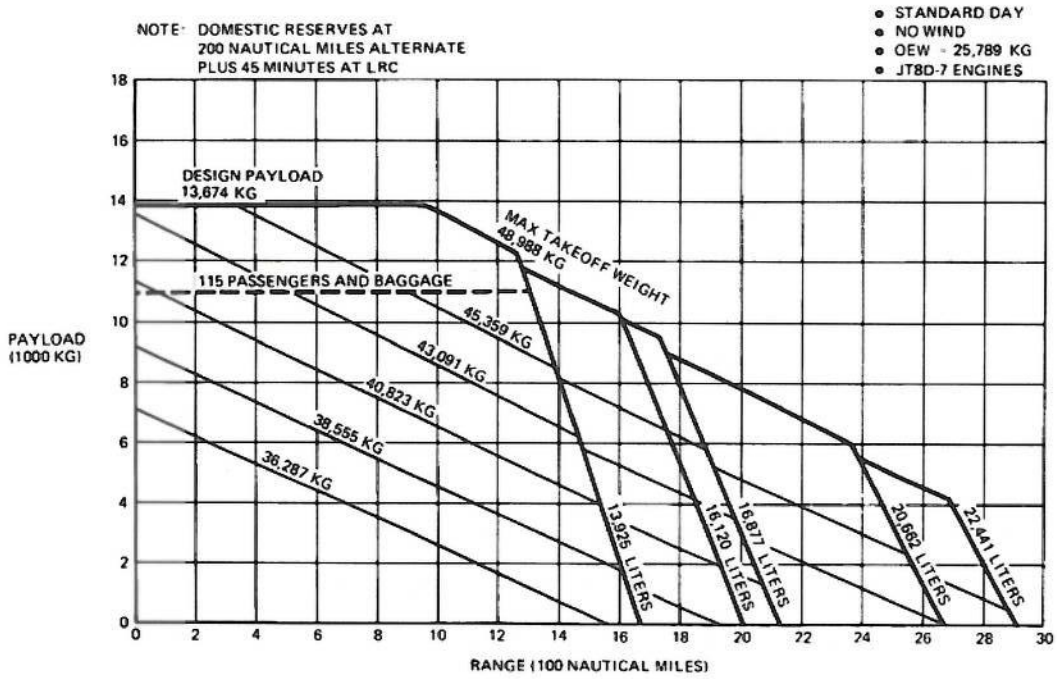

FigureA.3 Payload-range diagram of DC9-30

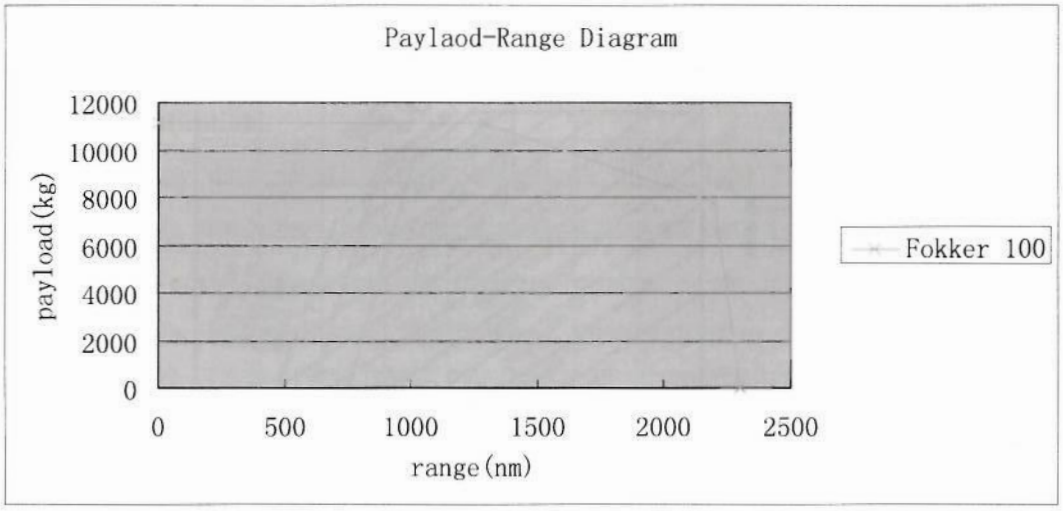

FigureA.4 Payload-range diagram of Fokker 100

A.2.2 Phase Two: Conceptual Design and Evaluation

Between this phase and the previous phase, we had a short course named Aircraft Conceptual Design, which introduced the procedure of aircraft design in conceptual design stage briefly, and gave methods which were developed by Denis Howe to do the initial mass estimation. And at the end of this course, we were divided into 4 teams and each team was assigned to work out an individual airliner configuration respectively.

A.2.2.1 Analysis of competitors

My team was red team and we had 6 team members totally. The first task of our team is to figure out what kind of airliner shall we work out, to decide the range, the maximum passenger capacity, the cross section of the cabin, etc. This decision should be done on base of comprehensive survey about aviation market nowadays and in the future. I analyzed competence of our main competitors, Boeing, Airbus, Embraer and Bombardier, through surveying and forecasting their manufacture capacities. Manufacture capacity has close relationship with delivery number and order number which are securable via these companies' official website.

Through the curves of delivery number and order number in recent years, we can see that these two curves cross each other alternately. The order number is influenced by many factors such as global economy, airlines' operating policy, and so on. We can get some idea about it from aviation industries' market reports. The ascent or drop of order

number will affect delivery number toward the same trend, but with 2 or 3 years delay. Delivery number is also limited by the manufacture capacities of aviation industries. Generally, manufacture capacities will be improved in adding product lines or building new plants when order number is far-forth higher than delivery number. And we can approximately regard delivery number as manufacture capacity of the enterprise when order number is higher than delivery number. All predictions in this paper are made under optimistic assumption that order number keeps raising trend.

A.2.2.1.1 Boeing 737 family

The order number and delivery number of Boeing 737 family from 1990 to 2007 are shown in Figure2-5. B737 family consists of 737-300, 737-400, 737-500 and 737 NG. We can see that there are two significant risings of order number in 1996 and 2005, and these two risings led to increases of delivery number in 1998 and 2007 respectively. Another information is that Boeing trend to improve their capacity rapidly and step by step like stairs. After rapid growth in 1998, the capacity keeps relatively stable around 300 for several years, even when order number raised above in 2000. Basing on this conclusion and sustaining growth of order number since 2005, we can predict Boeing's delivery number in future 5 years as shown in FigureA.5. And it is expected to reach 600 in the end of 2012. This number is also Boeing's capacity in term of Boeing 737 family.

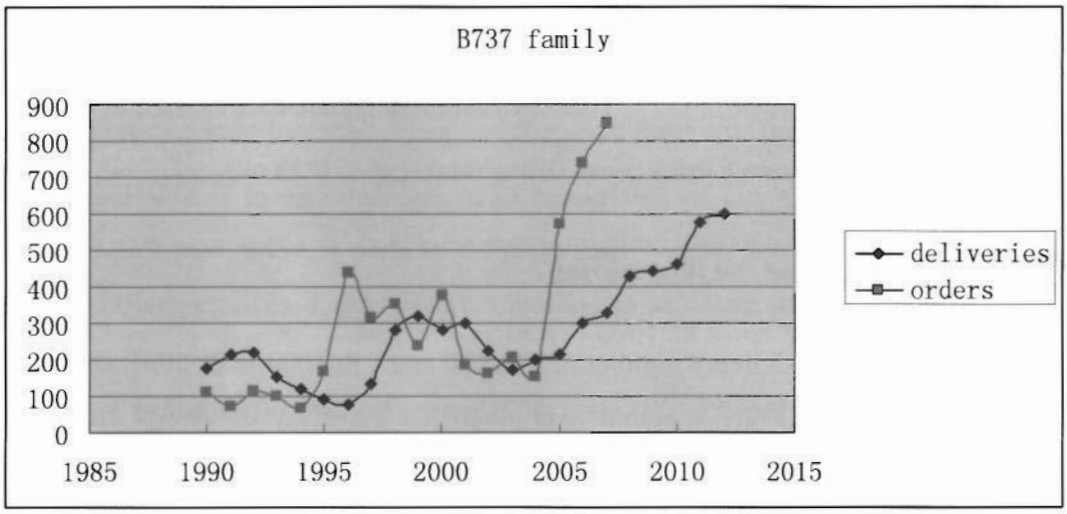

FigureA.5 Delivery and Order Number of B737 Family

Data coming from www.boeing.com

A.2.2.1.2 Airbus A320 family

The order number and delivery number of A320 family from 1990 to 2007 are shown in FigureA.6. A320 family consists of A318, A319, A320 and A321. We can see something similar with Boeing 737 family in Figure2-5. The order number of A320 family jumped up dramatically in 1996 and 2005, just exactly same with Boeing 737, and followed by growth of delivery number appearing in period from 1997 to 2001, and from 2005 to 2007. Different from Boeing's situation, the growth of delivery number of A320 family is more gradual and sustained. Therefore when order number dropped greatly in 2006, delivery number could keep rising. It owes to the multi-variant strategy of Airbus. Extending from such tendency, we can predict delivery number of A320 family in future 5 years which can arrive at 650 in the end of 2012. This number is also Airbus capacity in term of A320 family.

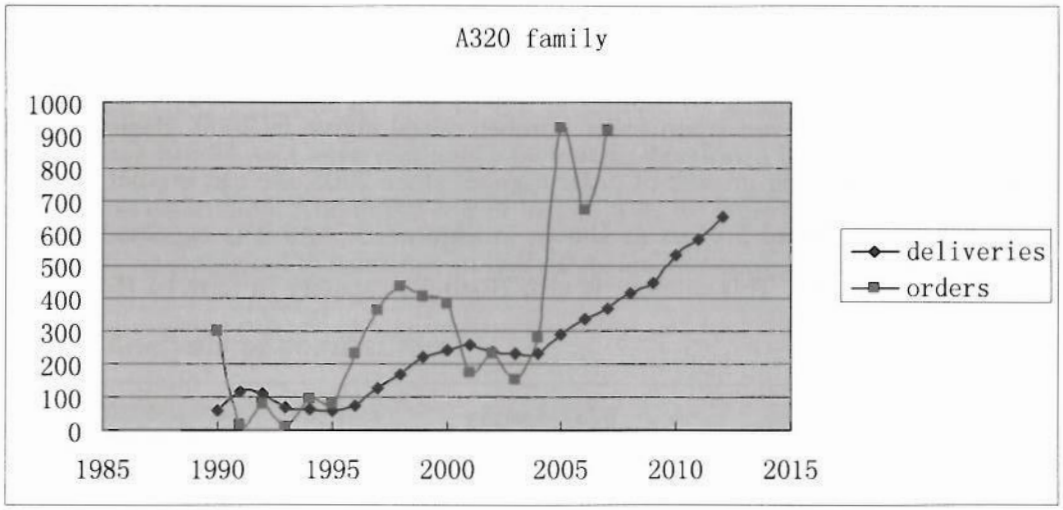

FigureA.6 Delivery and Order Number of A320 Family

Data coming from www.airbus.com

A.2.2.1.3 Bombardier CRJ900 series

The order number and delivery number of CRJ900 and CRJ1000 from 2001 to 2007 are shown in FigureA.7. In this diagram it is clear that the delay of change from order number to delivery number is shorter for regional airplane than that for main airliner. It is understandable because investment needed by producing smaller aircraft is lower than that by producing bigger aircraft. The developing model of Bombardier is similar to that of Boeing. After twice significant improvement of manufacture capacity happening in

2003 and 2006 respectively, the delivery number reached 56 in the end of 2007, and it is supposed to arrive at 100 in future five years under optimistic prediction. This number can be looked as manufacture capacity of Bombardier approximately.

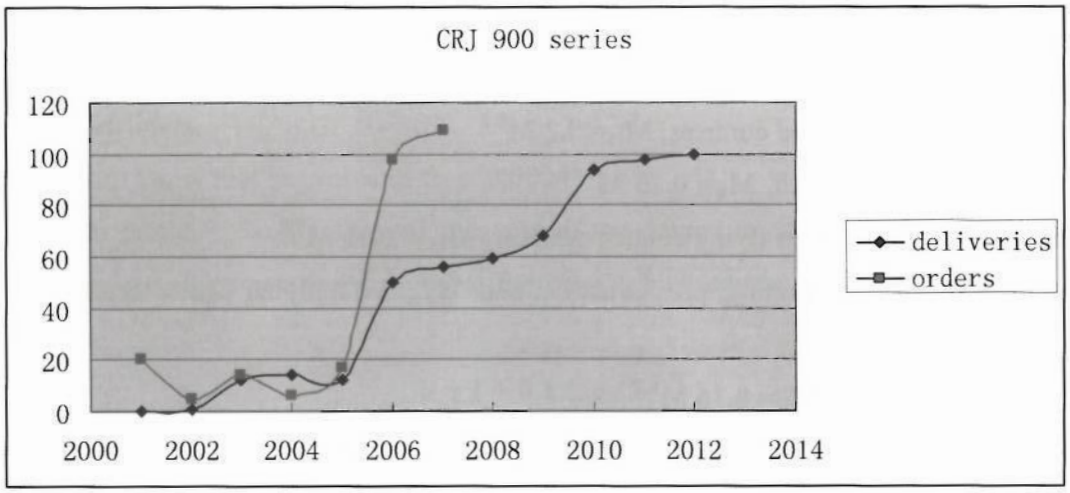

FigureA.7 Delivery and Order Number of CRJ 900 Series

Data coming from www.bombardier.com

Through investigating the aviation market and analyzing existing and potential competitors, we drew a conclusion that there is still much space in future middle range passenger aircraft to support our project, especially under the background that rapid increasing of Chinese economy. So, we aimed our project on middle range transport aircraft which can carry 150 passengers in maximum. To increase comfort and operating flexibility of our aircraft, we chose twin-aisle configuration.

A.2.2.2 Mass breakdown establishment

The second step is to establish the mass breakdown of our aircraft. We divided the whole aircraft into different parts to estimate their weight, and I was in charge of tail unit and power services. I used Howe's method to calculate initial weight of tail unit and power services.

In terms of tail unit, this method estimates its mass (M_{TU}) based on whole aircraft mass, and the formula is shown below:

$$M_{TU} = a\, M^{0.83}$$

Where a=0.14 for transport aircraft, and M is whole aircraft mass assumed on base of similar aircraft mass such as B737 and A320.

In terms of power services, this method divides it into 6 sub-systems: accessory drives and auxiliary power unit (M_{APU}), hydraulics and pneumatics (M_H), electrics (M_E), flying control systems (M_{FC}), environmental control (M_{AC}) and de-icing systems (M_D). The mass of power services is sum of mass of these 6 sub-systems.

For large airliner, $\mathbf{M_{APU}= 0.002\ M}$

For aircraft with powered controls, $\mathbf{M_H= 3.2\ M^{0.5}}$

For civil transport aircraft, $\mathbf{M_E= 0.75\ M^{0.67}}$

For aircraft with powered flying control systems, $\mathbf{M_{FC}= 0.11\ M^{0.8}}$

The mass of air conditioning, pressurization and oxygen supplying can be regarded as 5kg per passenger.

For transport aircraft, $\mathbf{M_D= 0.16\ M^{0.7}}$

We can get the mass of all parts of our aircraft structure and systems by such kind of empirical formulas. As I mentioned above, all these masses are calculated based on an assumed whole aircraft mass (M_{ass}). And after we plus all the results together, we can get another whole aircraft mass (M_{ite}). To adjust M_{ass} to make it equal to M_{ite} approximately and the final result is our aircraft mass.

The iterative result of M_{ass} is 64582kg, as a result we can get the value of M_{TU} and M_{PS}:

$M_{TU} = 0.14 \times 64582^{0.83} = 1376$ (kg)

$M_{PS} = M_{APU} + M_H + M_E + M_{FC} + M_{AC} + M_D$

$= 0.002 \times 64582 + 3.2 \times 64582^{0.5} + 0.75 \times 64582^{0.67} + 0.11 \times 64582^{0.8} + 5 \times 150$

$+0.16 \times 64582^{0.7} = 4093$ (kg)

I also calculated drag polar of our aircraft. The representation of fixed wing drag coefficient follows that of Kuchmann.

$$\mathbf{C_D= C_{DF} + C_{DLV} + C_{DW} + C_{DLW}}$$

Where C_{DF} is the incompressible flow zero lift drag coefficient

C_{DW} is the additional zero lift drag coefficient due to compressible air's wave drag effect

C_{DLV} is the vortex drag coefficient due to lift

C_{DLW} is the wave drag coefficient due to lift

An approximate definition of the skin friction coefficient which makes some allowance for both size and operating conditions is:

$$\mathbf{C_f = [0.0048 - 0.0006 \log_{10}(10.7\ S)]\ (1 - 0.2\ M_N)\ (1\text{-}2\ C_l / R)}$$

Where S is the wing area, and the value is 122.7 m^2

C_l is the fraction of the wing chord over which laminar boundary flow may be expected. Unless special considerations are given it should be taken as zero.

M_N is the operating Mach Number. Cruise Mach Number of our aircraft is 0.78.

R is ratio of overall wetted area to wing reference area, and the value is 5.5 for airliners.

So we can know that the value of C_f is 0.0024.

The size factor, F, is effectively a measure of the degree to which the inevitable gaps, leaks and small excrescences increase the drag, which can be calculated by following formula:

$$\mathbf{F = 1 + 0.1\ (20 / S)^{1/2}}$$

After applying our wing area into this formula, we can get the value of F, which is 1.04.

The incompressible flow zero lift drag coefficient is:

$$\mathbf{C_{DF} = R\ F\ T\ C_l}$$

Where T is type factor and equal 1.1 for jet airliners

So the value of C_{DF} is 0.0156.

A method of evaluating vortex drag factor K_V is given below:

$$\mathbf{K_V = 1 + (0.142 + 0.0062\ A)\ (10\ t / c)^{0.33} / (\cos \Lambda_{1/4})^2 + 0.1 / (4 + A)^{0.8}}$$

Where t/c is the aerofoil thickness to chord ratio, which is 0.12 in our aircraft

$\Lambda_{1/4}$ is the sweep of the wing 0.25 chord line, which is 25 deg in our aircraft

A is the wing aspect ratio which is 8 in our aircraft

So the value of K_V is 1.2614.

Then $\mathbf{C_{DLV} = K_V\ C_L^2 / (\pi\ A) = 0.0502\ C_L^2}$

Because cruise Mach number of our aircraft is 0.78, we need to consider increment on drag coefficient due to wave.

A specific relationship between C_{DW} and Mach number is given below:

$$C_{DW} = \frac{0.12 C_{DF}}{1 - 0.2 M_N} \left[\frac{M_N (\cos \Lambda_{1/4})^{1/2}}{A_f - t/c} \right]^{20}$$

Where A_f is a factor which depends upon the design standard of the aerofoil. Because we chose a supercritical aerofoil for our aircraft, this value should be 0.93.

So the value of C_{DW} is 0.0004.

In terms of wave drag due to lift, in practice the effect is Mach number dependent and it is suggested that

$$C_{DLW} = 0.12\ M_N^{6}\ C_{DLV}$$

Then $C_{DLW} = 0.0014\ C_L^{2}$

So far, we can get the drag polar of our aircraft shown below:

$$C_D = C_{DF} + C_{DW} + C_{DLV} + C_{DLW} = 0.016 + 0.0516\ C_L^{2}$$

This will be used in calculation of performance.

A.2.2.3 Cross-section and cabin layout drawing

Another work of mine in this stage was to draw 2-dimension cross-section and cabin layout configuration drawing.

The initial cross-section was designed with 4.6m width and 5.6m height. In this configuration, we can allocate 3 2-abreast seats and twin aisles in one row in the cabin, and under-floor cargo can hold 2 LD2 freight container abreast. But the cross-section area is too big which means this configuration will bring significant aerodynamic penalty. Finally, we decreased the width to 4.2m and the height to 4.1m, and gave up the idea of carrying ISO containers in under-floor cargo.

FigureA.8 and FigureA.9 is the initial design of cross-section and after modified respectively.

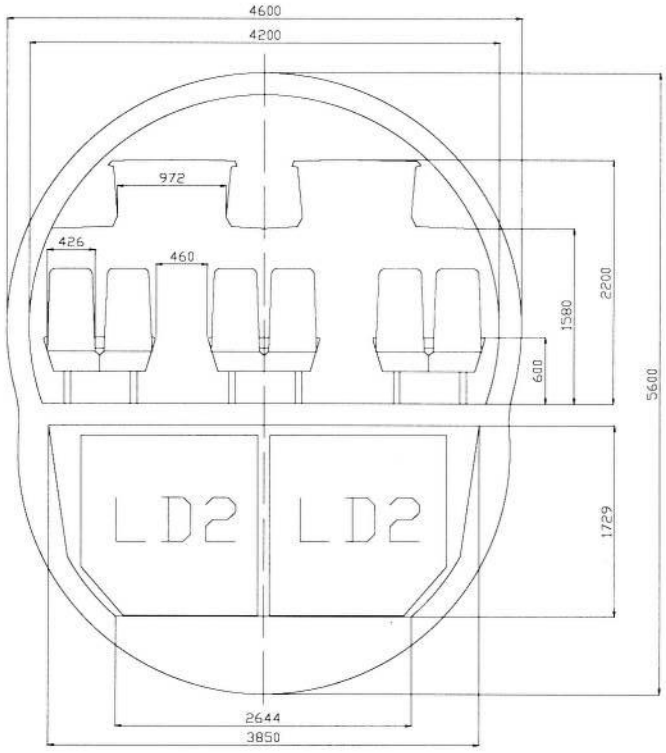

FigureA.8 Initial design of cross-section

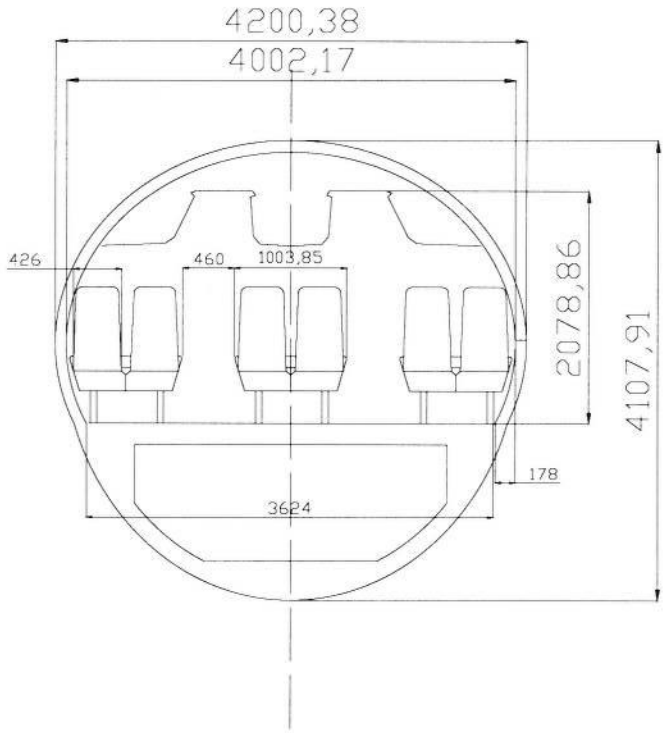

FigureA.9 Cross-section after modified

In terms of cabin layout, we had 3 different configurations: 156 economy seats in 30 inches seat pitch, 150 economy seats in 31 inches seat pitch, 10 business seats in 34 inches seat pitch and 118 economy seats in 32 inches seat pitch. Except passenger seats, cabin layout drawing also shows positions of two lavatories, two galleys, four attendant seats, two forward doors, two rear doors and two emergency exits. FigureA.10 is our cabin layout drawing.

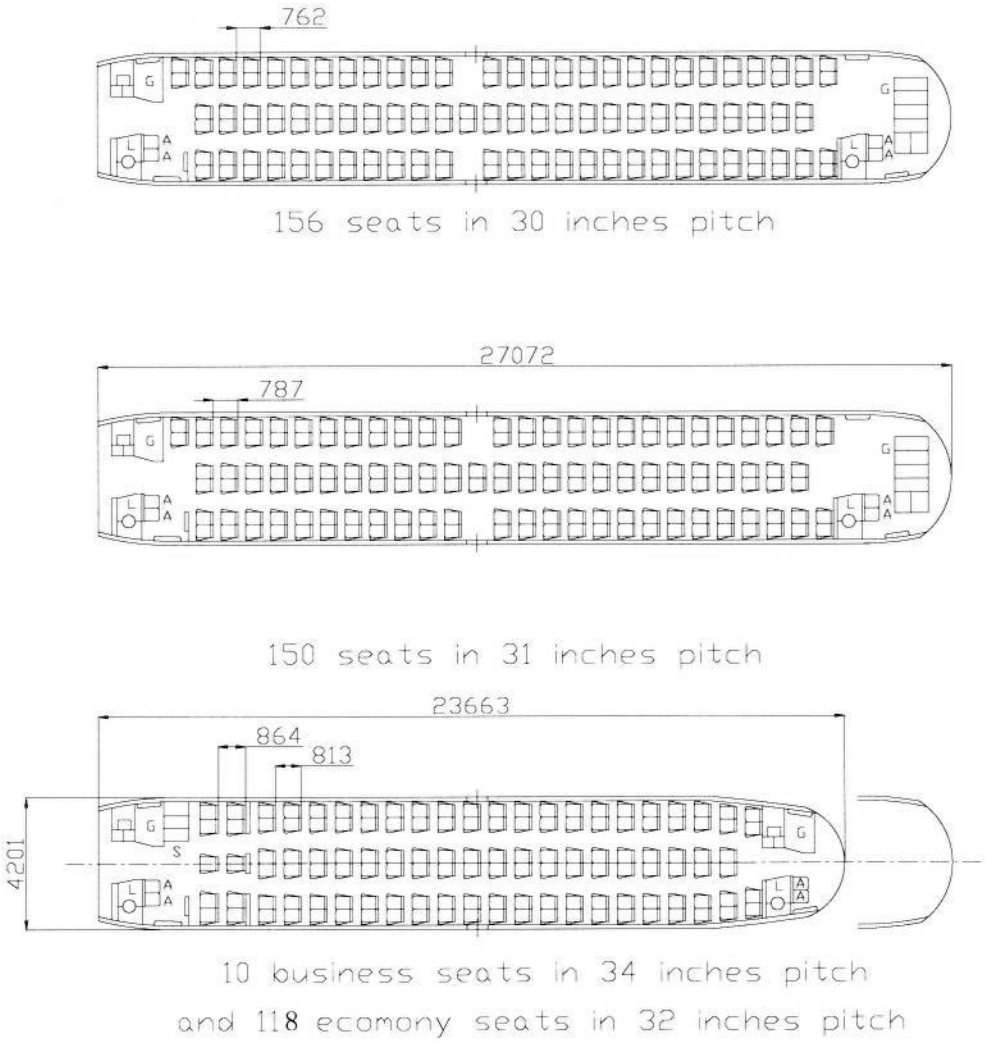

FigureA.10 Cabin layout

When I review this drawing now, I found some mistakes and some unreasonable design. For example, the length of fuselage in mixed-class and single-class configuration should be same to each other. In mixed-class configuration, the seat pitch of business class should be bigger to fulfill the requirement of comfort. Fortunately, those mistakes and shortcomings all were corrected or modified in further work.

A.2.3 Phase Three: Consolidation

A.2.3.1 Phase Three (i): Assessment Matrix

Task of this stage is to make criteria to evaluate the four aircraft concepts produced by the sub-teams in previous phase.

We were divided into 6 groups in this stage to evaluate score of the four aircraft concepts in terms of performance, certification, market, strategy and family issue respectively. There was one sub-team which was supposed to allocate a weighting factor to each sub-team mentioned above that signifies how important the aspect evaluated by this sub-team is to the project as a whole, and integrate the scores from the other sub-teams in addition to their weighting factors. I was in this sub-team.

The scores of the 4 aircraft concepts got in the 5 aspects and their own weighting factors were input into a table, and we got the order from high score to low, which was demonstrated in TableA.2.

TableA.2 Score of four aircraft concepts

Team	Configuration	Performance	General	Market	Strategy	Family	Score	Rank
Red	Twin Aisles	100	99	95	100	98	98.1	1
Blue	Single Aisle Conventional	90	100	97	97	95	95.3	2
Gold	Over Wing Engines	87	95	100	95	100	93.9	3
Yellow	Single Aisle Long Range	85	93	95	95	99	91.7	4
Weight Factor		0.25	0.24	0.28	0.12	0.11	1	

After working out this score table, we chose two configurations which got higher scores to run our project ahead. These two configurations are twin-aisle configuration and single-aisle conventional configuration.

A.2.3.2 Phase Three (ii): Amber and Jade

After evaluation in previous stage, we combined the original 4 configurations into 2 configurations: Amber and Jade. I was in Amber group and our aircraft had twin-aisle cabin design. The advantages brought by twin-aisle configuration are deflected in terms of safety aspect at first. Passengers in cabin have double escaping aisle than that in single-aisle configuration under emergency, and can escape from cabin in shorter time. Second, twin-aisle configuration provides more taking comfort to passenger. The seat arrangement of 2-2-2 makes everyone enjoy his (or her) trip. Seats in business class are bigger and more comfortable, which makes passengers don't feel tired at all in long journey. Meanwhile, twin-aisle configuration allows attendants to provide cabin service from two aisles at same time. It reduces passengers' waiting time and attendants' working burden. Moreover, it is good for operators. Twin-aisle configuration can improve operating efficiency by shortening boarding and deplane time greatly, and reduce DOC ultimately.

The main task of our group in this stage is to further develop the concept. Areas that might not have been explored need to be developed further. Firstly, we double checked former data to make sure that every parameter was correct so far. After that, we needed to do more detail works about our concept. My assignments were to optimize the design of cross-section and work out 3-dimension models of cabin inner components.

By adjusting shape of fuselage, there is more space in cabin. After considering about airworthiness regulations and comparing with other competitory prototypes, I increased width of economy seat to 17 inches and width of business seat to 20 inches. Width of aisle of economy class and business class is 17 inches and 18.9 inches respectively. Drawings of economy class cross-section and business class cross-section are shown below.

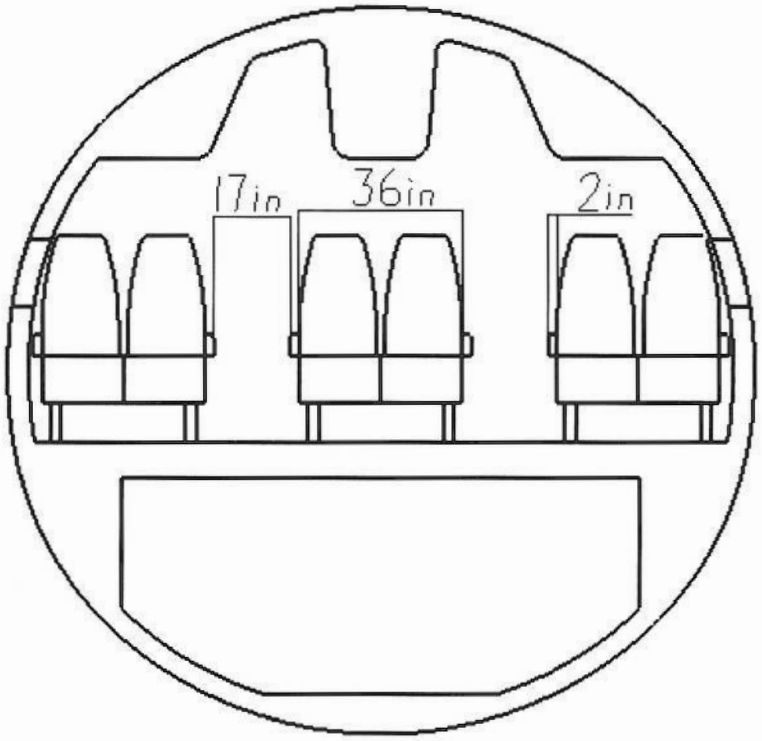

FigureA.11 Cross-section of Economy Class

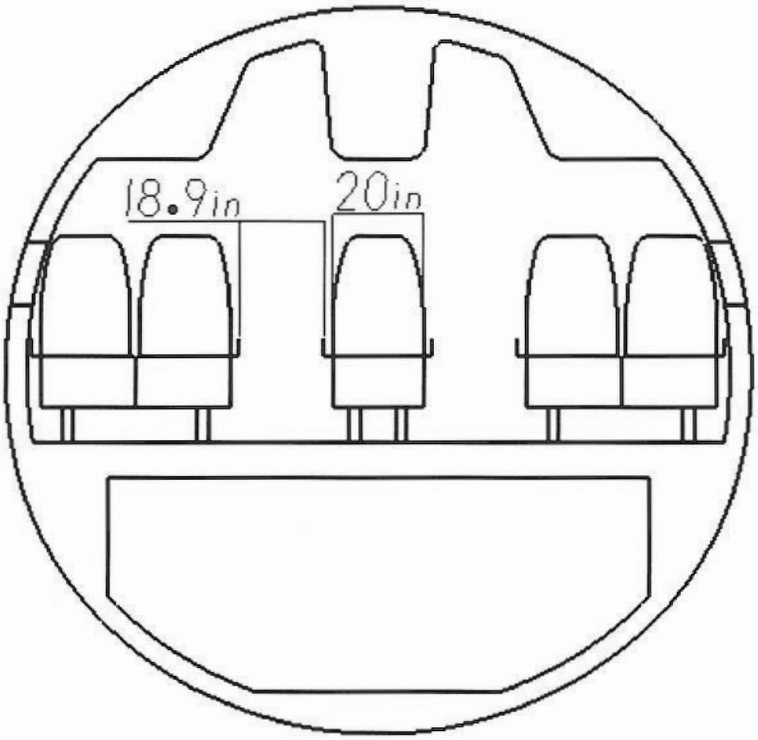

FigureA.12 Cross-section of Business Class

In terms of cabin layout drawing, I decreased seat pitch of economy class both in single-class configuration and in mixed-class configuration. So that length of cabin dropped to 23.7m. Seat pitch in single class configuration was 29 inches. Seat pitch of economy seat in mixed-class configuration was 31 inches, and that of business seat was 38 inches. Drawing of cabin layout is shown below.

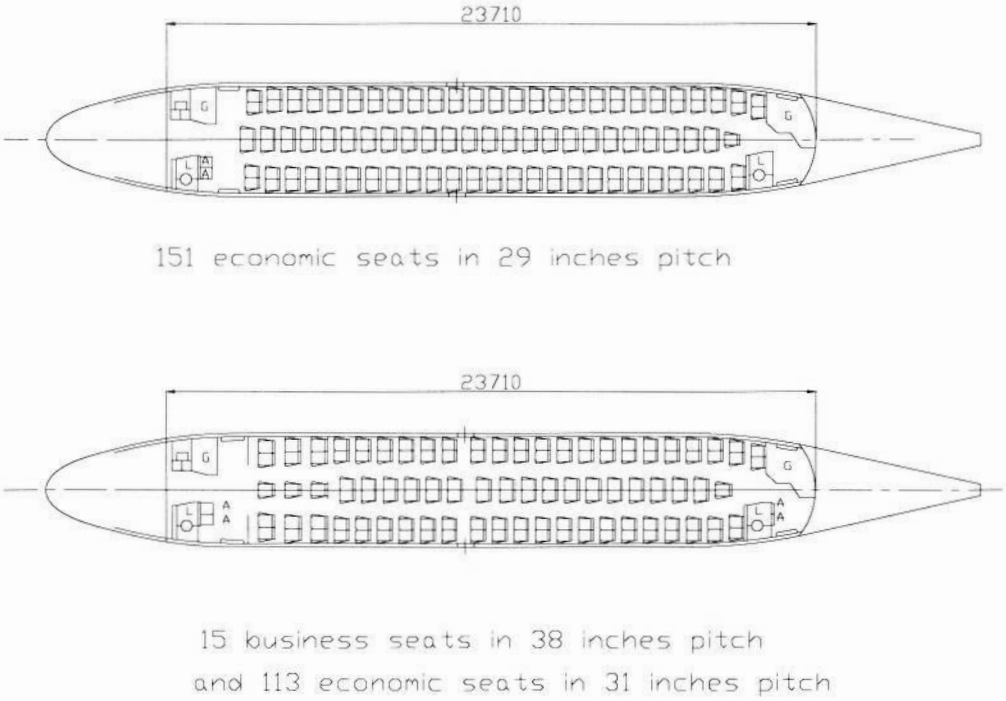

FigureA.13 Cabin layout of Ember

The 3-dimension models were also worked out in this phase, including passenger seat, walls, over-head luggage hold and under-floor cargo in cabin. Position and size of passenger doors, emergency exits, lavatories and galleys are also shown in these digital mock-ups.

A.2.4 Final Phase: Flying Crane

At the end of previous phase, we did the same work as in phase three (i) to compare Amber configuration and Jade configuration. Aspects to evaluate these two configurations consist of all up mass, fuel consumption per passenger and per kilometer, area for each passenger, boarding speed, operating flexibility, excess performance, technical risks and market risk. Comparing result is demonstrated in following table.

TableA.3 Comparison between Amber and Jade

	WEIGHT FACTOR	AMBER		JADE	
		RATE	SCORE	RATE	SCORE
ALL UP MASS	20	10	200	10.3	207
FUEL/PAS KM	15	10	150	10.4	155
AREA PER PASSENGER	8	10	80	10.9	87
BOARDING SPEED	4	10	40	5.9	24
FLEXIBILITY	5	10	50	9.0	45
EXCESS PERFORMANCE	7	10	70	9.5	66
TECHNICAL RISK	4	9	36	9.0	36
MARKET RISK	6	10	60	9.5	57
TOTAL SCORE			686		678

From above table we can see that Amber concept got a little bit high score than Jade. So we chose Amber concept as the base of the final configuration of our project. And we also absorbed some strong points into final design from Jade concept. After a comprehensive collection between members of our aircraft team, we chose a lovely name for this project as "Flying Crane". I was allocated in cabin group and main tasks of our group in this phase were to specify and consolidate the cabin design of Flying Crane, including rearranging the position of seats, walls and doors, adjusting seat width and seat pitch, modifying cross-section drawings and digital 3-dimension mock-ups.

In Amber concept, we chose twin-aisle configuration because it provides more space for passenger and shortens boarding and deplane time. But in the negative side, this configuration incurs that our seat width and aisle width are both narrower than our competitors such as B737-700 and A319 which will weaken comfort of our aircraft. After careful analysis of future aviation market and consideration about requirements of customers, we made a compromise that to add single-aisle configuration which based on Jade concept into our Flying Crane's cabin design. In this new single-aisle configuration, width of seat in economy class is 19 inches and width of aisle is 23 inches. As an alternative configuration, we can also reduce width of aisle to 20 inches and widen seat to 19.5 inches. Seat width and aisle width in business class are 21 inches and 34 inches respectively. Cross-section drawings of single-aisle configuration are displayed below.

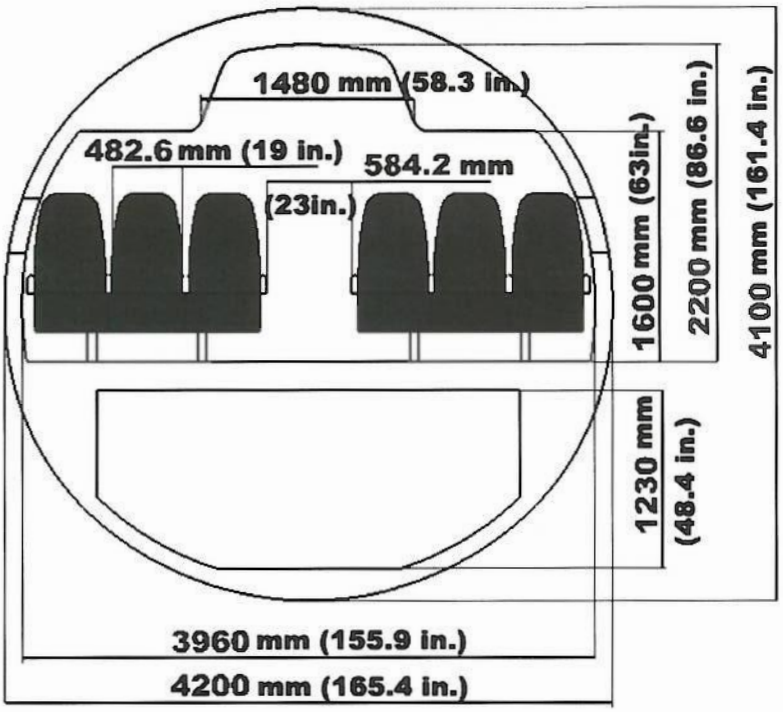

FigureA.14 Cross-section of economy class in single-aisle configuration

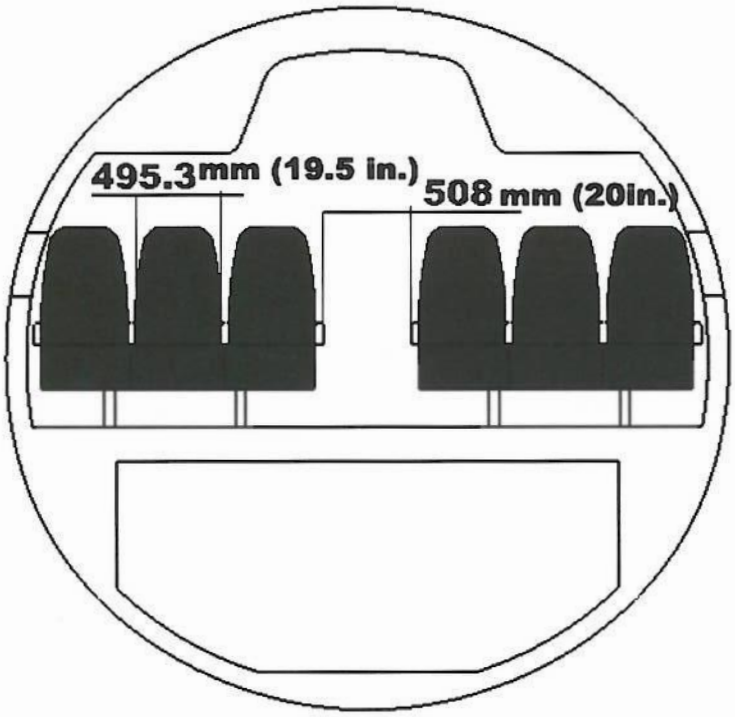

FigureA.15 Alternative Cross-section of economy class in single-aisle configuration

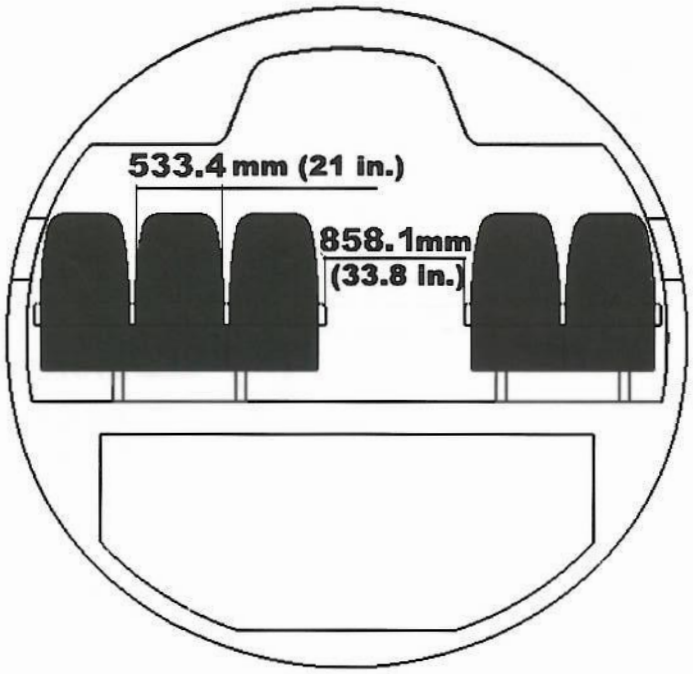

FigureA.16 Cross-section of business class in single-aisle configuration

Comparing with A319 and B737-700, which have similar passenger capacity and range to our Flying Crane, our concept has bigger seat and wider aisle, which means more cabin space for each passenger. FigureA.17 and FigureA.18 are cross-section comparison between Flying Crane and A319 and Flying Crane and B737-700 separately. The black line, blue line and red line demonstrate cross-section of Flying Crane, A319 and B737-700 respectively.

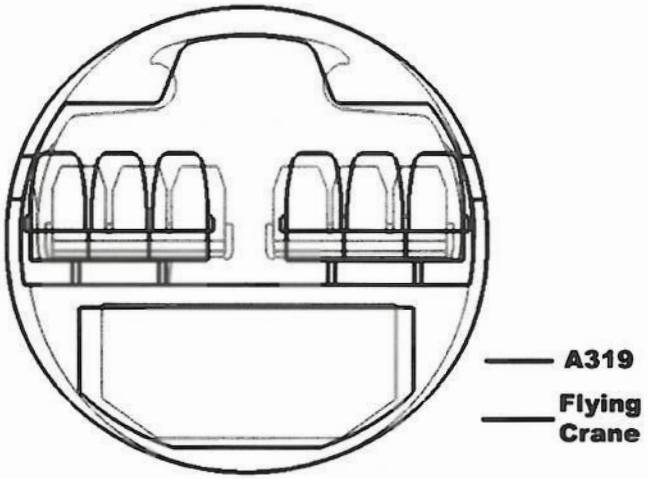

FigureA.17 Cross-section comparison between Flying Crane and A319

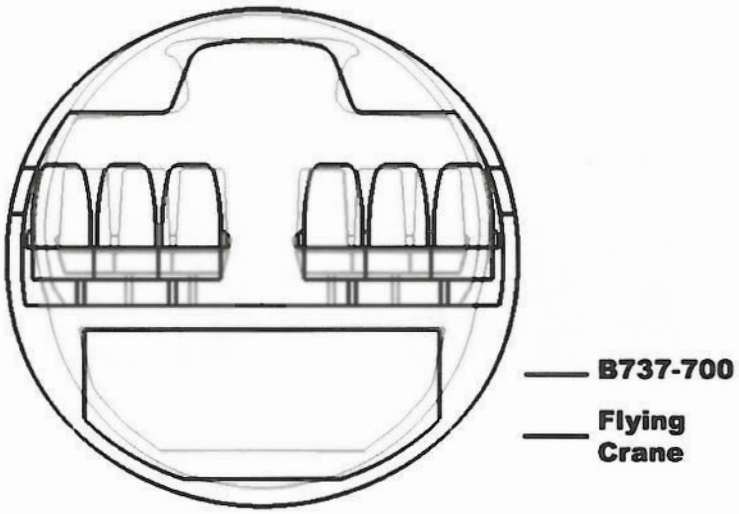

FigureA.18 Cross-section comparison between Flying Crane and B737-700

We also considered shifting the cabin into cargo configuration as an alternative. After all passenger seats are removed, the cabin can contain 8 ISO LD3 freight containers, or 8 LD4 containers, or 7 LD7 containers, or 8 standard pallet whose size is 3175mm× 2235mm.

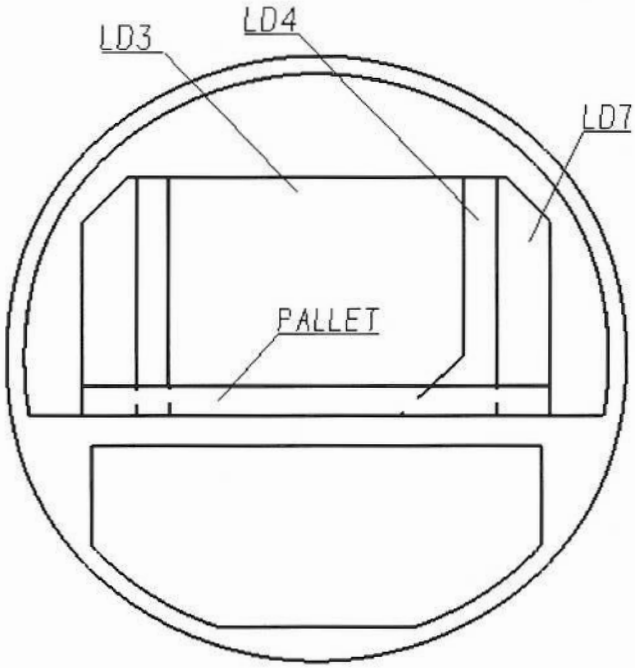

FigureA.19 Cross-section of cargo configuration

Digital mock-ups produced by CATIA of all the cabin configurations mentioned above were completed in this phase.

A.3 Conclusion

Through long time hard working and close cooperation, we worked out a brilliant new generation more comfortable airliner concept finally. This process consists of four phases which has close relationship to each other and lasts 6 months. We established it from totally blank sheet and experienced the whole procedure from initial data collection to final presentation. This is brand new experience for most of us and we all learned much from it.

Firstly, we learned how to start a new project with comprehensive survey of market to find position of our product in future competition and data collection about existing similar prototypes as reference. Secondly, we learned how to use several different methods to estimate some parameters and to evaluate accuracy of them, which provides input for next iterative process. Thirdly, we got some idea about which aspects should be considered and what weighting factor should be given to them respectively when we evaluate a concept. Last but not least, this group design project let us realize deeply that how important team-work is for success of a project.

Appendix B
Calculation about lift coefficient of Flying Crane's wing at low speed

B.1 Introduction

The main objective of calculations appearing in this chapter is to estimate the aerodynamic performance on Flying Crane's wing at low speed (M=0.2), such as take-off and landing, while high lift devices will be used. The estimated flaps position which is required by low speed configuration to obtain maximum performance would be defined through these calculations. The numerical methods used in these calculations are based on procedures derived in Engineering Sciences Data Unit (ESDU).

B.2 Airfoil datasheet

Data of baseline airfoil for Flying Crane, NASA SC(2)-0612, are presented in TableB.1 [2]. The first page of TableB.1 is coordinates of airfoil's upper surface with respect to horizontal axis from trailing edge to leading edge. The second page is coordinates of lower surface from leading edge to trailing edge. In order to permit convenient structure design and provide sufficient fuel volume, the airfoil is scaled at root (16% thick), kink (14%) and tip (10%).

B.3 Flying Crane's equivalent straight tapered wing planform

Calculations about aerodynamic properties in ESDU are applied on the case of straight swept tapered wing. So Flying Crane's wing which has a straight leading edge and a single crank trailing edge should be represented by an equivalent wing planform. FigureB.1 demonstrates relationship between the original wing and equivalent wing planform.

In FigureB.1, some parameters have been defined in Flying Crane Specification [2].

$s_0 = 2.1\text{m}$ $\quad c_b = 7.46\text{m}$

$s_1 = 6.537\text{m}$ $\quad c_1 = 3.176\text{m}$

$s = 16.74\text{m}$ $\quad c_t = 1.63\text{m}$

$\Lambda_0 = 28^\circ$ $\quad \Lambda_{1/4} = 25^\circ$

TableB. 1 NASA SC(2)-0612 Airfoil Datasheet [2]

1	-0.0067
0.99	-0.0041
0.98	-0.0016
0.97	0.0008
0.96	0.0031
0.95	0.0053
0.94	0.0075
0.93	0.0096
0.92	0.0117
0.91	0.0137
0.9	0.0157
0.89	0.0176
0.88	0.0195
0.87	0.0213
0.86	0.0231
0.85	0.0248
0.84	0.0265
0.83	0.0281
0.82	0.0297
0.81	0.0313
0.8	0.0328
0.79	0.0343
0.78	0.0357
0.77	0.0371
0.76	0.0384
0.75	0.0397
0.74	0.041
0.73	0.0422
0.72	0.0434
0.71	0.0445
0.7	0.0456
0.69	0.0466
0.68	0.0476
0.67	0.0486
0.66	0.0495

0.65	0.0504
0.64	0.0512
0.63	0.052
0.62	0.0527
0.61	0.0534
0.6	0.0541
0.59	0.0547
0.58	0.0553
0.57	0.0558
0.56	0.0563
0.55	0.0568
0.54	0.0572
0.53	0.0576
0.52	0.058
0.51	0.0583
0.5	0.0586
0.49	0.0589
0.48	0.0592
0.47	0.0594
0.46	0.0596
0.45	0.0598
0.44	0.0599
0.43	0.06
0.42	0.0601
0.41	0.0602
0.4	0.0602
0.39	0.0602
0.38	0.0602
0.37	0.0602
0.36	0.0601
0.35	0.06
0.34	0.0599
0.33	0.0597
0.32	0.0595
0.31	0.0593

0.3	0.0591
0.29	0.0588
0.28	0.0585
0.27	0.0581
0.26	0.0577
0.25	0.0573
0.24	0.0568
0.23	0.0563
0.22	0.0557
0.21	0.0551
0.2	0.0545
0.19	0.0538
0.18	0.0531
0.17	0.0523
0.16	0.0514
0.15	0.0505
0.14	0.0495
0.13	0.0484
0.12	0.0472
0.11	0.046
0.1	0.0447
0.09	0.0432
0.08	0.0416
0.07	0.0398
0.06	0.0378
0.05	0.0355
0.04	0.0329
0.03	0.0296
0.02	0.0252
0.01	0.019
0.005	0.0141
0.002	0.0092
0	0

TableB. 1 NASA SC(2)-0612 Airfoil Datasheet

0	0
0.002	-0.0092
0.005	-0.0141
0.01	-0.019
0.02	-0.0252
0.03	-0.0296
0.04	-0.0329
0.05	-0.0355
0.06	-0.0378
0.07	-0.0398
0.08	-0.0416
0.09	-0.0432
0.1	-0.0447
0.11	-0.046
0.12	-0.0473
0.13	-0.0485
0.14	-0.0496
0.15	-0.0506
0.16	-0.0515
0.17	-0.0524
0.18	-0.0532
0.19	-0.054
0.2	-0.0547
0.21	-0.0554
0.22	-0.056
0.23	-0.0565
0.24	-0.057
0.25	-0.0575
0.26	-0.0579
0.27	-0.0583
0.28	-0.0586
0.29	-0.0589
0.3	-0.0592
0.31	-0.0594
0.32	-0.0595
0.33	-0.0596
0.34	-0.0597
0.35	-0.0598
0.36	-0.0598
0.37	-0.0598
0.38	-0.0598
0.39	-0.0597
0.4	-0.0596
0.41	-0.0594
0.42	-0.0592
0.43	-0.0589

0.44	-0.0586
0.45	-0.0582
0.46	-0.0578
0.47	-0.0573
0.48	-0.0567
0.49	-0.0561
0.5	-0.0554
0.51	-0.0546
0.52	-0.0538
0.53	-0.0529
0.54	-0.0519
0.55	-0.0509
0.56	-0.0497
0.57	-0.0485
0.58	-0.0472
0.59	-0.0458
0.6	-0.0444
0.61	-0.0429
0.62	-0.0414
0.63	-0.0398
0.64	-0.0382
0.65	-0.0365
0.66	-0.0348
0.67	-0.033
0.68	-0.0312
0.69	-0.0294
0.7	-0.0276
0.71	-0.0258
0.72	-0.024
0.73	-0.0222
0.74	-0.0204
0.75	-0.0186
0.76	-0.0168
0.77	-0.015
0.78	-0.0133
0.79	-0.0117
0.8	-0.0102
0.81	-0.0087
0.82	-0.0073
0.83	-0.006
0.84	-0.0048
0.85	-0.0037
0.86	-0.0028
0.87	-0.0021
0.88	-0.0016
0.89	-0.0012

0.9	-0.001
0.91	-0.001
0.92	-0.0013
0.93	-0.0018
0.94	-0.0025
0.95	-0.0035
0.96	-0.0048
0.97	-0.0063
0.98	-0.0081
0.99	-0.0102
1	-0.0125

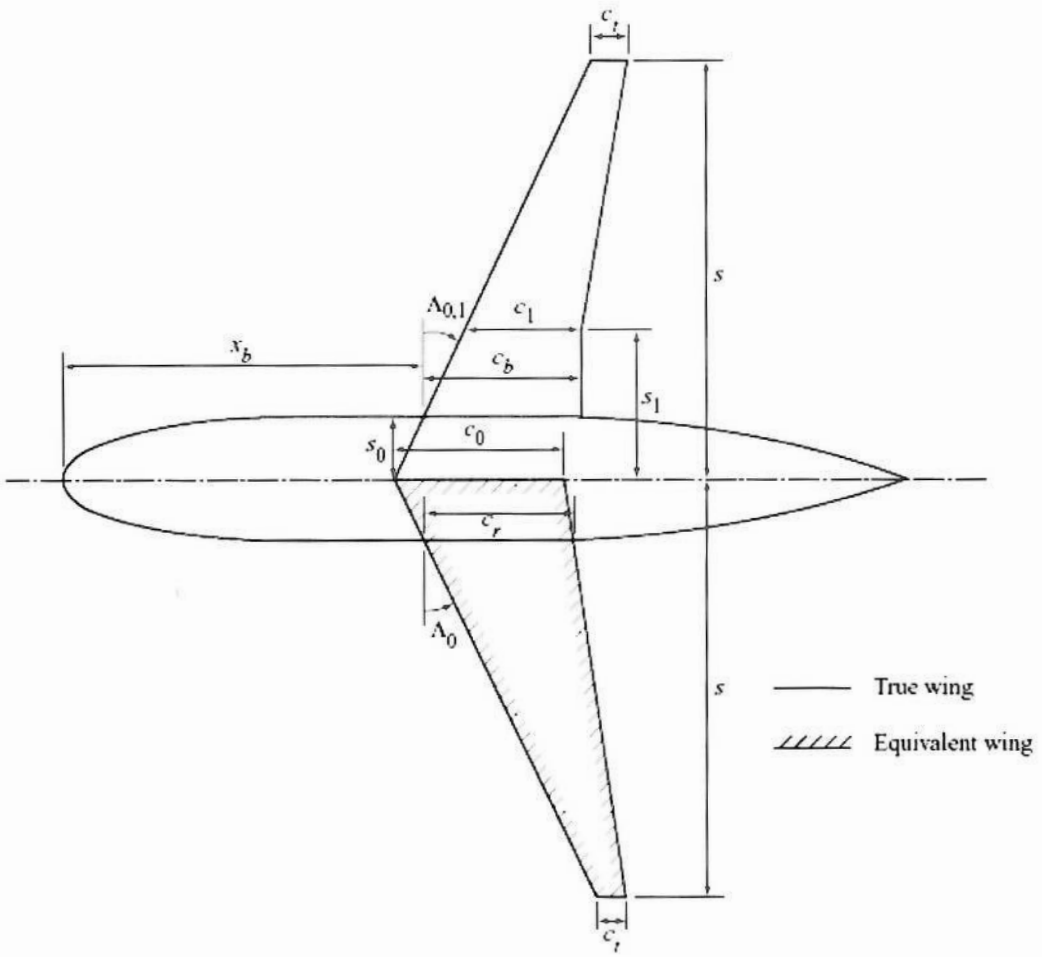

FigureB.1 Equivalent Straight Swept Tapered Wing Planform [11]

Via equations coming from reference [11], the calculating process could be run as below.

The equivalent wing area is given by

$$S_e = (c_b + c_1)(s_1 - s_0) + (c_1 + c_t)(s - s_1) \qquad \text{(A4.1) [11]}$$

$$= (7.46+3.176)(6.537-2.1)+(3.176-1.63)(16.74-6.537)$$

$$= 96.227\text{m}^2$$

The equivalent root chord is given by,

$$c_r = \frac{S_e}{s - s_0} - c_t \qquad \text{(A4.2) [11]}$$

$$= \frac{96.227}{16.74 - 2.1} - 1.63$$

$= 4.943\text{m}$

The centre-line chord of the equivalent wing planform is given by

$$c_0 = \frac{sc_r - s_0 c_t}{s - s_0} \qquad \text{(A3.4) [11]}$$

$$= \frac{16.74 \times 4.943 - 2.1 \times 1.63}{16.74 - 2.1}$$

$$= 5.418\text{m}$$

The taper ratio is given by

$$\lambda = \frac{c_t}{c_0} = \frac{1.63}{5.418} = 0.301 \qquad \text{(A3.5) [11]}$$

The standard mean chord is given by

$$\bar{c} = c_0 \frac{1+\lambda}{2} \qquad \text{(A3.6) [11]}$$

$$= 5.418 \times \frac{1+0.301}{2}$$

$$= 3.524\text{m}$$

The aerodynamic mean chord is given by

$$\bar{\bar{c}} = \frac{2}{3} c_0 \left(\frac{1+\lambda+\lambda^2}{1+\lambda} \right) \qquad \text{(A3.7) [11]}$$

$$= \frac{2}{3} \times 5.418 \times \frac{1+0.301+0.301^2}{1+0.301}$$

$$= 3.863\text{m}$$

The aspect ratio is given by

$$A = \frac{2s}{\bar{c}} = \frac{2 \times 16.74}{3.524} = 9.5 \qquad \text{(A3.8) [11]}$$

The gross wing area is given by

$$S = 2s\bar{c} = 2 \times 16.74 \times 3.524 = 117.985\text{m}^2 \qquad \text{(A3.9) [11]}$$

The equivalent wing sweepback of the half-chord line is given by

$$\Lambda_{1/2} = \tan^{-1}\left[\tan \Lambda_0 - \frac{2}{A}\left(\frac{1-\lambda}{1+\lambda} \right) \right] \qquad \text{(A3.11) [11]}$$

$$= \tan^{-1}\left[\tan 28^\circ - \frac{2}{9.5}\left(\frac{1-0.301}{1+0.301}\right)\right]$$

$$= 22.71^\circ$$

B.4 Maximum lift coefficient of Flying Crane's basic clean wing

These calculations are based on the procedure presented in reference [12] [13] [14] [15] [16].

The wing taper parameter for a straight tapered wing is given by

$$\kappa = \frac{1+2\lambda}{3(1+\lambda)} = \frac{1+2\times 0.301}{3\times(1+0.301)} = 0.410 \qquad (4.1)\ [12]$$

Due to the high lift devices are only deployed at low speed, in which Mach number (M) is defined as 0.2, hence

$$\beta = \sqrt{1-M^2} = \sqrt{1-0.2^2} = 0.9798$$

$\beta A = 0.9798\times 9.5 = 9.308$

$A \tan \Lambda_{1/2} = 9.5\times\tan(22.71^\circ) = 3.977$

From figures 1 to 5 of reference [13], values of spanwise center of pressure position ($\bar{\eta}$) could be obtained for $A \tan \Lambda_{1/2} = 3.977$, $\kappa = 0.410$, $\beta A = 1.5$, 3, 5, 8 and 12 respectively. The results are tabulated in TableB.2 and plotted on FigureB.2. Meanwhile, the value of $\bar{\eta}$ for $\beta A = 9.308$ could also be gotten by means of linear interpolation.

$\bar{\eta} = 0.432$ when $\beta A = 9.308$

βA	1.5	3	5	8	12
$\bar{\eta}$	0.4475	0.4446	0.4406	0.4349	0.4311

TableB.2 Tabulated spanwise center of pressure

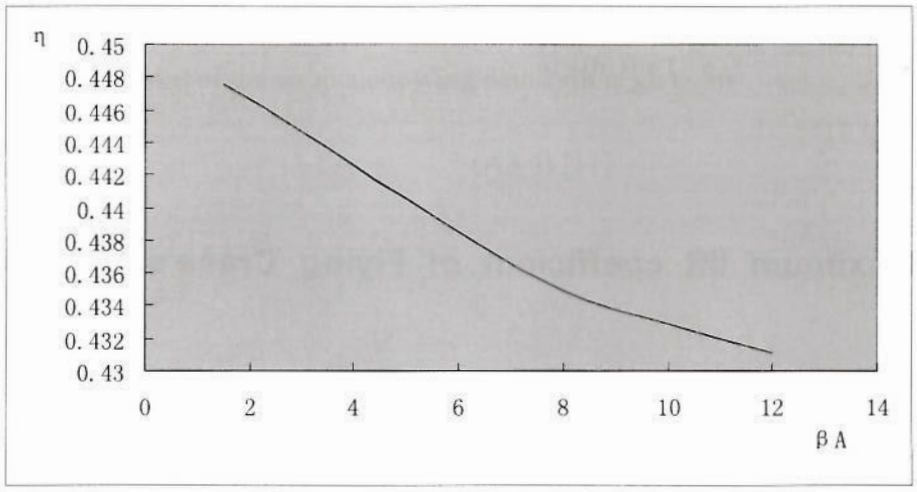

FigureB.2 β A vs. $\bar{\eta}$

From figures 1 and 2 of reference [12], value of ηp and μp for $\bar{\eta}$=0.432 and λ =0.301 is 0.716 and 1.186 respectively.

So the Reynolds number at ηp could be calculated as shown below:

$$c_p \Big/ \bar{c} = \frac{3}{2}\left(\frac{1+\lambda}{1+\lambda+\lambda^2}\right)\left(1-\eta_p+\lambda\eta_p\right) \qquad (8.2)\ [14]$$

$$= \frac{3}{2}\left(\frac{1+0.301}{1+0.301+0.301^2}\right)\left(1-0.716+0.301\times 0.716\right)$$

$$= 0.717$$

$$R_{cp} = R_c \times c_p \Big/ \bar{c} \qquad (8.5)\ [14]$$

$$= 15.4\times 10^6 \times 0.717$$

$$= 11.04\times 10^6$$

Hence,

$R_{cp}\cos^2\Lambda_0 = 11.04\times 10^6 \times \cos^2 28^\circ = 8.6\times 10^6$

As the baseline airfoil has been defined, following values could be measured from the airfoil sketch.

For root section:

η=0

$z_{u1.25}/c = 0.0335$; $x_{um}/c = 0.3330$; $z_{um}/c = 0.0741$

For tip section:

$\eta = 1$

$z_{u1.25}/c = 0.0195$; $x_{um}/c = 0.4625$; $z_{um}/c = 0.0698$

Interpolation gives the section for $\eta_p = 0.716$:

$z_{u1.25}/c = 0.0235$; $x_{um}/c = 0.4257$; $z_{um}/c = 0.0710$

Hence,

$$\tan \tau_u = \frac{z_{um}/c}{1 - x_{um}/c} = \frac{0.0710}{1 - 0.4257} = 0.124 \qquad (3.1)\ [14]$$

From figure2 of reference [14], when $R_{cp} \cos^2 \Lambda_0 = 8.6 \times 10^6$, $z_{u1.25}/c = 0.0235$ and $\tan \tau_u = 0.124$, the increment of lift coefficient, $\Delta C_L \cong 1.83$. Assuming in ideal situation there is no twist at wing tip section, the lift coefficient at zero incidence (C_{L0}) and increment in lift coefficient due to wing twist (ΔC_{LT}) are both zero.

Maximum wing lift coefficient is given by

$$C_{Lm} = \Delta C_L + C_{L0} \sec \Lambda_0$$

$= 1.83 + 0$

$= 1.83$

When

$M \cos \Lambda_0 = 0.2 \times \cos 28^\circ = 0.177$

$$\zeta_p = (z_{u1.25}/c)_p \sec \Lambda_0$$

$= 0.0235 \times \sec 28^\circ$

$= 0.0266$

From figure3 of reference [16], the increment of wing maximum lift coefficient due to Mach number is given by

$$\Delta C_{LM} / \cos^4 \Lambda_0 = -0.15$$

Hence,

$$\Delta C_{LM} = -0.15 \times \cos^4 (28^\circ) = -0.09$$

Since $\Lambda_0 < 37°$, figure4 of reference [16] gives the increment of lift coefficient caused by Reynolds number (ΔC_{LR}) is zero. And for $\Lambda_0 = 28°$, $\zeta p = 0.0266$, figure5b gives the increment of lift coefficient due to sweepback ($\Delta C_{L\Lambda}$) is 0.049.

The maximum lift coefficient of basic Flying Crane's clean wing is given by

$$C_{L\max} = C_{Lm}/\mu_p + \Delta C_{LM} + \Delta C_{LR} + \Delta C_{L\Lambda} + \Delta C_{LT} \qquad (6.9)\ [13]$$

$$= (1.83 / 1.186) - 0.09 + 0 + 0.049 + 0$$

$$= 1.50$$

B.5 Maximum increment in wing lift coefficient due to trailing edge flaps

Single slotted Fowler flap was chosen as trailing edge high lift device for Flying Crane aircraft. And theoretically, chord of flap airfoil takes 30 percent proportion of local wing chord. Flap deflection in take-off and landing configuration is 25° and 45° respectively. [2] Trailing edge flaps are divided into inboard and outboard flap by the single crank on wing trailing edge. Hinge lines of flaps are approximately parallel to rear spar of the wing. In planform, inboard flap is square and outboard flap is tapered because of taper ratio of the wing. Therefore, reference [15] (for airfoil) and reference [16] (for wing) are used to calculate the increment in maximum lift coefficient yielded by deployment of single slotted Fowler flap.

The shape of wing's trailing edge is formed by upper and lower surface of trailing edge flaps. Thus, the airfoil of flap could be drafted in CATIA sketch according to the trailing edge of NASA SC(2)-0612 section. Other constraints for the flap airfoil are its 30 percent proportion in local wing chord and its leading edge shape should be smooth. Coordinates of Flying Crane's flap airfoil at kink section are presented in TableB.3. Data at other sections could be obtained by scaling values in TableB.3 with ratio of local chord length.

TableB.3 Flying Crane's Flap Airfoil Coordinates (mm)

3865	-48.3125
3859.274	-47.2712
3845.871	-44.8306
3822.51	-40.6005
3790.421	-35.199
3750.043	-29.5444
3702.032	-23.917
3647.174	-18.5753
3586.353	-14.229
3520.544	-11.7802
3450.815	-11.7099
3378.317	-13.8134
3304.246	-17.9009
3229.816	-23.9324
3156.255	-31.6684
3084.776	-40.6747
3016.563	-50.4917
2952.745	-60.6879
2894.374	-70.8441
2842.446	-79.4653
2797.978	-80.456
2761.767	-71.3311
2734.279	-56.9816
2715.929	-38.8655
2710.284	-28.3641
2707.025	-17.0427
2706.159	-5.24624
2707.673	6.534012
2711.553	17.8612
2717.777	28.50784
2726.323	38.44149
2737.155	47.70694
2750.229	56.33665
2765.494	64.33563
2782.889	71.70234
2802.342	78.4472
2823.776	84.58722
2847.103	90.12432
2872.226	95.02877
2899.044	99.2488
2927.443	102.7365
2957.306	105.4715
3020.933	108.683
3088.882	108.8812
3160.037	106.0756
3233.228	100.316
3307.253	91.5843
3380.917	80.84458
3453.046	69.49962
3522.443	57.35245
3587.965	44.45211
3648.539	31.12228
3703.176	17.74456
3750.995	5.086393
3791.231	-5.78002
3823.226	-14.424
3846.553	-20.7533
3854.644	-22.9471
3859.854	-24.3584
3865	-25.7485

The maximum lift coefficient of the basic airfoil, $(C_{LmB})_d$ and the slope of lift coefficient curve, $(a_1)_0$ are calculated in advance with the means presented in reference [14] and [17] respectively.

In NASA SC(2)-0612 two-dimensional airfoil,

$t/c = 0.12$, $y_{90}/c = 0.0166$, $y_{99}/c = 0.0061$, and $\tau = 1.42°$

Where y90, y99 and τ is defined as shown in FigureB.3.

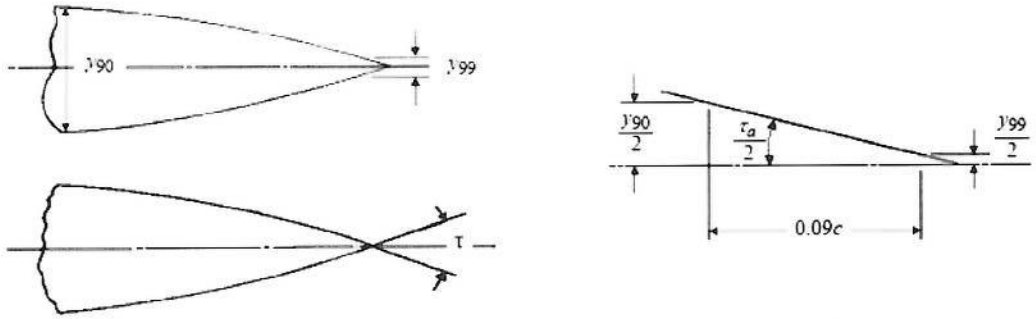

FigureB.3 Symbol definition on wing's trailing edge [17]

From figure1 of reference [17], it can be read that

$(a_1)_0/(a_1)_{0T} = 0.918$

Knowing

$\log_{10} R = \log_{10}(15.4\times10^6) = 7.19$

And

$\tan(\tau_a/2) = (y_{90}/2 - y_{99}/2)/(0.09c)$

$= (y90/c - y99/c)/(2\times0.09)$

$= (\ 0.0166 - 0.0061\ ) / 0.18$

$= 0.059$

From figure3 of reference [11] for $t/c = 0.12$ and $\tau = 1.42°$,

$(a_1)_{0T} = 6.85$

Hence the slope of lift curve for two-dimensional airfoil NASA SC(2)-0612 section is

$(a_1)_0 = 6.288$

The zero lift angle is given by

$$\alpha_0 = -\frac{\pi}{90}\sum_{i=1}^{14}(B_i z_{ci}/c) \qquad (5.1)\ [14]$$

Where

$$z_{ci} = (z_{ui} + z_{li})/2 \qquad (5.2)\ [14]$$

The coefficients B_i are defined in Table5.1 of reference [14] as function of x_i/c. The value of $\sum(B_i z_{ci}/c)$ for NASA SC(2)-0612 airfoil is shown in TableB.3.

Therefore

$$\alpha_0 = -\frac{\pi}{90}\sum_{i=1}^{14}(B_i z_{ci}/c) = -\frac{\pi}{90}\times 1.693 = -0.0591$$

And the lift coefficient at zero incidence is given by

$$C_{L0} = -\alpha_0 (a_1)_0 = -(-0.0591\times 6.288) = 0.3715 \qquad (5.3)\ [14]$$

i	x_i/c	B_i	z_{ui}	z_{li}	z_{ci}	$B_i\ z_{ci}/c$
1	0	1.45	0	0	0	0
2	0.025	2.11	108.318	-104.736	1.791	0.000978
3	0.05	1.56	140.058	-134.394	2.832	0.001143
4	0.1	2.41	177.923	-167.655	5.134	0.003201
5	0.2	2.94	220.502	-201.595	9.4535	0.00719
6	0.3	2.88	243.01	-214.259	14.3755	0.010711
7	0.4	3.13	252.023	-211.084	20.4695	0.016576
8	0.5	3.67	250.571	-190.162	30.2045	0.028678
9	0.6	4.69	237.911	-142.889	47.511	0.057648
10	0.7	6.72	209.799	-73.025	68.387	0.118894
11	0.8	11.75	165.125	-0.775	82.175	0.249801
12	0.9	21.72	103.916	39.625	71.7705	0.403295
13	0.95	99.85	66.204	32.325	49.2645	1.27262
14	1	-164.88	22.417	0	11.2085	-0.47811
$\Sigma\ (B_i\ z_{ci}/c)$						1.69262

TableB.3 Calculation of sum $B_i\ z_{ci}/c$

τ_u is specified as the angle between the chord line and a line drawn from the maximum upper surface ordinate to the trailing edge point, shown in FigureB.4. And

its value is given by

$$\tan\tau_u = (z_{um}/c)/(1-x_{um}/c) \qquad (3.1)\ [14]$$

Where $z_{um}/c = 0.0649$, $x_{um}/c = 0.3792$

Hence $\tan\tau_u = 0.0649/(1-3792) = 0.105$

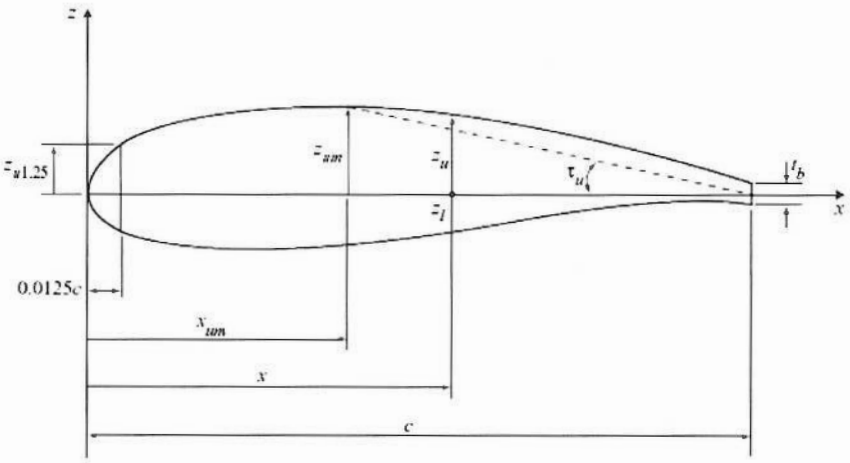

FigureB.4 Airfoil geometry [14]

From figure2 of reference [14] for $z_{u1.25}/c = 0.0212$, $R_c = 15.4\times10^6$, $\tan\tau_u = 0.105$

$\Delta C_L = 1.66$

From figure5 of [14] for $R_c = 15.4\times10^6$

$F_S = 1.145$

From figure6 of [14] for M=0.2

$F_1 = 0.0375$

From figure7 of [14] for $(z_{u0.05} - z_{u0.01})/c = 0.0169$

$F_2 = 2.225$

The Mach number factor is given by

$F_M = 1\text{-}F_1F_2 = 0.9166$ (7.1) [14]

The maximum lift coefficient of NASA SC(2)-0612 basic airfoil is given by

$$(C_{LmB})_d = (C_{L0} + \Delta C_L)F_S F_M \qquad (2.1)\ [14]$$

$= (0.3715+1.66) \times 1.145 \times 0.9166$

$= 2.13$

Parameters involved in the calculation about ΔC_{Lmt} for single slotted flap in NASA SC(2)-0612 airfoil without considering leading edge device are shown in FigureB.5. The calculation is based on the procedures provided by reference [15].

For landing configuration, relevant parameters are tabulated in TableB.4. Unit is millimeter for lengths and degree for angles. Those values are measured from wing cross-section at kink point of the wing [2].

Airfoil		Flap	
t/c	0.12	c_{t1}	940.78
c	3135.9	δ_{t1}	45
$z_{u1.25}/c$	0.0212	Δc_{t1}	0
x_{um}/c	0.3792	x_{ts}	2799.4
$\Delta c_l/c$	0.0651	c_{t1}'/c'	0.2428
c'/c	1.2354		

TableB.4 Airfoil and Flap's parameters

The flow conditions are M=0.2 and R=15.4×10^6

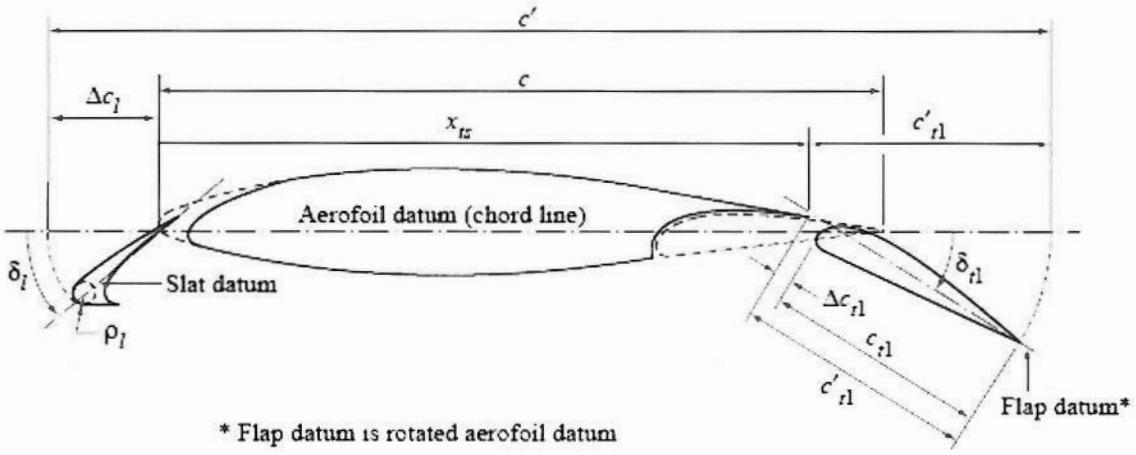

FigureB.5 Single-slotted trailing edge flap with typical leading edge slat [15]

From figure1 of reference [15] for δ tl = 45°

$J_{tl} = 1.17$

From figure2 of [15] for δ tl = 45° and $c_{tl}'/c' = 0.2428$

$\Delta C'_{L1} = 1.41$

The increment in lift coefficient at zero angle of attack due to the deployment of single slotted trailing edge flap is given by

$$\Delta C'_{L0t} = J_{t1}\Delta C'_{L1}(a_1)_0 / 2\pi \qquad (4.1)\ [15]$$

$= 1.17\times1.41\times6.288/2\ \pi$

$= 1.651$

Hence

$$\Delta C_{L0t} = \frac{c'}{c}\Delta C'_{L0t} \qquad (3.3)\ [15]$$

$=1.2354\times1.651$

$= 2.04$

From figure3 of [15] for $z_{u1.25}/c = 0.0212$, $x_{um}/c = 0.3792$

$K_T = 2.45$

From figure4 of [15] for δ tl = 45°

$K_{t1} = 0.35$

The increment in maximum lift coefficient due to the deployment of single slotted trailing edge flap is given by

$$\Delta C'_{Lmt} = (1-c/c')(1-\sin\delta_{t1})(C_{LmB})_d + K_T K_{t1} J_{t1}\Delta C'_{L1} \qquad (4.9)\ [15]$$

$= (1\text{-}1/1.2354)(1\text{-}\sin45^\circ)\times2.13 + 2.45\times0.35\times1.17\times1.41$

$= 1.53$

The factor for effect of Reynolds number is given by

$$F_R = 0.153\log_{10} R_c \qquad (3.5)\ [15]$$

$= 0.153\times\log_{10}(15.4\times10^6)$

$= 1.10$

Therefore

$$\Delta C_{Lmt} = F_R\frac{c'}{c}\Delta C'_{Lmt} \qquad (3.4)\ [15]$$

$= 1.10\times1.2354\times1.53$

$= 2.08$

ΔC_{Lmt} is used to calculate increment in wing maximum lift coefficient. Calculating method comes from reference [16].

In spanwise of Flying Crane wing, the distance between inboard and outboard flaps'

border and aircraft center line is presented by symbol s_i and s_o respectively, and the value is

$s_i = 2.3$ m

$s_o = 12.221$ m

Knowing

$$A\tan\Lambda_{1/2} - 8\lambda = 9.5\times\tan(22.71^\circ) - 8\times 0.3008 = 1.570$$

From figure3b for $\eta_i = \frac{s_i}{s} = \frac{2.3}{16.74} = 0.1374$

$\Phi i = 0.11$

For $\eta_o = \frac{s_o}{s} = \frac{12.221}{16.74} = 0.73$

$\Phi o = 0.88$

The increment in wing maximum lift coefficient due to deployment of trailing edge flaps for swept wing is given by

$$\Delta C_{L\max t} = K_f K_{\Lambda t}\cos(\Lambda_h) F_R(\Delta C_{Lmt}/\mu_p)(\Phi_o - \Phi_i) \qquad (6.5)\ [16]$$

Where factor $K_{\Lambda t}$ is given by

$$K_{\Lambda t} = \cos^{2.5}\Lambda_{1/4} = \cos^{2.5}(25^\circ) = 0.782 \qquad (6.7)\ [16]$$

The hinge line sweep back angle of 70 percent chord line is given by

$$\Lambda_h = \tan^{-1}\left[\tan\Lambda_{1/4} + \frac{4}{A}\left(\frac{1}{4} - 0.70\right)\left(\frac{1-\lambda}{1+\lambda}\right)\right]$$

$$= \tan^{-1}\left[\tan 25^\circ + \frac{4}{9.5}\left(\frac{1}{4} - 0.70\right)\left(\frac{1-0.301}{1+0.301}\right)\right]$$

$$= 20.026^\circ$$

For a slotted flap, the factor $K_f = 1.1$. Therefore

$$\Delta C_{L\max t} = 1.1\times 0.782\times\cos(20.026^\circ)\times 1.10\times(2.08/1.186)(0.88-0.11) = 1.202$$

For take-off configuration, flap parameters are shown in TableB.5. Unit is millimeter for lengths and degree for angle.

C_{t1}	940. 78
δ_{t1}	25
Δc_{t1}	0
c'	3373. 3
c_{t1}'/ c'	0. 2789
c'/c	1. 0757

TableB.5 Parameters for take-off configuration

Thus, the value of $\Delta C_{L\max t}$ in take-off position could be obtained by the means having been done in landing position.

$J_{tl} = 1.17$ figure1 [15]

$\Delta C'_{L1} = 1.18$ figure2 [15]

$$\Delta C'_{L0t} = J_{t1}\Delta C'_{L1}(a_1)_0 / 2\pi = 1.382 \qquad (4.1)\ [15]$$

$$\Delta C_{L0t} = \frac{c'}{c}\Delta C'_{L0t} = 1.486 \qquad (3.3)\ [15]$$

$K_T = 2.45$ figure3 [15]

$K_{tl} = 0.35$ figure4 [15]

$$\Delta C'_{Lmt} = (1 - c/c')(1 - \sin\delta_{t1})(C_{LmB})_d + K_T K_{t1} J_{t1}\Delta C'_{L1} = 1.27 \qquad (4.9)\ [15]$$

$$\Delta C_{Lmt} = F_R \frac{c'}{c}\Delta C'_{Lmt} = 1.50 \qquad (3.4)\ [15]$$

$$\Delta C_{L\max t} = K_f K_{\Lambda t}\cos(\Lambda_h) F_R (\Delta C_{Lmt} / \mu_p)(\Phi_o - \Phi_i) = 0.867 \qquad (6.5)\ [16]$$

B6 SUMMARY

As a conclusion, by using the procedure coming from ESDU and presented in this chapter, the maximum lift coefficient of Flying Crane's basic clean wing is 1.50. Additional lift coefficient is acquired by means of deploying trailing edge and leading edge high lift devices. This increment due to single slotted Fowler flaps is 1.202 and 0.867 when they are landing and take-off position respectively. And the increment due to leading edge devices is assumed to be 0.5 which is based on empirical data provided by reference [7].

Thus, the total lift coefficient is

Take-off = 1.50 + 0.867 + 0.5 = 2.867

Landing = 1.50 + 1.202 + 0.5 = 3.202

It could fulfil the lift capability required by Flying Crane's specification [2], which is 2.5 and 3.0 for take-off and landing configuration respectively.

Appendix C

Flap motion validation

Data about flap status in different positions are presented in TableC.1. FigureC.1 to FigureC.5 illustrate the relationship between flap deflection, flap Fowler motion and swing angle of swing arms. FigureC.6 illustrates flap Fowler motion statistic data about 12 existing trailing edge flap mechanisms for airliner. FigureC.7 to FigureC.14 demonstrate detailed flap motion trails of the swing arm mechanism and some other types flap mechanism which are applied in several commercial airliners [18].

		swing angle (deg)	deflection (deg)	Fowler motion /Cw	gap/Cw
retracted	inboard	0	0	0	-
	outboard	0	0	0	-
take-off	inboard	23	24.6	0.082	-
	outboard	23	24.8	0.082	-
landing	inboard	61	44.9	1.183	0.022
	outboard	61	45	1.181	0.013

TableC.1 Flap status data

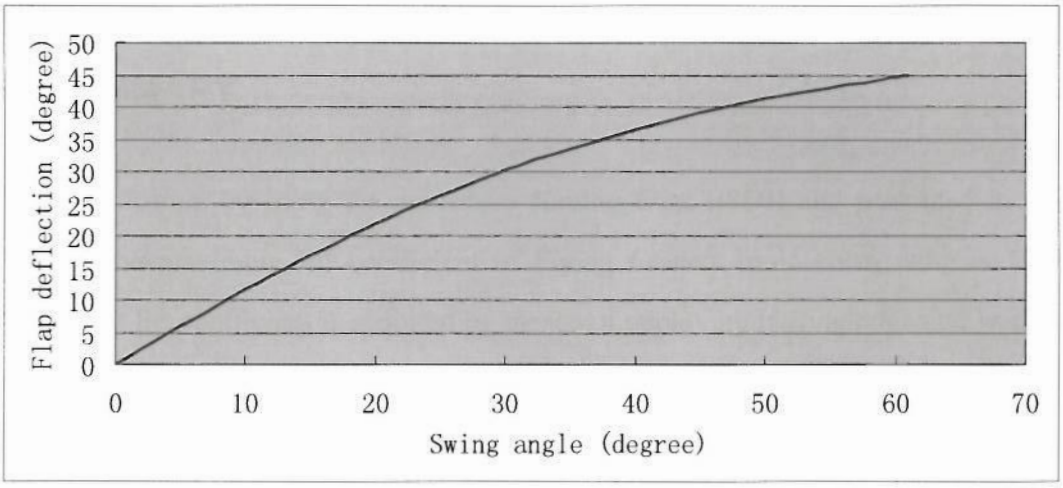

FigureC.1 Inboard flap deflection

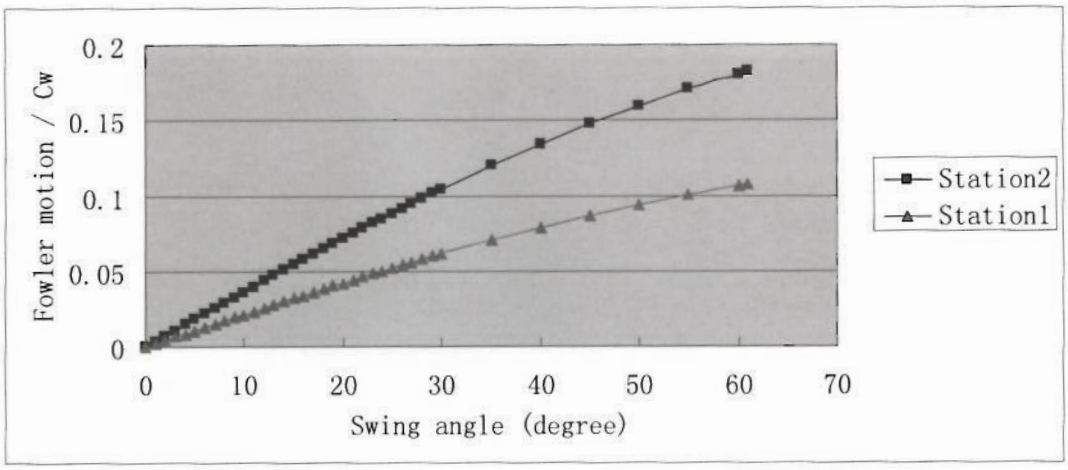

FigureC.2 Inboard flap Fowler motion

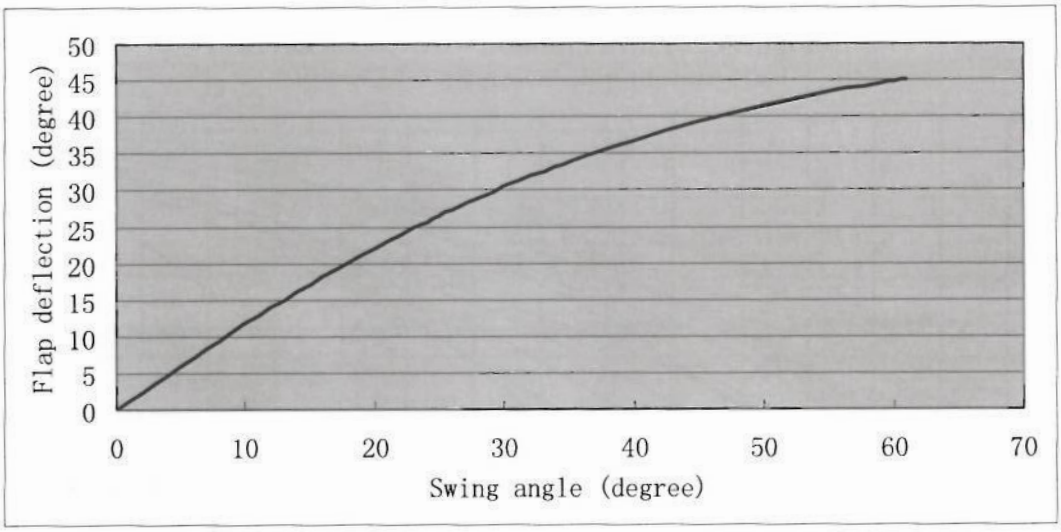

FigureC.3 Outboard flap deflection

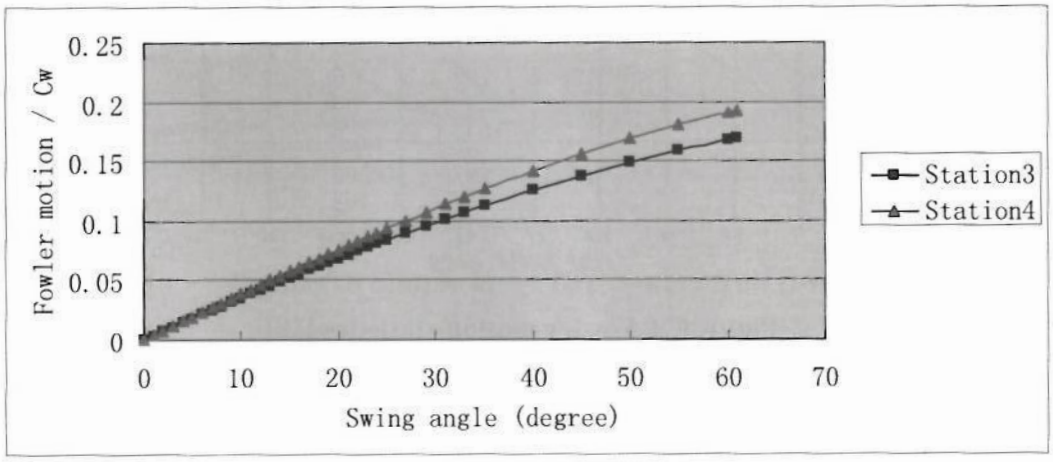

FigureC.4 Outboard flap Fowler motion

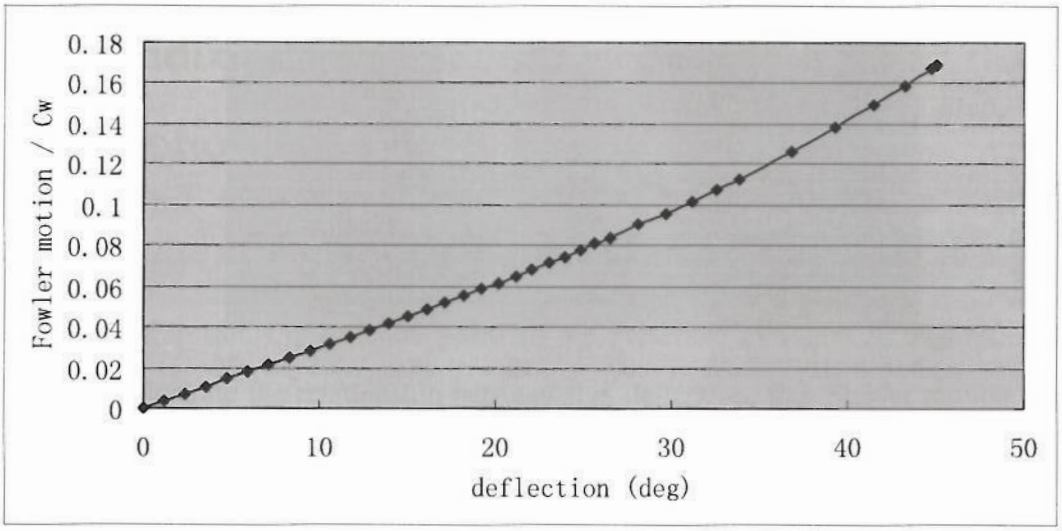

FigureC.5 Fowler motion – deflection curve

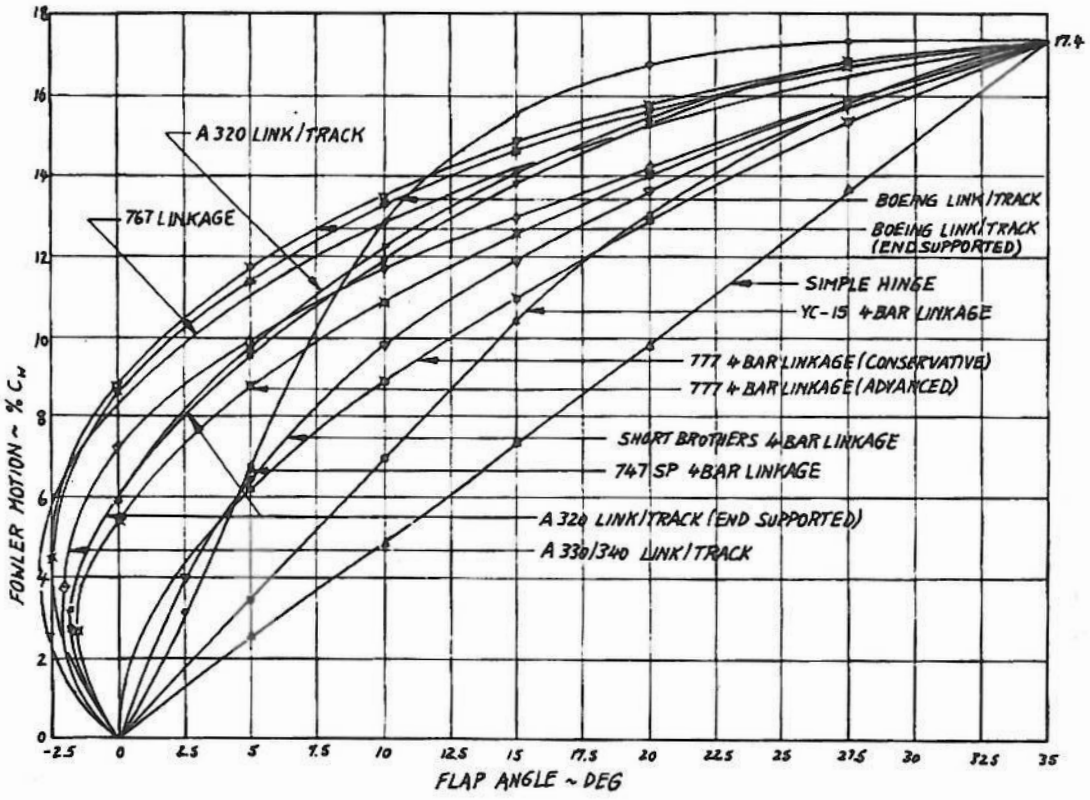

FigureC.6 Fowler motion statistics [18]

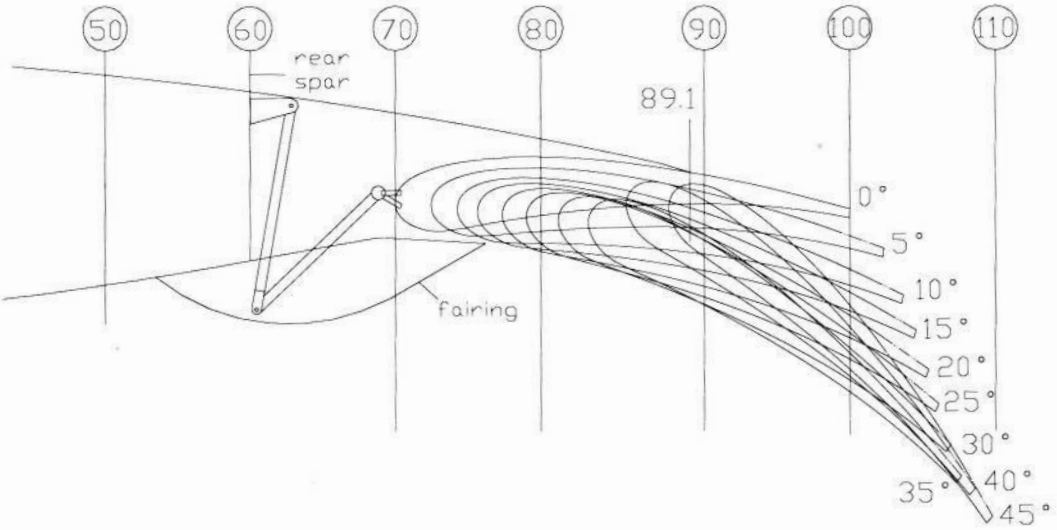

FigureC.7 Swing arm flap motion trail

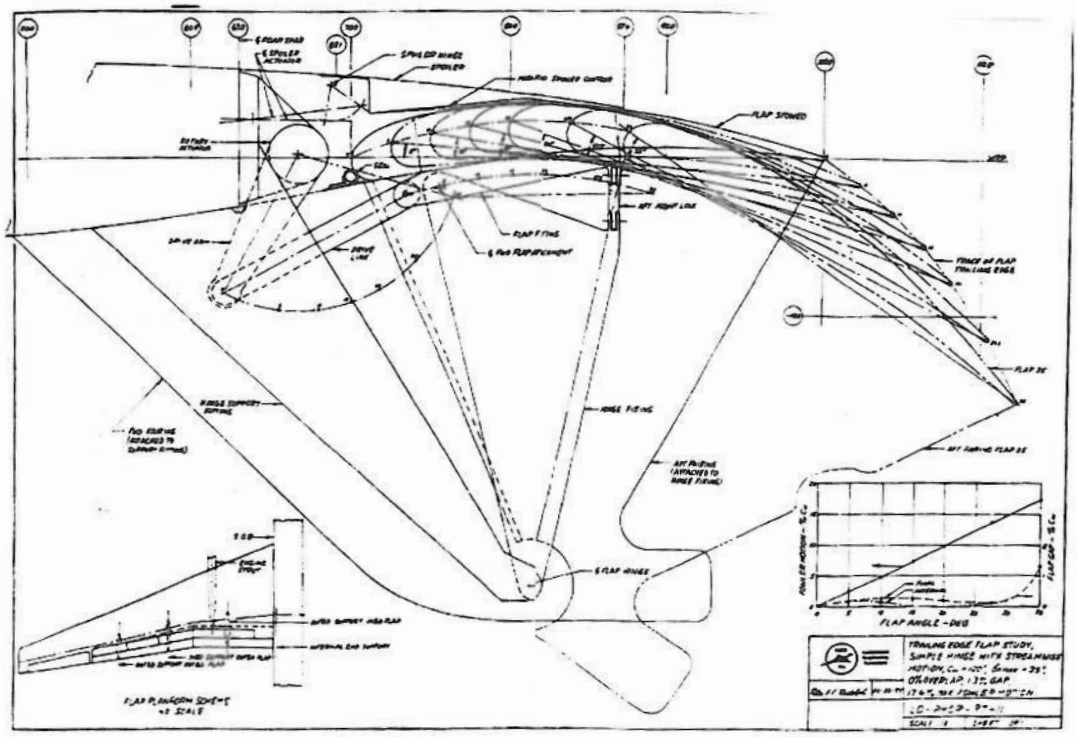

FigureC.8 Simple hinge flap motion trail [18]

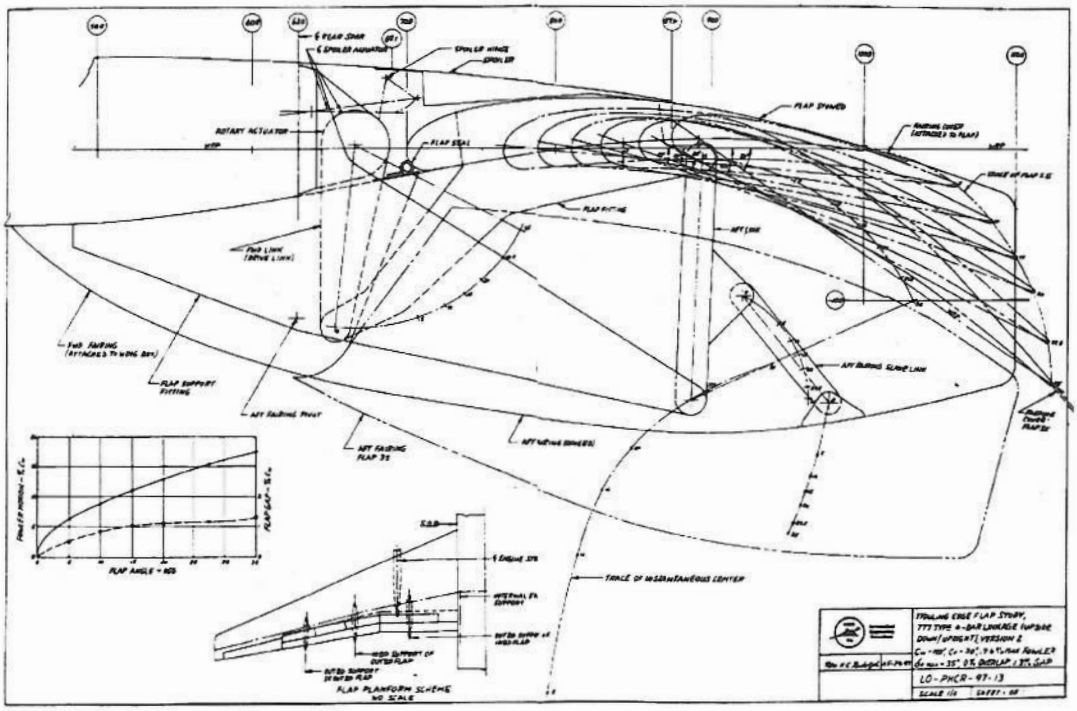

FigureC.9 Boeing777 four-bar linkage flap motion trail [18]

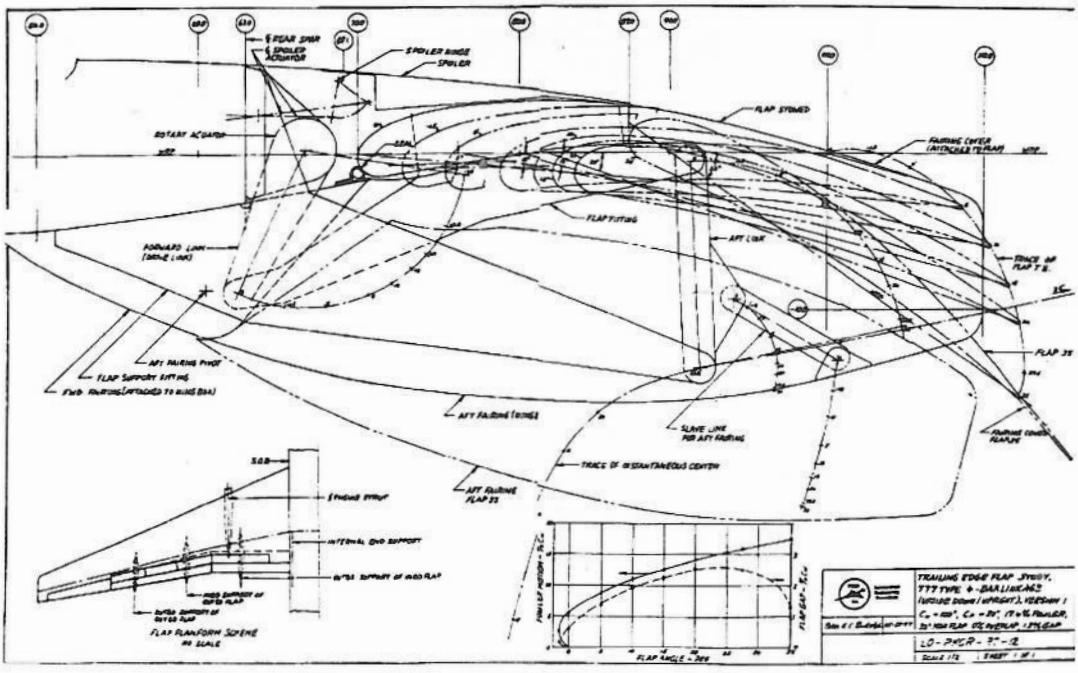

FigureC.10 Boeing777 upside down/upright four-bar linkage flap motion trail [18]

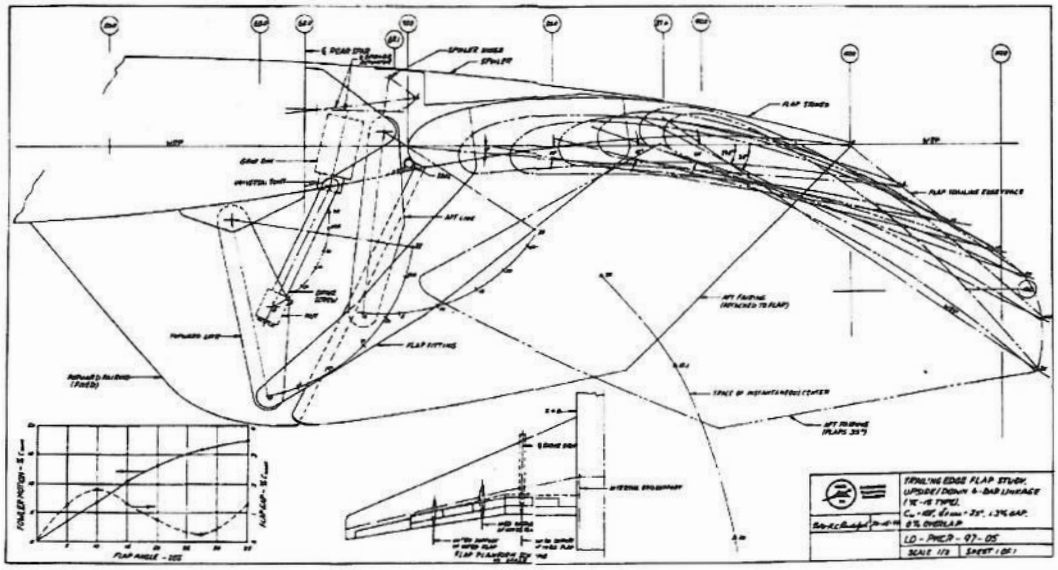

FigureC.11 YC15 upside down four-bar linkage flap motion trail [18]

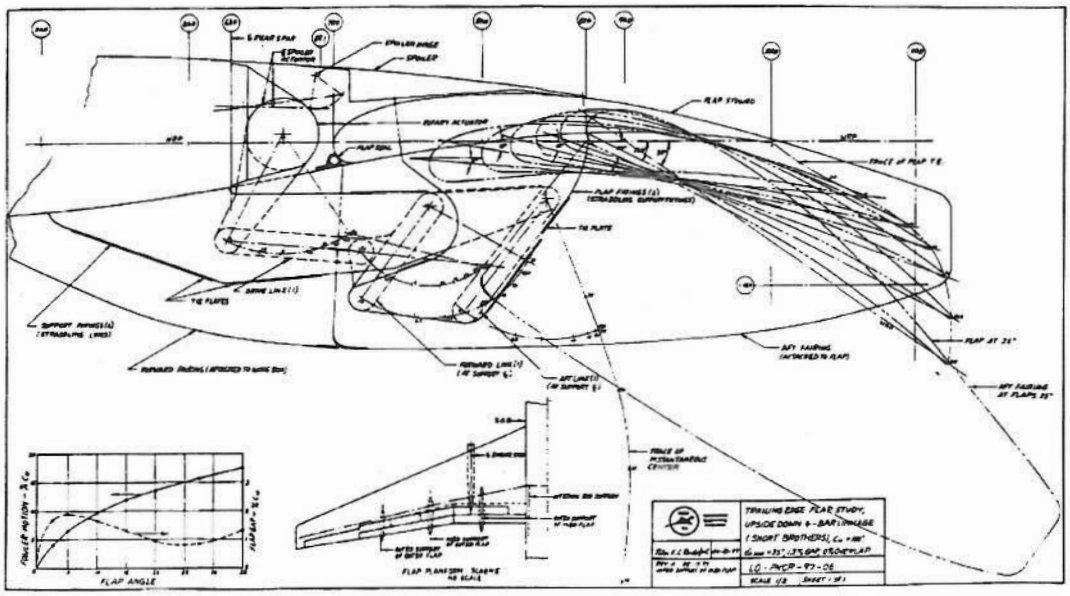

FigureC.12 Short Brothers upside down four-bar linkage flap motion trail [18]

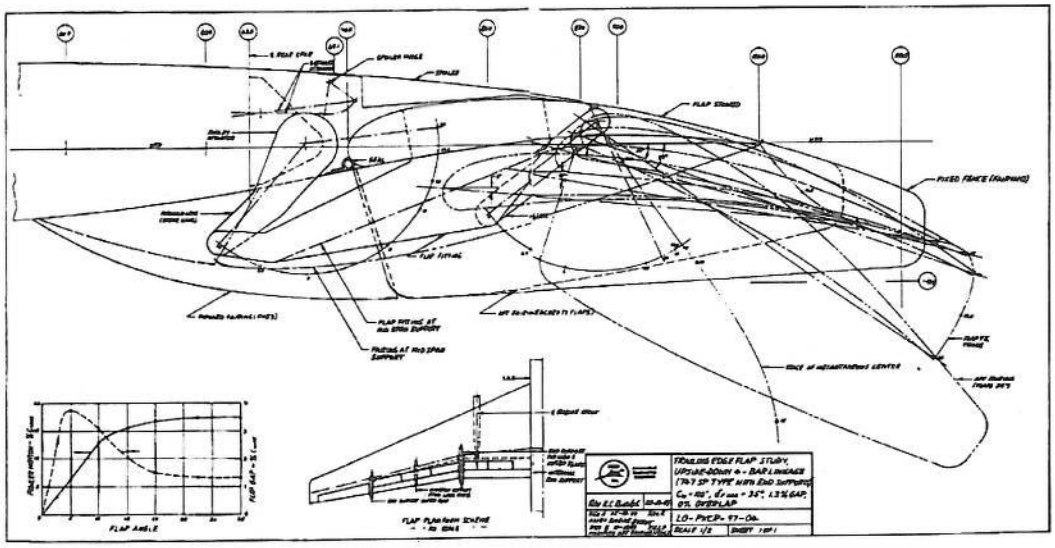

FigureC.13 Boeing747 four-bar linkage flap motion trail [18]

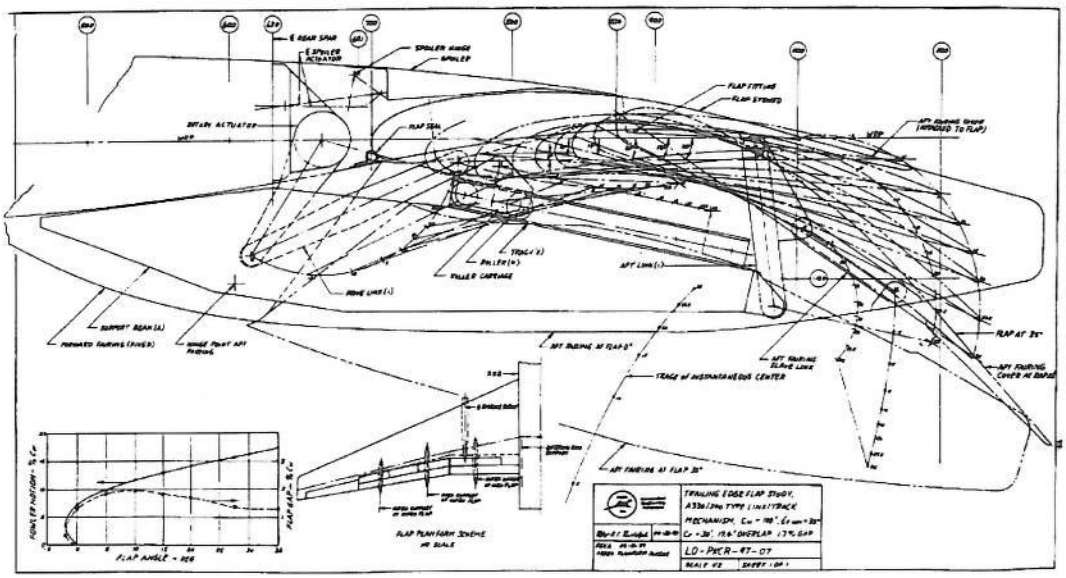

FigureC.14 Airbus A330/340 link/track flap motion trail [18]

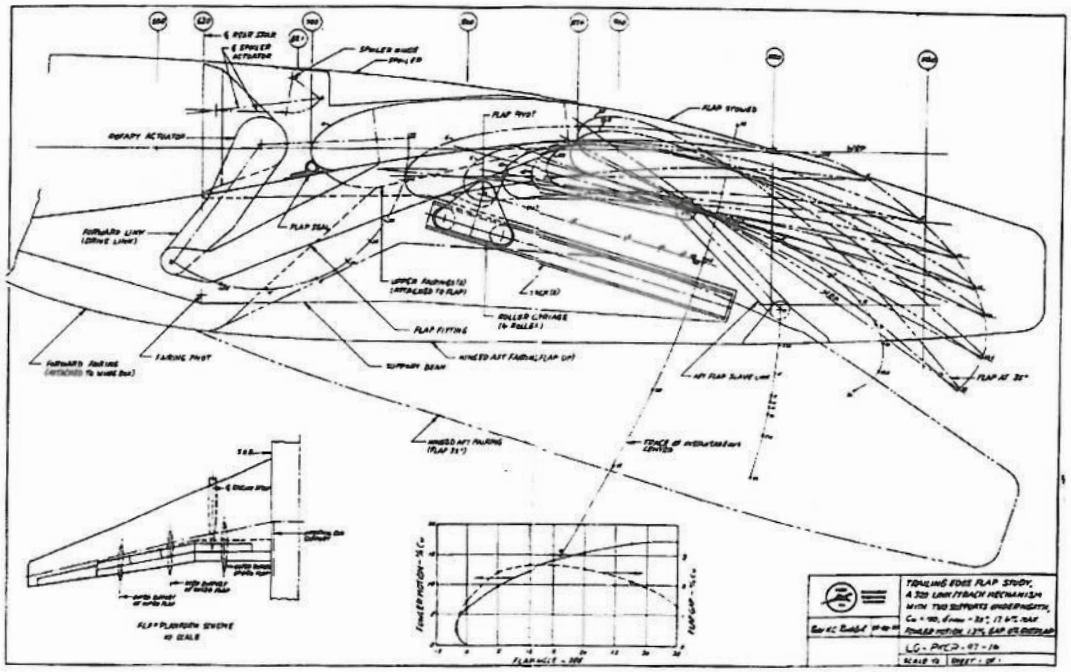

FigureC.15 Airbus A320 conservative link/track flap motion trail [18]

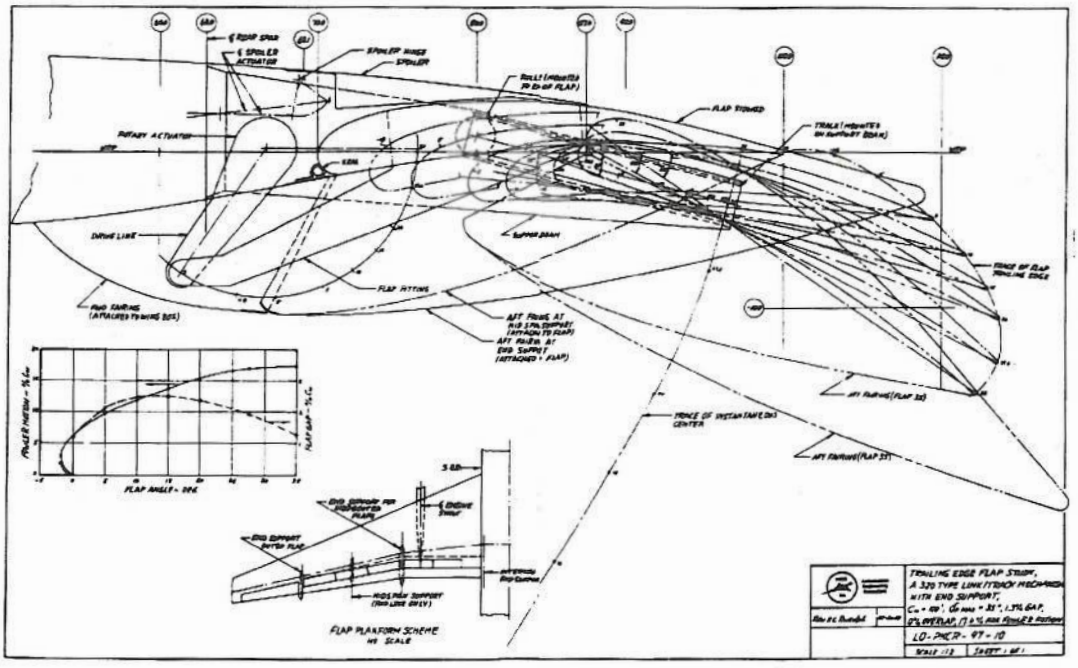

FigureC.16 Airbus A320 end supported link/track flap motion trail [18]

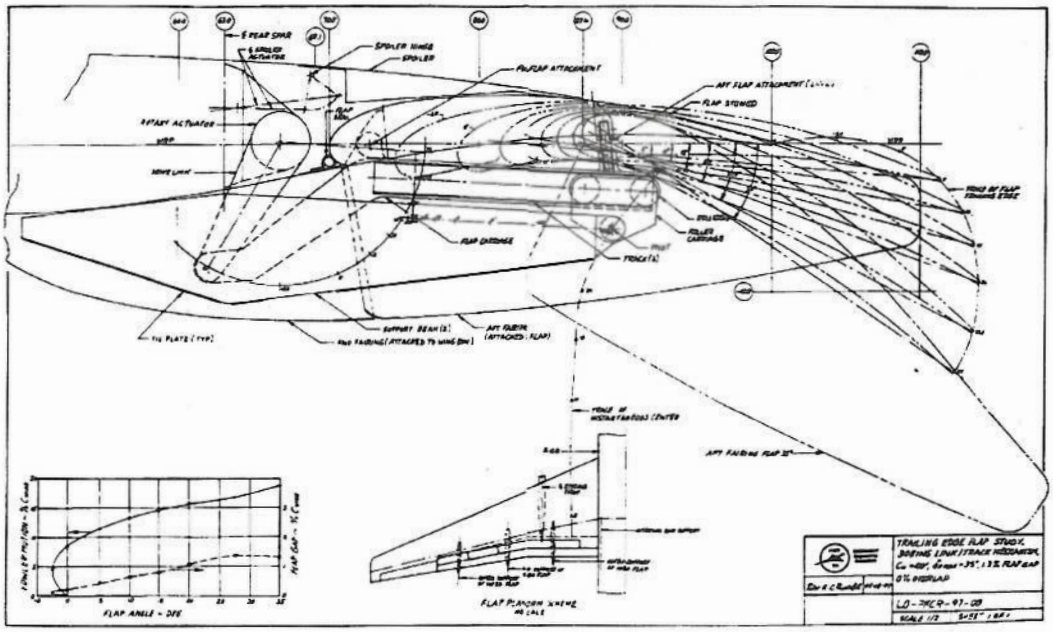

FigureC.17 Boeing conservative link/track flap motion trail [18]

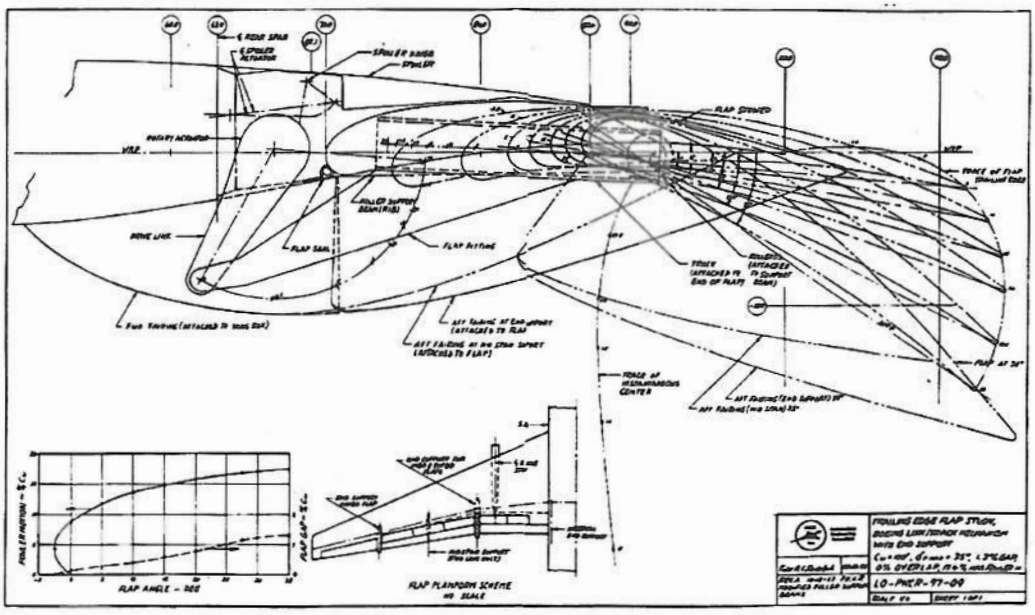

FigureC.18 Boeing end supported link/track flap motion trail [18]

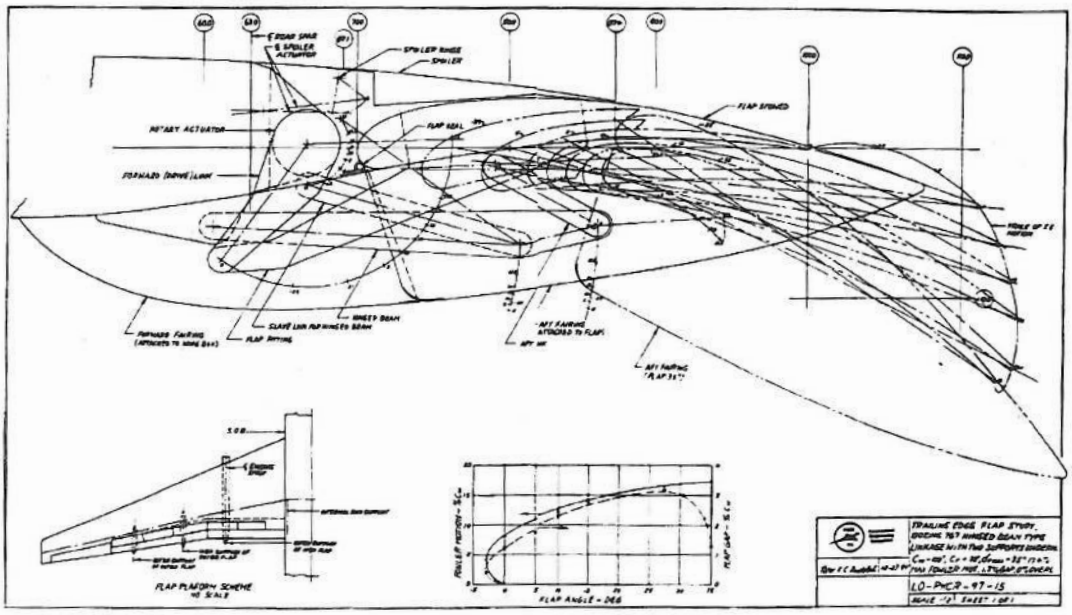

FigureC.19 Boeing767 hinged beam four-bar linkage flap motion trail [18]

Appendix D

Mechanical stress analysis

D.1 Forces on flap panel

Forces on flap panel consist of three types:

- Aerodynamic loading
- Gravity
- Support forces coming from hinge points

Magnitude and location of aerodynamic loading is given by paragraph3.6. It is regarded as mean load along flap span and acts at 36.4 percent of flap chord from its leading edge on chordwise. And the direction of aerodynamic loading could be simplified as perpendicular to flap chord.

The flap panels' gravity could be estimated by an empirical equation provided by reference [21], and the value is 1052.5N. This value is only 1.2% and 1.3% with respect to aerodynamic loading on flap panels in take-off and landing position respectively. Hence, it was ignored in stress analysis.

To avoid mathematical complexity, some simplifications are made in calculation. The hinge line of flap is regarded as superposing with flap leading edge, and always is parallel to the spar which mechanism is attached to during whole deploying process.

Forces on inboard and outboard flap panels are presented in FigureD.1. The four spherical joints on each flap panel are named by number from 1 to 4 which are defined as FigureD.1. Support force on each joint is analyzed into spanwise force (P_s), chordwise force (not including deflection) (P_c), and vertical force (P_v). Slide joints allow spanwise motion, thus spanwise force at point 4 equal zero. And the lever pairs can only provide constraint perpendicular to streamwise. Thus for inboard flap, $P_{3C}=0$; for outboard flap, $P_{3S}/P_{3C} = \tan \Lambda_h$, where Λ_h is sweepback of flap hinge line which equals 22.5° .

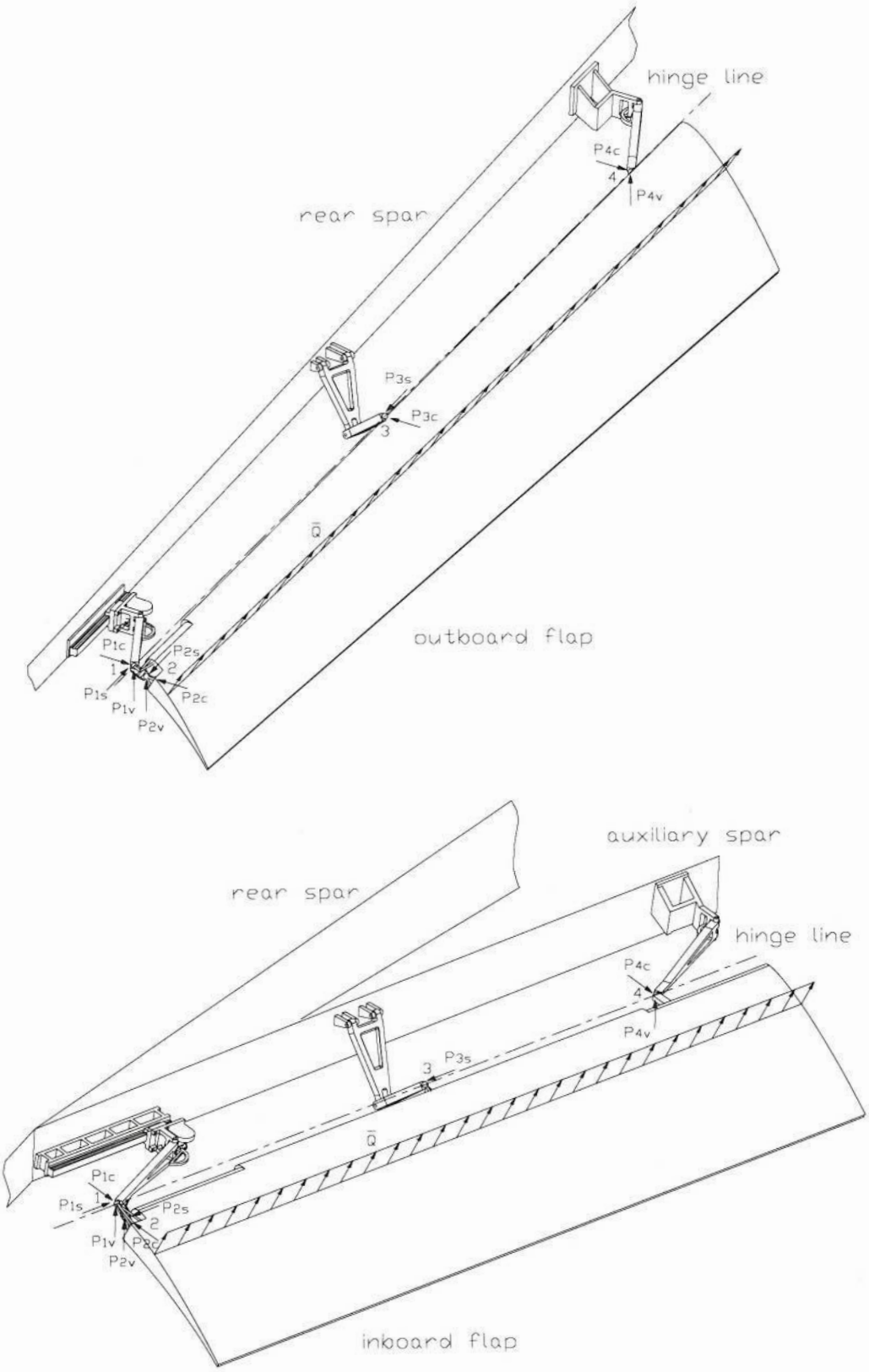

FigureD.1 Forces on flap panels

Taking inboard flap in take-off position as an example, moment yielded by aerodynamic loading with aspect to hinge line is given by

$$M_z = L \bullet P_c$$

Where L is aerodynamic loading calculated in paragraph3.6, P_c is length from pressure center to flap leading edge, and is equal to 342.2mm.

Hence,

$$M_z = 41662 \times 342.2 = 1.425 \times 10^7 (N \bullet mm)$$

This moment should be balanced by support force on point2 (P_2) because other three spherical joints are all on hinge line. Meanwhile, the direction of P_2 is supposed to be parallel to symmetrical plane of the control arm because there is no force to balance the arm against any moment around its rotation axis. Assume P_2 is parallel to control arm's rotation axis, thus distance between P_2 and hinge line (l_2) equals to the equivalent length of control arm, which is 80mm.

Therefore,

$$P_2 = \frac{M_z}{l_2} = \frac{1.425 \times 10^7}{80} = 17819(N)$$

Angles between P_{2v}, P_{2s}, P_{2c} and P_2 could be measured from the kinematic model and are listed below:

$\gamma_{2v} = 50^\circ$, $\gamma_{2s} = 45.2^\circ$, $\gamma_{2v} = 72.6^\circ$

and

$$P_{2v} = -P_2 \cos\gamma_{2v} = -17819 \times \cos 50^\circ = -11454(N)$$

$$P_{2s} = -P_2 \cos\gamma_{2s} = -17819 \times \cos 45.2^\circ = -12565(N)$$

$$P_{2c} = P_2 \cos\gamma_{2c} = 17819 \times \cos 72.6^\circ = 5334(N)$$

Direction of these forces is defined in FigureD.1.

For the arms and slide block assembly at station2 (defined as Figure3.4), there is no spanwise outside force besides P_{1s} and P_{2s}. Therefore $P_{1s} = P_{2s} = -12565$ N.

By solving mechanical equations about flap panel, other forces could be obtained.

$$P_{4v} = -\frac{4200}{2} \times \frac{L\cos\delta}{3527.6} = -\frac{4200 \times 41662 \times \cos 25^\circ}{2 \times 3527.6} = -2248(N)$$

$$P_{4c} = -\frac{\frac{4200}{2} L\sin\delta + 70.16 P_{2s}}{3527.6}$$

$$= -\frac{2100 \times 41662 \times \sin 25^\circ - 70.16 \times 12565}{3527.6}$$

$$= -798(N)$$

$$P_{1v} = -(L\cos\delta + P_{2v} + P_{4v}) = -(41662 \times \cos 25^\circ - 11454 - 2248) = 9926(N)$$

$$P_{1c} = P_{2c} - P_{4c} - L\sin\delta = 5334 + 798 - 41662 \times \sin 25^\circ = 4371(N)$$

$$P_{3s} = P_{1s} - P_{2s} = 0$$

Resultant forces on four points are given by

$$P_1 = \sqrt{P_{1v}{}^2 + P_{1s}{}^2 + P_{1c}{}^2} = 16598(N)$$

$$P_2 = \sqrt{P_{2v}{}^2 + P_{2s}{}^2 + P_{2c}{}^2} = 17819(N)$$

$$P_3 = P_{3s} = 0$$

$$P_4 = \sqrt{P_{4v}{}^2 + P_{4c}{}^2} = 2385(N)$$

The above steps were carried out on inboard and outboard flaps in both take-off and landing position. Calculation results are tabulated in tableD.1. It could be seen that most critical situation occurred at inboard flap, and the difference of support forces on point1 and point2 between take-off position and landing position is not very significant. Hence, assembly at station2 is chosen for strength verification in next part of this chapter.

		take-off	landing			take-off	landing
P_{1v} (N)	inboard	9925.3	9733.1	P_1 (N)	inboard	16597.9	15351.7
	outboard	3576.7	3531.1				
P_{1s} (N)	inboard	-12564.6	-6232.8				
	outboard	-6055.5	-2873.9		outboard	7269.5	6048.5
P_{1c} (N)	inboard	4371.1	10104.2				
	outboard	1839.6	3982.0				
P_{2v} (N)	inboard	-11453.6	-10787.6	P_2 (N)	inboard	17818.6	16782.6
	outboard	-5520.0	-4974.2				
P_{2s} (N)	inboard	-12564.6	-6232.8				
	outboard	-6055.5	-2873.9		outboard	8587.6	7738.5
P_{2c} (N)	inboard	5333.5	11244.3				
	outboard	2570.5	5184.8				
P_{3s} (N)	inboard	0	0	P_3 (N)	inboard	0	0
	outboard	1773.2	1597.8				
P_{3c} (N)	inboard	0	0		outboard	1898.6	1710.9
	outboard	678.6	611.5				
P_{4v} (N)	inboard	-2247.8	-2481.9	P_4 (N)	inboard	2385.3	3449.9
	outboard	-1936.5	-1284.6				
P_{4c} (N)	inboard	-798.3	-2396.3		outboard	1977.3	1576.2
	outboard	-399.7	-913.5				

TableD.1 Support forces on spherical joints

D.2 Stresses in control arm

As mentioned in previous paragraphs, the assembly at outside of inboard flap (station2 defined as Figure3.4) is chosen for checkout strength. And the aim of design reserve factor is to be higher than 1.5 which is recommended for civil aircraft. Taking take-off position as an example, forces on the control arm are presented in FigureD.2.

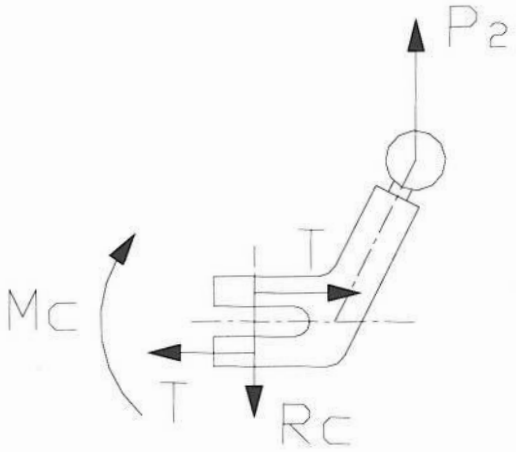

FigureD.2 Forces on control arm

P_2 was calculated in paragraph D.1, which equals to 17818.6 N. Value of forces demonstrated in FigureD.2 could be gotten by solving mechanical equations.

$$R_c = P_2 = 17818.6N$$

$$M_c = 80 \times P_2 = 1425486N \bullet mm$$

$$T = M_c / 7.5 = 47516.2N$$

Stress yielded by bending moment at cross-section through pivot axis is given by

$$\sigma = \frac{M_c y}{I}$$

Where $I = 2 \times (\frac{40 \times 15^3}{12} + 40 \times 15 \times 15^2) = 292500mm^4$, y = 22.5mm. Hence,

$$\sigma = \frac{1425486 \times 22.5}{292500} = 109.7N/mm^2$$

Material of control arm is S98, and its mechanical properties could be found in reference [6].

$$f_t = 1158N/mm^2$$

Therefore,

$$R.F. = \frac{f_t}{\sigma} = \frac{1158}{109.7} = 10.6$$

To check the stresses in lugs located in root part of the control arm.

The dimensions of the lug are:

a = 20mm, c = 12.5mm, d = 15mm, t = 15mm

d / t = 1, a / d =1.33

The multiplying factor for allowable shear stress is:

$$f = 0.4 \times (1 + a/d) = 0.933$$

The reduction factor used for proof stresses equals 0.8 for flap attachments.

Stresses applied on lug are given by

$$Tensile = \frac{T}{2ct} = \frac{47516.2}{2 \times 12.5 \times 15} = 126.7 N/mm^2$$

$$Shear = \frac{T}{2at} = \frac{47516.2}{2 \times 20 \times 15} = 79.2 N/mm^2$$

$$Bearing = \frac{T}{dt} = \frac{47516.2}{15 \times 15} = 211.2 N/mm^2$$

Stressing data of S98 are tabulated in TableD.2.

	Failing	Proof×1.5×0.8	Allowable stresses
Tensile (MPa)	984	1005.6	984
Shear (MPa)	389.2	350.56	350.56
Bearing (MPa)	-	1542	1542

TableD.2 Stressing data sheet of S98

Hence reserve factor for tensile, shear and bearing is 7.77, 4.43 and 7.30 respectively.

Same steps were run again with landing data to calculate stresses in landing position.

The results are tabulated in TableD.3.

Validating Part		Reserve Factor	
		take-off	landing
pivot axis		10.56	11.21
lugs	Tensile	7.77	8.25
	Shear	4.43	4.7
	Bearing	7.3	7.75

TableD.3 Reserve factors of control arm

The conclusion is that control arm is strong enough to carry design loading.

D.3 Stresses in swing arm

Strength validation process about swing arm is similar to that about control arm. Force diagram of swing arm is shown in FigureD.3, and FigureD.4 presents bending moment diagram along its top.

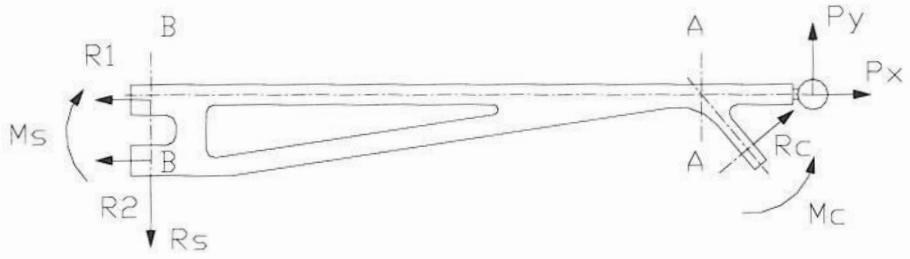

FigureD.3 Forces on swing arm

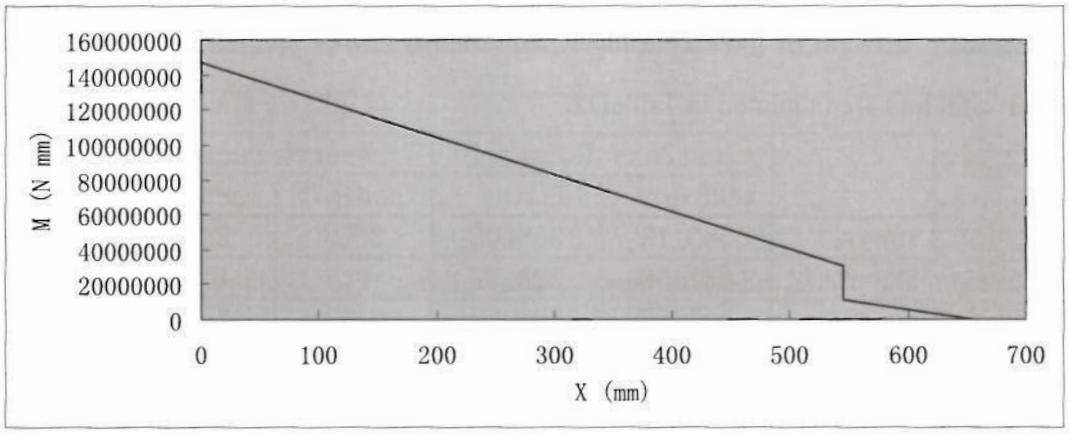

FigureD.4 Bending moment diagram of swing arm

Values of forces and moments are tabulated in TableD.4. The cross-sections which were chosen to validate strength are plan A-A and plan B-B defined as FigureD.3, because maximum bending moment occurred on plan B-B, while cross-section on plan A-A has minimum area. Reserve factors are tabulated in TableD.5.

	take-off	landing
Px (N)	13273.7094	11859.0153
Py (N)	9925.47029	9733.12217
Rc (N)	17818.5756	16782.5662
Mc (N mm)	1425486.05	1342605.29
Rs (N)	21379.0299	20520.7478
Ms (N mm)	14689423.4	14087353.8
R_1 (N)	-215656.56	-208014.42
R_2 (N)	202580.095	200029.63

TableD.4 Values of forces and moments on swing arm

Validating Part		Reserve Factor	
		take-off	landing
plan A-A		1.00	1.05
plan B-B		4.73	4.95
lugs	Tensile	3.04	3.17
	Shear	1.73	1.81
	Bearing	2.86	2.98

TableD.5 Reserve factors of swing arm

Reserve factor of cross-section on plan A-A is less than 1.5, which means swing arm will fail on this cross-section under act of design loading. Add the thickness of top of swing arm from origin 20mm to 30mm, then the reserve factor will be enlarged to 2.24 and 2.35 in take-off and landing position respectively. Thus the swing arm could fulfil the strength requirement.

To validate strength of the single lug which control arm is pivoted on. Stresses and reserve factors are tabulated in TableD.6.

	stress (N/mm^2)		reserve factor	
	take-off	landing	take-off	landing
Tensile	380.13	358.03	2.59	2.75
Shear	237.58	223.77	1.48	1.57
Bearing	633.55	596.71	2.43	2.58

TableD.6 Stress and R.F. on single lug

The reserve factor of shear in take-off position is too small to carry design loading. Hence this part needs to be reinforced. This factor would rise to 1.97 after thickness of the lug was enlarged to 20mm.

To check strength of the bolt that pivots swing arm on sliding block. Its diameter is 15mm and material is defined as S99. Thus its allowable single shear strength is 154kN (according to the datum of 5/8" UNF bolt provided by reference [6]).

D / t = 15 / 30 =0.5, so factor k is 1.

This bolt is in double shear case, so $Q = 2kQ_0 = 308$ kN

R.F. = $Q / R_2 = 1.52$

So this bolt is regarded as having capability to carry design loading.

D.4 Stresses in lever pair

The inertia loads acting parallel to the hinge line of control surfaces are regulated to be equal to K • W both in CS-25 (reference [24]) and in FAR-25 (reference [25]), where K is equal to 12 for horizontal surfaces. This figure was regarded as maximum load on lever pair.

Basing on the method provided by reference [21], the masses of inboard and outboard flap panel were calculated and tabulated in TableD.7.

	inboard	outboard
a_1 (lb/ft^2)	2.7	
STE (m^2)	3.95	4.2
Wpanel (kg)	52.06	55.33

TableD.7 Weights of flap panels

Load on lever pair is give by

$$L = \frac{K \cdot W}{\cos \Lambda_h}$$

Where Λh is sweepback of hinge line and is equal to 0 and 22.5° for inboard and outboard flap respectively. Hence load on inboard and outboard lever pair is 6128.5N and 6513.4N respectively.

According to methods used in paragraphD.2 and D.3, forces acting on levers and stresses in them could be carried out. FigureD.5 and FigureD.6 demonstrates forces and bending moment on second lever, as well as FigureD.7 and FigureD.8 illustrates those on first lever. And results of reserve factors for these levers are presented in TableD.8 and TableD.9.

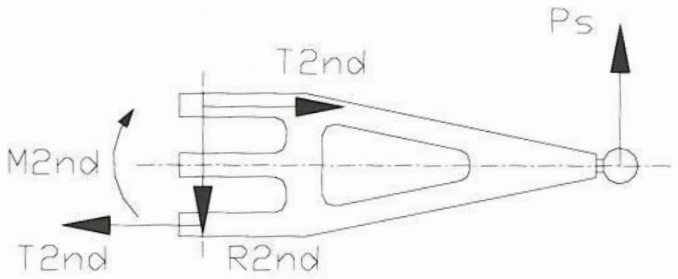

FigureD.5 Forces on second lever

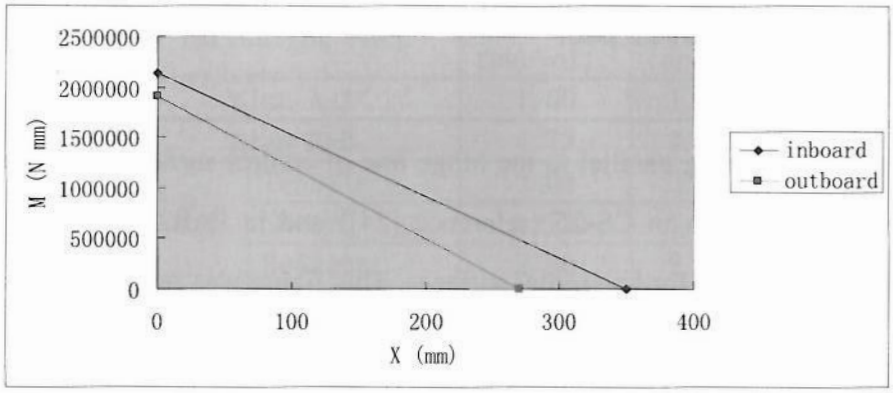

FigureD.6 Bending moments on second levers

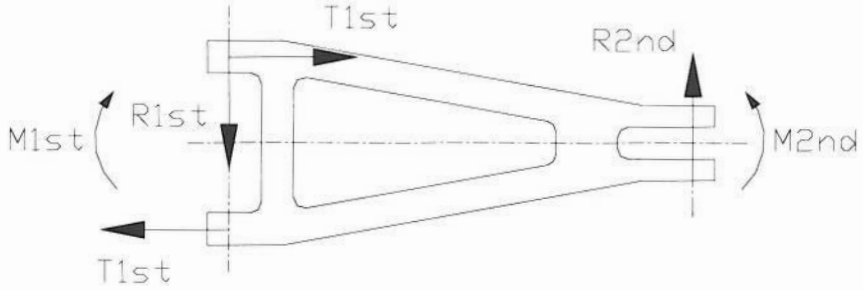

FigureD.7 Forces on first lever

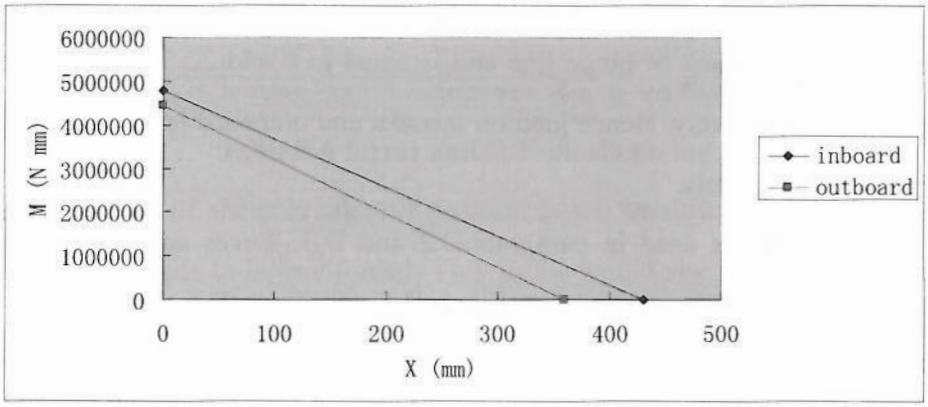

FigureD.8 Bending moments on first levers

	inboard	outboard
T_{2nd} (N)	21449.76	19035.28
M_{2nd} (N mm)	2144976	1903528
Izz (mm^4)	4080000	
y (mm)	60	
σ m (N/mm^2)	31.54377	27.99306
σ t (N/mm^2)	26.8122	23.7941
σ (N/mm^2)	58.35597	51.78717
R.F.	19.84373	22.36075

TableD.8 Reserve factors of second levers

	inboard	outboard
T_{1st} (N)	29876.45	27759.79
M_{1st} (N mm)	4780232	4441566
Izz (mm^4)	15540000	
y (mm)	95	
σ m (N/mm^2)	29.22279	27.15243
σ t (N/mm^2)	24.89704	23.13316
σ (N/mm^2)	54.11983	50.28559
R.F.	21.39696	23.02847

TableD.9 Reserve factors of first levers

About stresses of lever lugs, only inboard lever pair was chosen to validate because stress in it is higher than that in outboard one. Calculating method has been described in paragraphD.2 and results are tabulated in TableD.10.

		2nd lever	1st lever	
			wing end	flap end
a (mm)		20	20	20
c (mm)		12.5	12.5	12.5
d (mm)		15	15	15
t (mm)		20	30	20
T (N)		21449.7612	29876.453	30642.516
stress (MPa)	tensile	42.8995224	39.835271	61.285032
	share	26.8122015	24.897044	38.303145
	bending	71.499204	66.392118	102.14172
R.F.	tensile	22.9373183	24.701727	16.056123
	share	13.0746444	14.080386	9.1522511
	bending	21.5666737	23.225649	15.096672

TableD.10 Lug stress analysis

Reserve factors of these levers are much higher than 1.5, thus the material of levers could be change into aluminum alloy to get benefit from weight saving.

D.5 Alternative material

According to the fact that most of the reserve factors gotten from former paragraphs of this chapter, lighter alternative materials with low allowable stress such as aluminum alloy and titanium alloy were considered being used to take the place of steel in order to reduce mechanism's weight. Stress data of L168 (20mm<D<75mm) and TA49 could be found in reference [6] and is presented in TableD.11 and

TableD.12 respectively, while these data of S98 is presented in TableD.2.

	Failing	Proof×1.5×0.8	Allowable stresses
Tensile (MPa)	424	456	424
Shear (MPa)	168	159.04	159.04
Bearing (MPa)	-	684	684

TableD.11 Stress data sheet of L168

	Failing	Proof×1.5×0.8	Allowable stresses
Tensile (MPa)	876	765.6	765.6
Shear (MPa)	346.3	299.04	299.04
Bearing (MPa)	-	1340.4	1340.4

TableD.12 Stress data sheet of TA49

Apply these allowable stresses into steps presented in the three paragraphs above, thus reserve factors of new materials could be obtained. Calculating results are tabulated in following four tables. All these calculation were carried out under the loading in take-off position because it is higher than that in landing position.

Validating Part		Reserve Factor
pivot axis		4.55
lugs	Tensile	3.35
	Shear	2.01
	Bearing	3.24

TableD.13 Reserve factors of control arm made by L168

Validating Part		Reserve Factor		
		2nd lever	1st lever	
			Wing end	Flap end
pivot axis		8.55	9.22	
lugs	Tensile	9.88	10.64	6.92
	Shear	5.93	6.39	4.15
	Bearing	9.57	10.3	6.70

TableD.14 Reserve factors of lever pair made by L168

Validating Part		Reserve Factor	
		take-off	landing
plan A-A		0.96	1.01
plan B-B		2.04	2.13
lugs	Tensile	1.31	1.37
	Shear	0.79	0.82
	Bearing	1.27	1.32

TableD.15 Reserve factors of swing arm made by L168

Validating Part		Reserve Factor	
		take-off	landing
plan A-A		1.99	2.09
plan B-B		4.20	4.40
lugs	Tensile	2.37	2.47
	Shear	1.58	1.64
	Bearing	2.49	2.59

TableD.16 Reserve factors of swing arm made by TA49

It could be seen that aluminum alloy (L168) is strong enough for control arm and lever pair components. However, in the case of swing arm, reserve factors for several parts are smaller than 1.5 when using aluminum material. Thus, titanium alloy (TA49) was chosen as the material of swing arms.

Significant weight saving could be achieved by using new materials due to their low densities. The control arm and lever pair could get weight saving of about 65%, and the swing arm could get weight saving of about 43%. However, the manufacture cost will rise because titanium is more expensive than steel.

D.6 Summary

The outside end arm assembly of inboard flap was chosen as the most critical components to do the strength check. It has been validated that the control arm and connecting bolts are all capable to carry design loading. However, reserve factors at two sections on the swing arm are less than 1.5. Hence, the thickness of top bar and single lug of swing arm need to be enlarged to reinforce these weak areas.

Aluminum alloy and titanium alloy were validated to be acceptable alternative materials for different components of this new mechanism which could provide significant weight saving.